Reports on Progress in **Physics**

PURPOSE-LED PUBLISHING™

**PAPER** • **OPEN ACCESS**

# Measurement of off-shell Higgs boson production in the $H^* \to ZZ \to 4\ell$ decay channel using a neural simulation-based inference technique in 13 TeV *pp* collisions with the ATLAS detector

To cite this article: The ATLAS Collaboration 2025 *Rep. Prog. Phys.* **88** 057803

View the article online for updates and enhancements.

You may also like

- Dark matter search with a resonantly-coupled hybrid spin system
Kai Wei, Zitong Xu, Yuxuan He et al.
- 70 years of hyperon spectroscopy: a review of strange , baryons, and the spectrum of charmed and bottom baryons
Volker Crede and John Yelton
- Divergence beneath the Brillouin sphere and the phenomenology of prediction error in spherical harmonic series approximations of the gravitational field
M Bevis, C Ogle, O Costin et al.

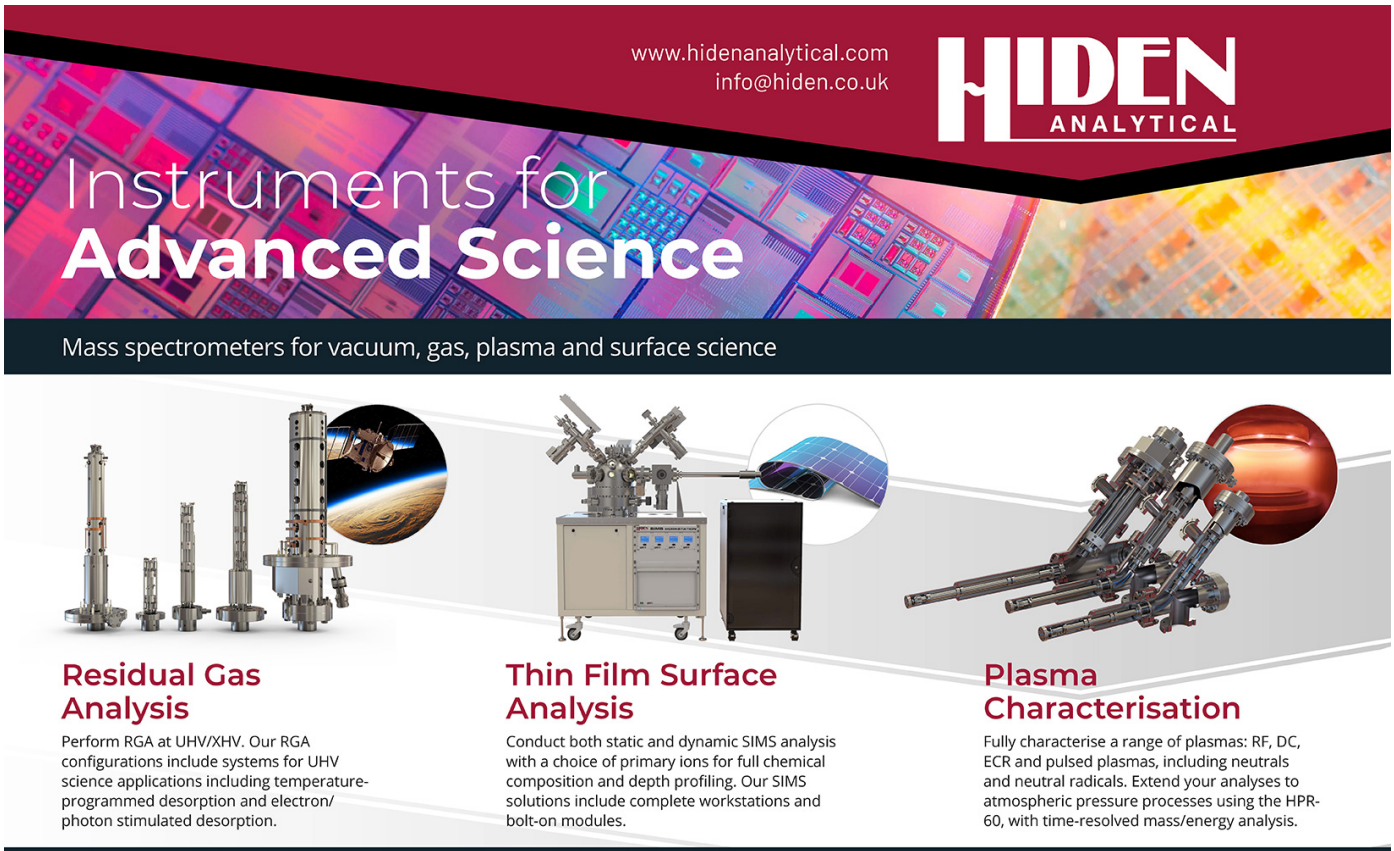


This content was downloaded from IP address 79.35.252.254 on 05/10/2025 at 12:57

OPEN ACCESS
IOP Publishing
Reports on Progress in Physics
Rep. Prog. Phys. **88** (2025) 057803 (38pp)
https://doi.org/10.1088/1361-6633/adcd9a

# Measurement of off-shell Higgs boson production in the $H^* \to ZZ \to 4\ell$ decay channel using a neural simulation-based inference technique in 13 TeV *pp* collisions with the ATLAS detector

**The ATLAS Collaboration**

E-mail: atlas.publications@cern.ch

Received 3 December 2024, revised 2 April 2025
Accepted for publication 16 April 2025
Published 15 May 2025

Corresponding editor: Dr Paul Mabey

**Abstract**

A measurement of off-shell Higgs boson production in the $H^* \to ZZ \to 4\ell$ decay channel is presented. The measurement uses 140 fb$^{-1}$ of proton–proton collisions at $\sqrt{s} = 13$ TeV collected by the ATLAS detector at the Large Hadron Collider and supersedes the previous result in this decay channel using the same dataset. The data analysis is performed using a neural simulation-based inference method, which builds per-event likelihood ratios using neural networks. The observed (expected) off-shell Higgs boson production signal strength in the $ZZ \to 4\ell$ decay channel at 68% CL is $0.87^{+0.75}_{-0.54}$ ($1.00^{+1.04}_{-0.95}$). The evidence for off-shell Higgs boson production using the $ZZ \to 4\ell$ decay channel has an observed (expected) significance of $2.5\sigma$ ($1.3\sigma$). The expected result represents a significant improvement relative to that of the previous analysis of the same dataset, which obtained an expected significance of $0.5\sigma$. When combined with the most recent ATLAS measurement in the $ZZ \to 2\ell 2\nu$ decay channel, the evidence for off-shell Higgs boson production has an observed (expected) significance of $3.7\sigma$ ($2.4\sigma$). The off-shell measurements are combined with the measurement of on-shell Higgs boson production to obtain constraints on the Higgs boson total width. The observed (expected) value of the Higgs boson width at 68% CL is $4.3^{+2.7}_{-1.9}$ ($4.1^{+3.5}_{-3.4}$) MeV.

Supplementary material for this article is available online

Keywords: machine learning, likelihood-free inference, neural simulation-based inference, parameter inference, frequentist statistics

Original Content from this work may be used under the terms of the Creative Commons Attribution 4.0 licence. Any further distribution of this work must maintain attribution to the author(s) and the title of the work, journal citation and DOI.


© 2025 The Author(s). Published by IOP Publishing Ltd

## Contents


1. Introduction 2
2. ATLAS detector 3
3. Modeling of off-shell Higgs boson production 3
4. Data and simulated event samples 5
5. Object reconstruction, event selection and description 7
   5.1. Object reconstruction 7
   5.2. Event selection and description 7
6. Neural simulation-based inference 8
   6.1. Signal and control regions 9
   6.2. Probability density ratio estimation 10
   6.3. Systematic uncertainties 12
7. Statistical analysis and results 14
   7.1. Combination with the analysis in the $2\ell 2\nu$ decay channel 18
   7.2. Combination with on-shell $4\ell$ analysis and Higgs boson width interpretation 19
8. Conclusion 20
Data availability statement 21
Acknowledgment 21
References 35


## 1. Introduction

The Higgs boson was observed in 2012 by the ATLAS [1] and CMS [2] collaborations at the Large Hadron Collider (LHC). Since then, a series of measurements were performed to establish the fundamental nature of this new particle. Measurements of the spin [3, 4], mass [5–7], and couplings [8, 9] of the Higgs boson have been performed in several decay channels. The total width of the Higgs boson ($\Gamma_H$) in the Standard Model (SM) is calculated to be 4.10 MeV [10], and is a particularly challenging parameter to be measured. Direct measurements of the Higgs boson lineshape are unable to reach the precision required to measure the Higgs boson width due to limited detector resolution, $\mathcal{O}$(1.5–3 GeV) [7, 11].

Due to the small total width, the differential cross-section with respect to the four-lepton invariant mass $\mathrm{d}\sigma/\mathrm{d}m_{4\ell}$ in the $H \to ZZ \to 4\ell$ decay channel falls steeply for invariant masses larger than the Higgs boson mass of 125 GeV. Several authors have pointed out that this differential cross-section increases again at the kinematic threshold at twice the $Z$ boson pole mass $m_{4\ell} = 2m_Z$ to a level that could be probed by the LHC experiments [12–14]. Similar kinematic thresholds can be exploited at twice the pole mass of the $W$ boson [15] and of the top quark [16] in different production and decay channels. Both the ATLAS and CMS collaborations have recently reported evidence for the production of off-shell Higgs bosons using the $H^* \to ZZ \to 4\ell$ and $H^* \to ZZ \to 2\ell 2\nu$ decay channels [7, 17, 18].

Measurements of the Higgs boson production rate in $H \to VV$ decay channels, where $V = Z$ or $W$, are used to probe the Higgs boson couplings to vector bosons and fermions. These measurements depend on the Higgs boson total width if performed with on-shell Higgs bosons, but are independent of the width if the Higgs boson is off-shell, as can be seen from the Breit–Wigner model of the Higgs boson's resonance:

$$\begin{aligned} \frac{\mathrm{d}\sigma^{H\to VV}}{\mathrm{d}m_{VV}^2} &\propto \frac{g_{\mathrm{prod}}^2(\hat{s})\, g_{\mathrm{decay}}^2(\hat{s})}{\left(m_{VV}^2 - m_H^2\right)^2 + m_H^2\Gamma_H^2} \\ &\Rightarrow \frac{\mathrm{d}\sigma_{\text{off-shell}}^{H^*\to VV}}{\mathrm{d}m_{VV}^2} \propto g_{\mathrm{prod}}^2(\hat{s})\, g_{\mathrm{decay}}^2(\hat{s}), \\ \sigma_{\text{on-shell}}^{H\to VV} &\propto \frac{g_{\mathrm{prod}}^2(m_H)\, g_{\mathrm{decay}}^2(m_H)}{\Gamma_H}, \end{aligned} \tag{1}$$

where $g_{\mathrm{prod}}(\hat{s})$ and $g_{\mathrm{decay}}(\hat{s})$ are, respectively, the effective couplings of Higgs boson production and decay, as a function of the Higgs boson virtuality $\hat{s}$. A comparison of the off-shell and on-shell Higgs boson production rates allows an indirect measurement of the Higgs boson total width assuming that there is no beyond SM (BSM) physics that alters the on-shell and off-shell couplings differently [13, 14, 19].

In the presence of light BSM states, off-shell Higgs boson production can probe new kinematic thresholds produced by one-loop electroweak (EW) corrections [20]. Off-shell Higgs boson production can also be used to constrain BSM physics at high energy. Using the formalism of SM Effective Field Theory [21–23], off-shell Higgs boson production breaks the degeneracy between the top-quark Yukawa and Higgs-gluon interaction which exists for on-shell Higgs boson production [24]. In these cases, using the SM prediction for on-shell and off-shell Higgs boson production would no longer provide an indirect measurement of the Higgs boson total width, since the new states can have a non-negligible contribution to the Higgs boson propagator and decay. The ATLAS Collaboration has recently reported limits on dimension-6 operators that modify the production of off-shell Higgs bosons [25], while the CMS Collaboration reported limits on dimension-6 operators that modify both production and decay [18, 26].

This paper reports a new measurement of off-shell Higgs boson production in the $H^* \to ZZ \to 4\ell$ decay channel using a novel method to interpret the data. The method, known as neural simulation-based inference (NSBI) [27–30], uses neural networks (NNs) to estimate the per-event likelihood ratio of different hypotheses instead of using histograms of kinematic observables as an approximation to probability density ratios. The specific implementation of NSBI used in this paper is described in section 6 and in more detail in [31].

The NSBI method improves several aspects of a histogram-based analysis by providing a better approximation of the exact likelihood ratio between different hypotheses [27]. The likelihood ratio obtained by the NSBI approach is optimally sensitive to any value of the off-shell Higgs boson production signal strength. This cannot be achieved by analyses that interpret a ratio of likelihoods constructed from a single observable when the signal model is non-linear, even if this observable is optimal for a given parameter value [31]. Multidimensional optimal observables [32] and parameterized optimal observables [33] can alternatively be used with the same goal. In addition, the NSBI construction allows for unbinned measurements of parameters. Binned histograms treat all events inside a given bin as equivalent leading to an unavoidable loss in the power to separate different hypotheses. These losses can

be minimized by choosing bin widths compatible with the observable resolution. This optimization may be challenging in high-resolution final states and may require large simulated samples, while an unbinned NSBI analysis can make better use of limited-size simulation samples.

The NSBI construction can be understood as a machine learning approach to the matrix-element method [34, 35] where NNs learn both the theory dependency of the likelihood ratio relative to a high-dimensional final-state phase space and the complex detector response using simulated samples. The use of large NN models and the unbinned character of the NSBI analysis require a more advanced computational infrastructure than that used in histogram-based analyses [36].

The results of this paper supersede those of [17] for the $4\ell$ channel, using the same dataset, object selection, and event selection. The measurement is combined with the $2\ell 2\nu$ channel, which is not re-analyzed, applying the same method for its interpretation as in [17].

## 2. ATLAS detector

The ATLAS detector [37] at the LHC covers nearly the entire solid angle around the collision point[1]. It consists of an inner tracking detector surrounded by a thin superconducting solenoid, electromagnetic and hadronic calorimeters, and a muon spectrometer incorporating three large superconducting air-core toroidal magnets.

The inner-detector (ID) system is immersed in a 2 T axial magnetic field and provides charged-particle tracking in the range $|\eta| < 2.5$. The high-granularity silicon pixel detector covers the vertex region and typically provides four measurements per track, the first hit generally being in the insertable B-layer (IBL) installed before Run 2 [38, 39]. It is followed by the SemiConductor Tracker (SCT), which usually provides eight measurements per track. These silicon detectors are complemented by the transition radiation tracker (TRT), which enables radially extended track reconstruction up to $|\eta| = 2.0$. The TRT also provides electron identification information based on the fraction of hits (typically 30 in total) above a higher energy-deposit threshold corresponding to transition radiation.

The calorimeter system covers the pseudorapidity range $|\eta| < 4.9$. Within the region $|\eta| < 3.2$, electromagnetic calorimetry is provided by barrel and endcap high-granularity lead/liquid-argon (LAr) calorimeters, with an additional thin LAr presampler covering $|\eta| < 1.8$ to correct for energy loss in material upstream of the calorimeters. Hadronic calorimetry is provided by the steel/scintillator-tile calorimeter, segmented into three barrel structures within $|\eta| < 1.7$, and two copper/LAr hadronic endcap calorimeters. The solid angle coverage is completed with forward copper/LAr and tungsten/LAr calorimeter modules optimized for electromagnetic and hadronic energy measurements respectively.

The muon spectrometer (MS) comprises separate trigger and high-precision tracking chambers measuring the deflection of muons in a magnetic field generated by the superconducting air-core toroidal magnets. The field integral of the toroids ranges between 2.0 and 6.0 T m across most of the detector. Three layers of precision chambers, each consisting of layers of monitored drift tubes, cover the region $|\eta| < 2.7$, complemented by cathode-strip chambers in the forward region, where the background is highest. The muon trigger system covers the range $|\eta| < 2.4$ with resistive-plate chambers in the barrel, and thin-gap chambers in the endcap regions.

The luminosity is measured mainly by the LUCID–2 [40] detector that records Cherenkov light produced in the quartz windows of photomultipliers located close to the beampipe.

Events are selected by the first-level trigger system implemented in custom hardware, followed by selections made by algorithms implemented in software in the high-level trigger [41]. The first-level trigger accepts events from the 40 MHz bunch crossings at a rate below 100 kHz, which the high-level trigger further reduces in order to record complete events to disk at about 1 kHz.

A software suite [42] is used in data simulation, in the reconstruction and analysis of real and simulated data, in detector operations, and in the trigger and data acquisition systems of the experiment.

## 3. Modeling of off-shell Higgs boson production

The measurement of off-shell Higgs boson production presented in this paper is interpreted using a model in which the effective couplings of the Higgs boson to gluons and to EW vector bosons in the SM can have anomalous scalar modifications. This analysis framework, known as the $\kappa$-framework [43], allows changes in the overall cross-section without changing the process kinematics, and can be understood as a sector of a larger Higgs Effective Field Theory (HEFT) [44].

The gluon–gluon fusion (ggF) off-shell Higgs boson production and subsequent decay into a $ZZ$ pair, $gg \to ZZ$, can be described by using the Higgs boson effective coupling constants $g_g(\hat{s})$ and $g_V(\hat{s})$ to gluons and vector bosons, shown in figure 1(a). The effective couplings $g_g$ and $g_V$ depend on the Higgs boson virtuality $\hat{s}$, but the notation is suppressed hereafter for simplicity. The Higgs boson is represented by $H^*$ to denote explicitly that its virtuality is well above the pole mass $m_H = 125$ GeV [45].

In $gg \to ZZ$ production, the *signal* (S) component is defined at leading order (LO) in perturbation theory by the absolute value squared of the amplitude of the diagram in figure 1(a).

[1] ATLAS uses a right-handed coordinate system with its origin at the nominal interaction point (IP) in the center of the detector and the $z$-axis along the beam pipe. The $x$-axis points from the IP to the center of the LHC ring, and the $y$-axis points upwards. Polar coordinates $(r, \phi)$ are used in the transverse plane, $\phi$ being the azimuthal angle around the $z$-axis. The pseudorapidity is defined in terms of the polar angle $\theta$ as $\eta = -\ln\tan(\theta/2)$ and is equal to the rapidity $y = \frac{1}{2}\ln\left(\frac{E+p_z}{E-p_z}\right)$ in the relativistic limit. Angular distance is measured in units of $\Delta R \equiv \sqrt{(\Delta y)^2 + (\Delta\phi)^2}$.

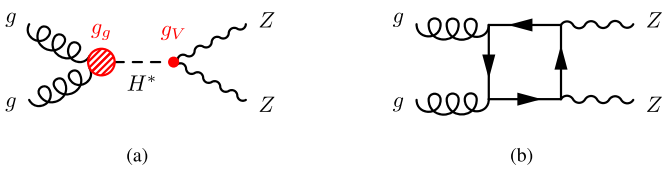


**Figure 1.** Illustrative leading-order Feynman diagrams for $gg \to ZZ$ production. The diagrams indicate the effective couplings $g_g$ and $g_V$. Diagram (a) corresponds to the signal component and diagram (b) corresponds to the background component. A large destructive interference between the two components is present in the off-shell regime.

The signal contribution scales as $g_g^2 g_V^2$. The *background* (B) component is defined at LO in perturbation theory by the absolute value squared of the amplitude of the diagram in figure 1(b). The background component is independent of $g_g$ and $g_V$. The *interference* (I) between the two diagrams scales as $g_g g_V$. The integrated interference between the two diagrams is negative, as required by perturbative unitarity conservation [46].

The effective coupling between gluons and the Higgs boson $g_g$ is represented by a blob in figure 1(a) since in the SM, at LO in perturbation theory, it can be resolved to a fermion triangle loop dominated by the top-quark contribution. In several BSM scenarios, the contribution of new heavy particles cannot be resolved at the scales probed by this measurement, but can modify the Higgs boson effective couplings as well as the background process.

The same concepts can be applied to the EW production of $qq \to ZZ + 2j \to 4\ell + 2j$. In this case, the *signal* scales as $g_V^4$, the *interference* scales as $g_V^2$, and the *background* component is independent of $g_V$. Similar to the case of ggF production, a negative interference is present in the off-shell regime between the EW signal background components. The LO Feynman diagrams for the production of EW $qq \to ZZ + 2j \to 4\ell + 2j$ are shown in figure 2.

The scaling of the cross-sections with the effective couplings $g_g$ and $g_V$ defines uniquely each component (signal, interference, and background) in the ggF and EW production of off-shell Higgs bosons. The probability density model used to measure the off-shell Higgs boson production is defined as function of the coupling modifiers $\kappa_g = g_g/g_{g,\mathrm{SM}}$ and $\kappa_V = g_V/g_{V,\mathrm{SM}}$, independently of the Higgs boson virtuality, which are used to define the signal strengths:

$$\mu^{\mathrm{ggF}}_{\text{off-shell}} = \kappa^2_{g,\text{off-shell}}\kappa^2_{V,\text{off-shell}}, \qquad \mu^{\mathrm{EW}}_{\text{off-shell}} = \kappa^4_{V,\text{off-shell}}, \quad (2)$$

where the subscript *off-shell* indicates that the modifier only affects processes with virtuality sufficiently above the pole mass. These signal strengths are used in the definition of a probability density model that is used to interpret the collected data:

$$\begin{aligned} p\left(x|\mu^{\mathrm{ggF}}_{\text{off-shell}}, \mu^{\mathrm{EW}}_{\text{off-shell}}\right) = & \frac{1}{\nu\left(\mu^{\mathrm{ggF}}_{\text{off-shell}}, \mu^{\mathrm{EW}}_{\text{off-shell}}\right)} \\ & \times \Bigg[\mu^{\mathrm{ggF}}_{\text{off-shell}}\nu^{\mathrm{ggF}}_{\mathrm{S}} p^{\mathrm{ggF}}_{\mathrm{S}}(x) \\ & + \sqrt{\mu^{\mathrm{ggF}}_{\text{off-shell}}}\nu^{\mathrm{ggF}}_{\mathrm{I}} p^{\mathrm{ggF}}_{\mathrm{I}}(x) \\ & + \nu^{\mathrm{ggF}}_{\mathrm{B}} p^{\mathrm{ggF}}_{\mathrm{B}}(x) + \mu^{\mathrm{EW}}_{\text{off-shell}}\nu^{\mathrm{EW}}_{\mathrm{S}} p^{\mathrm{EW}}_{\mathrm{S}}(x) \\ & + \sqrt{\mu^{\mathrm{EW}}_{\text{off-shell}}}\nu^{\mathrm{EW}}_{\mathrm{I}} p^{\mathrm{EW}}_{\mathrm{I}}(x) \\ & + \nu^{\mathrm{EW}}_{\mathrm{B}} p^{\mathrm{EW}}_{\mathrm{B}}(x) + \nu_{\mathrm{NI}} p_{\mathrm{NI}}(x)\Bigg], \end{aligned} \quad (3)$$

where $x$ is a vector of reconstructed observables, which are defined in section 5.2, and where $p_{\mathrm{X}}(x)$ and $\nu_{\mathrm{X}}$ are the probability density function and the expected yield for process X, respectively. The expected number of events $\nu(\mu^{\mathrm{ggF}}_{\text{off-shell}}, \mu^{\mathrm{EW}}_{\text{off-shell}})$ can be written as a function of the expected number of events $\nu_{\mathrm{X}}$ for each process. The term $p_{\mathrm{NI}}(x)$ represents the probability density for processes that do not interfere with the ggF and EW processes described above. The leading non-interfering process is $q\bar{q} \to ZZ \to 4\ell$ production via a $t$-channel exchange at LO. Non-interfering triboson $VVV$ processes, including those from top-quark decays $t\bar{t}V$, are subleading processes, but are also included in the analysis. The exception is the interfering $ZZZ \to 4\ell + \text{jets}$ process, which is modeled as part of the EW B process. Figure 3(a) shows the LO Feynman diagram of the leading non-interfering $q\bar{q} \to ZZ$ process ($q\bar{q}ZZ$) and figure 3(b) shows the corresponding LO Feynman diagram of the subleading non-interfering top-quark-induced $VVV$ process.

Monte Carlo (MC) simulated samples are used to describe the expected event yields $\nu_{\mathrm{X}}$ and probability densities $p_{\mathrm{X}}(x)$ in equation (3). Due to the technical challenges associated with the efficient production of interference-only MC simulations [47], the interference terms in equation (3) are not generated separately, but inferred from samples generated with signal, interference, and background terms (SBI sample, where SBI = S + I + B). For ggF production, a single SBI sample is generated and the interference term $\nu^{\mathrm{ggF}}_{I} p^{\mathrm{ggF}}_{I}(x)$ is calculated as the difference of the SBI sample and the S and B samples (I = SBI − S + B):

$$\nu^{\mathrm{ggF}}_{\mathrm{I}} p^{\mathrm{ggF}}_{\mathrm{I}}(x) = \nu^{\mathrm{ggF}}_{\mathrm{SBI}} p^{\mathrm{ggF}}_{\mathrm{SBI}}(x) - \nu^{\mathrm{ggF}}_{\mathrm{S}} p^{\mathrm{ggF}}_{\mathrm{S}}(x) - \nu^{\mathrm{ggF}}_{\mathrm{B}} p^{\mathrm{ggF}}_{\mathrm{B}}(x). \quad (4)$$

In the simulation of EW production, it is impossible to generate an off-shell signal-only sample. Due to the diagram shown in figure 2(b), where an $s$-channel Higgs boson propagator is absent, and in figure 2(c), where the Higgs boson can decay as $H^* \to ZZ \to 2\ell 2q$, there is always contamination of on-shell events. Any on-shell contamination is formally part of the EW background process, since it does not scale with $\mu_{\text{off-shell}}$. Instead of generating pure signal and interference

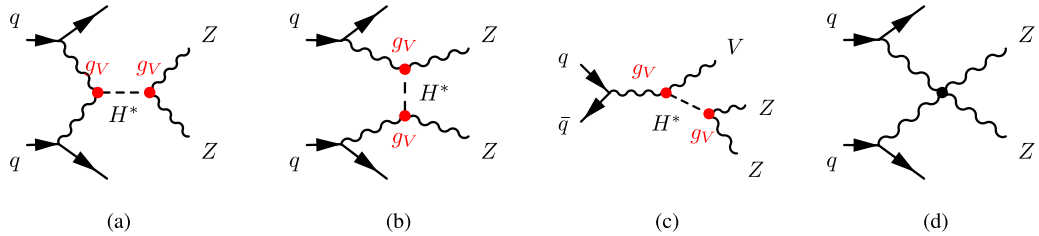


**Figure 2.** Illustrative leading-order Feynman diagrams for the electroweak $qq \to ZZ + 2j$ processes. The diagrams indicate the effective couplings $g_V$ used to define the off-shell Higgs boson production signal strengths. Diagrams (a)–(c) correspond to the vector boson fusion, $t$-channel and $VH$ signal components, respectively. In diagram (c), one of the vector bosons decays into a $q\bar{q}$ pair. Diagram (d) corresponds to the electroweak background component. A large destructive interference is present in the off-shell regime between the vector boson fusion signal and the background components.

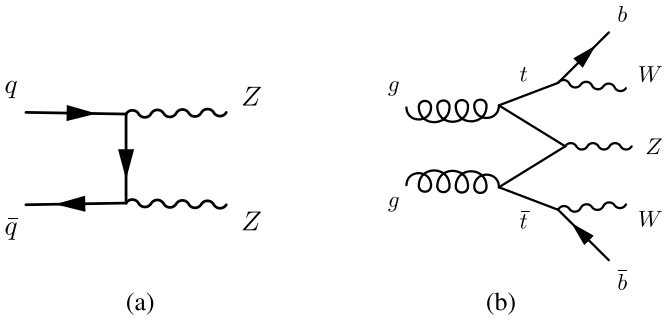


**Figure 3.** Illustrative leading-order Feynman diagrams for non-interfering background processes. Diagram (a) shows the leading $q\bar{q}ZZ$ process and diagram (b) shows the top-quark induced sub-leading $VVV$ process. The leptonic decays of the $Z$ and $W$ bosons are not shown.

samples, two linear combinations ($\mathrm{EWSBI}_1$ and $\mathrm{EWSBI}_{10}$) are used to model the EW processes:

$$\nu^{\mathrm{EW}}_{\mathrm{SBI}_1} p^{\mathrm{EW}}_{\mathrm{SBI}_1}(x) = \nu^{\mathrm{EW}}_{\mathrm{S}} p^{\mathrm{EW}}_{\mathrm{S}}(x) + \nu^{\mathrm{EW}}_{\mathrm{I}} p^{\mathrm{EW}}_{\mathrm{I}}(x) + \nu^{\mathrm{EW}}_{\mathrm{B}} p^{\mathrm{EW}}_{\mathrm{B}}(x),$$
$$\nu^{\mathrm{EW}}_{\mathrm{SBI}_{10}} p^{\mathrm{EW}}_{\mathrm{SBI}_{10}}(x) = 10\nu^{\mathrm{EW}}_{\mathrm{S}} p^{\mathrm{EW}}_{\mathrm{S}}(x) + \sqrt{10}\nu^{\mathrm{EW}}_{\mathrm{I}} p^{\mathrm{EW}}_{\mathrm{I}}(x) + \nu^{\mathrm{EW}}_{\mathrm{B}} p^{\mathrm{EW}}_{\mathrm{B}}(x). \quad (5)$$

These samples contain the signal, interference, and background components, including any possible on-shell contamination, albeit with different fractions. An additional sample is generated exclusively modeling the diagram in figure 2(d) to describe the EW B process $\nu^{\mathrm{EW}}_{\mathrm{B}} p^{\mathrm{EW}}_{\mathrm{B}}(x)$. While this sample does not contain the on-shell contamination from diagrams figures 2(b) and (c) discussed above, it was found that considering the contribution of these terms only in $\mathrm{EWSBI}_1$ and $\mathrm{EWSBI}_{10}$ is a good approximation.

The EW $\mathrm{SBI}_{10}$ sample is simulated by choosing the effective coupling between the Higgs boson and the EW vector bosons to achieve an EW signal cross-section ten times larger than the SM value ($\kappa_V^4 = 10$). The change of the effective coupling scales the interference component by a factor $\sqrt{10}$, yielding the expression in equation (5). When simulating the EW $\mathrm{SBI}_{10}$ sample, the Higgs boson width is modified to keep the on-shell effective coupling unchanged at $g_V^4/\Gamma_H$. Linear combinations of the EW B, EW $\mathrm{SBI}_1$, and EW $\mathrm{SBI}_{10}$ samples can be inverted to obtain the EW signal, interference and background processes separately, as shown in table 1.

As described earlier, the non-interfering background process $\nu_{\mathrm{NI}} p_{\mathrm{NI}}(x)$ in equation (3) contains both the leading $q\bar{q}ZZ$ and the subleading $VVV$ processes:

$$\nu_{\mathrm{NI}} p_{\mathrm{NI}}(x) = \nu_{q\bar{q}ZZ} p_{q\bar{q}ZZ}(x) + \nu_{VVV} p_{VVV}(x). \quad (6)$$

All $VVV$ processes are considered separately as a single non-interfering background process, except for the $ZZZ \to 4\ell +$ jets sample is modeled as part of the EW background process.

A data-driven normalization is introduced for the leading $q\bar{q} \to ZZ$ process as a function of the number of reconstructed jets, which is one of the observables in the vector $x$ defined in section 5.2:

$$\nu_{\mathrm{NI}} p_{\mathrm{NI}}(x) = \theta^{\mathrm{incl}}_{q\bar{q}ZZ} \nu^{0j}_{q\bar{q}ZZ} p^{0j}_{q\bar{q}ZZ}(x) + \theta^{\mathrm{incl}}_{q\bar{q}ZZ} \theta^{1j}_{q\bar{q}ZZ} \nu^{1j}_{q\bar{q}ZZ} p^{1j}_{q\bar{q}ZZ}(x) + \theta^{\mathrm{incl}}_{q\bar{q}ZZ} \theta^{1j}_{q\bar{q}ZZ} \theta^{2j}_{q\bar{q}ZZ} \nu^{2j}_{q\bar{q}ZZ} p^{2j}_{q\bar{q}ZZ}(x) + \nu_{VVV} p_{VVV}(x). \quad (7)$$

The parameter $\theta^{\mathrm{incl}}_{q\bar{q}ZZ}$ provides a data-driven normalization for the total $q\bar{q} \to ZZ \to 4\ell$ observed yield. The parameter $\theta^{1j}_{q\bar{q}ZZ}$ ($\theta^{2j}_{q\bar{q}ZZ}$) provides a data-driven normalization for the ratio of the observed yield of $q\bar{q} \to ZZ \to 4\ell$ events with one (at least two) reconstructed jet and that with zero (one) reconstructed jets. The process referred to as $\nu^{2j}_{q\bar{q}ZZ} p^{2j}_{q\bar{q}ZZ}(x)$ includes all events with at least two reconstructed jets.

Table 1 summarizes the processes that are used in the model after all transformations, as well as the simulated samples used to describe them.

## 4. Data and simulated event samples

The analysis uses $pp$ collision data collected with the ATLAS detector in Run 2 of the LHC, at a center-of-mass energy of $\sqrt{s} = 13\,\mathrm{TeV}$, corresponding to a total integrated luminosity of $140\,\mathrm{fb}^{-1}$ [48] after data-quality requirements [49]. Events were recorded using a combination of single-lepton, dilepton and trilepton triggers [50–52] with either a low transverse momentum, $p_{\mathrm{T}}$, threshold and a lepton isolation requirement, or a higher threshold but a looser identification criterion and without any isolation requirement. The overall trigger efficiency for the ggF signal process is more than 98% in

**Table 1.** Definition of processes in the probability model used to interpret the data and the simulated samples used to describe them. The multipliers define both the measured off-shell Higgs boson production signal strength and the data-driven normalization of leading backgrounds. The $(H^* \to)$ notation is used for the SBI process. The multipliers are obtained after substituting the interference terms of equations (4) and (5) into equation (3), since interference-only samples are not simulated. For instance, in the case of ggF production: $\mu\nu_{\mathrm{S}} + \sqrt{\mu}\nu_{\mathrm{I}} + \nu_{\mathrm{B}} = (\mu - \sqrt{\mu})\nu_{\mathrm{S}} + \sqrt{\mu}(\nu_{\mathrm{S}} + \nu_{\mathrm{I}} + \nu_{\mathrm{B}}) + (1 - \sqrt{\mu})\nu_{\mathrm{B}}$.

| Process | Multipliers | Samples |
|---|---|---|
| ggF S | $\mu^{\mathrm{ggF}}_{\text{off-shell}} - \sqrt{\mu^{\mathrm{ggF}}_{\text{off-shell}}}$ | $gg \to H^* \to ZZ \to 4\ell$ |
| ggF SBI | $\sqrt{\mu^{\mathrm{ggF}}_{\text{off-shell}}}$ | $gg \to (H^* \to)ZZ \to 4\ell$<br>$(\kappa_V^2 = 1)$ |
| ggF B | $1 - \sqrt{\mu^{\mathrm{ggF}}_{\text{off-shell}}}$ | $gg \to ZZ \to 4\ell$<br>$(\kappa_V^2 = 0)$ |
| EW B | $\dfrac{(1-\sqrt{10})\mu^{\mathrm{EW}}_{\text{off-shell}} + 9\sqrt{\mu^{\mathrm{EW}}_{\text{off-shell}}} - 10 + \sqrt{10}}{-10+\sqrt{10}}$ | EW $qq \to ZZ + 2j \to 4\ell + 2j$<br>$(\kappa_V^4 = 0)$<br>$ZZZ \to 4\ell + 2j$ |
| EW $\mathrm{SBI}_1$ | $\dfrac{\sqrt{10}\mu^{\mathrm{EW}}_{\text{off-shell}} - 10\sqrt{\mu^{\mathrm{EW}}_{\text{off-shell}}}}{-10+\sqrt{10}}$ | EW $qq \to (H^* \to)ZZ + 2j \to 4\ell + 2j$<br>$(\kappa_V^4 = 1)$<br>$ZZZ \to 4\ell + 2j$ |
| EW $\mathrm{SBI}_{10}$ | $\dfrac{-\mu^{\mathrm{EW}}_{\text{off-shell}} + \sqrt{\mu^{\mathrm{EW}}_{\text{off-shell}}}}{-10+\sqrt{10}}$ | EW $qq \to (H^* \to)ZZ + 2j \to 4\ell + 2j$<br>$(\kappa_V^4 = 10)$<br>$ZZZ \to 4\ell + 2j$ |
| $q\bar{q}ZZ\ n_{\mathrm{jets}} = 0$ | $\theta^{\mathrm{incl}}_{q\bar{q}ZZ}$ | $q\bar{q} \to ZZ \to 4\ell$ |
| $q\bar{q}ZZ\ n_{\mathrm{jets}} = 1$ | $\theta^{\mathrm{incl}}_{q\bar{q}ZZ}\theta^{1j}_{q\bar{q}ZZ}$ | $q\bar{q} \to ZZ \to 4\ell$ |
| $q\bar{q}ZZ\ n_{\mathrm{jets}} \geqslant 2$ | $\theta^{\mathrm{incl}}_{q\bar{q}ZZ}\theta^{1j}_{q\bar{q}ZZ}\theta^{2j}_{q\bar{q}ZZ}$ | $q\bar{q} \to ZZ \to 4\ell$ |
| $VVV$ | — | $WWZ \to 4\ell$<br>$WZZ \to 4\ell$<br>$t\bar{t}Z \to 4\ell$ |

each final state after object selection and after imposing the $180 < m_{4\ell} < 2000\,\mathrm{GeV}$ requirement.

The $gg \to ZZ \to 4\ell$ samples (ggF S, ggF B, and ggF SBI) are generated with Sherpa v2.2.2 [53] and OpenLoops [54–56] at LO accuracy in quantum chromodynamics (QCD), with up to one additional parton in the final state, using the NNPDF3.0 NNLO parton distribution function (PDF) set [57]. The merging with the parton shower was performed using the MEPS@NLO prescription [58, 59] and the Sherpa built-in algorithm was used for parton showering and hadronization. Next-to-leading-order (NLO) QCD corrections are included as a function of the invariant mass of the two $Z$ bosons, $m_{ZZ}$, separately for the ggF B, S, and SBI processes [60]. Fully differential next-to-next-to-leading-order (NNLO) corrections to the $gg \to H \to ZZ$ signal process are known [61–63], but not for the interference and background components. A common, average NNLO/NLO correction of 1.2 is applied to the signal, interference, and background components of the $gg \to ZZ$ process. Inclusive next-to-next-to-next-to-leading-order ($\mathrm{N^3LO}$) corrections to the $gg \to H \to ZZ$ signal process are known [64], dominated by the on-shell Higgs boson contribution. Currently, $\mathrm{N^3LO}$ corrections in the off-shell region and for the interference and background components are not available. An average, common $\mathrm{N^3LO/NNLO}$ correction of 1.1 is extrapolated to the off-shell region and applied to the signal, interference, and background components of the $gg \to ZZ$ process [65].

The EW $qq \to ZZ + 2j \to 4\ell + 2j$ samples (EW B, EW $\mathrm{SBI}_1$, and EW $\mathrm{SBI}_{10}$) are generated with MadGraph5_aMC@NLO [66] at LO QCD and LO EW accuracy using the NNPDF3.0 NLO PDF set [57]. The Pythia 8.2 [67] program was used for parton showering and hadronization with the A14 set of tuned parameters (A14 tune) for the underlying event [68] and NNPDF2.3 LO PDF set [69].

The $q\bar{q} \to ZZ$ sample is generated with Sherpa v2.2.2 and OpenLoops using the NNPDF3.0 NNLO PDF set. The matrix elements (ME) are calculated to NLO accuracy in QCD for 0- and 1-jet final states, and to LO accuracy for 2- and 3-jet final states. The merging with the Sherpa parton shower was performed using the MEPS@NLO prescription. The NLO EW corrections are included as a function of $m_{ZZ}$ [70, 71].

The triboson samples $ZZZ$, $WZZ$, and $WWZ$ with fully leptonic decays were modeled with Sherpa v2.2.2 at NLO QCD accuracy. The $ZZZ \to 4\ell + 2j$ process is included in the EW $q\bar{q} \to ZZ + 2j$ sample described above. The simulation of $t\bar{t}V$ production with at least one of the top quarks decaying leptonically and the vector boson decaying inclusively into either quarks or leptons was performed with

**Table 2.** Matrix element generator, parton shower (PS), and higher-order corrections used to describe the different samples in the measurement. The notation $[Xj]$ indicates that up to $X$ jets are included in the hard-scatter matrix element calculation.

| Sample | ME generator | PS | Higher-order correction |
|---|---|---|---|
| $gg \to ZZ$ | SHERPA 2.2.2<br>(LO [1j]) | SHERPA 2.2.2 | NLO QCD ($m_{ZZ}$ dependent) [60]<br>Approx. NNLO QCD (global) [61–63]<br>Approx. N3LO QCD (global) [65] |
| EW $q\bar{q} \to ZZ + 2j$ | MG5_AMC@NLO 2.3.3 | PYTHIA 8.244 | — |
| $q\bar{q} \to ZZ$ | SHERPA 2.2.2<br>(NLO [1j], LO [3j]) | SHERPA 2.2.2 | NLO EW ($m_{ZZ}$ dependent) [70, 71] |
| $WWZ$, $WZZ$, $ZZZ$ | SHERPA 2.2.2 | SHERPA 2.2.2 | — |
| $t\bar{t}$ Z | MG5_AMC@NLO 2.3.3 | PYTHIA 8.210 | NLO QCD + NLO EW (global) [72] |

MADGRAPH5_AMC@NLO interfaced to PYTHIA 8.2 for parton showering and hadronization with the A14 tune. The total cross-sections for the $t\bar{t}V$ backgrounds were normalized to the NLO QCD and EW predictions from [72].

Table 2 summarizes the order in perturbation theory with which each simulated sample was generated and the source of higher-order correction ($K$-factors) used to improve the modeling. All simulated samples are processed with the ATLAS detector simulation [73] based on GEANT4 [74]. The effects of multiple inelastic interactions in the same and neighboring bunch crossings (pileup) were modeled by overlaying each simulated hard-scattering event with inelastic $pp$ events generated with PYTHIA 8.186 [75] using the NNPDF2.3 LO PDF set and the A3 tune [76]. Simulated events are reweighted to match the pileup conditions observed in the full Run 2 dataset. Simulated events are reconstructed with the same algorithms and analysis chain as the data.

## 5. Object reconstruction, event selection and description

The measurement of the off-shell Higgs boson production is performed in the $H^* \to ZZ \to 4\ell$ decay channel, where $\ell$ is either an electron or a muon. The object and event selections aim to identify opposite-charged electron or muon pairs consistent with the decay of a $Z$ boson. A quadruplet is formed from two pairs with a common production vertex and invariant mass above the $ZZ$ threshold. The selection criteria are optimized to increase the acceptance of $H^* \to ZZ \to 4\ell$ events while maintaining negligible levels of non-prompt background events. The object and event reconstruction used in this analysis is exactly the same as in the previous result [17] and only a short summary is provided here.

### 5.1. Object reconstruction

Muons are identified by tracks or segments reconstructed in the MS and matched to tracks reconstructed in the ID, with exceptions in areas where the MS lacks coverage. In the region $2.5 < |\eta| < 2.7$, muons can also be identified by tracks from the MS alone. In the central gap region ($|\eta| < 0.1$) of the MS, muons can be identified by a track from the ID associated with a compatible calorimeter energy deposit (calorimeter-tagged muons). Candidate muons are required to have $p_T > 5$ GeV and $|\eta| < 2.7$, except calorimeter-tagged muons for which the $p_T$ threshold is raised to 15 GeV. Muons must satisfy the *loose* identification criterion [77] with at most one standalone or calorimeter-tagged muon allowed per Higgs boson candidate. Electrons are reconstructed from energy deposits in the electromagnetic calorimeter matched to a track in the ID. Candidate electrons must have $p_T > 7$ GeV and $|\eta| < 2.47$, and satisfy the *loose* identification criteria [78].

All electrons and muons used in both channels must be isolated, satisfying a *loose* isolation criteria [77, 78]. Furthermore, electrons (muons) are required to have associated tracks satisfying $|d_0/\sigma_{d_0}| < 5$ (3) and $|z_0 \sin\theta| < 0.5$ mm, where $d_0$ is the transverse impact parameter relative to the beam line, $\sigma_{d_0}$ is its uncertainty, and $z_0$ is the $z$ coordinate of the $r$-$\phi$ impact point, defined relative to the primary vertex. The event is rejected if the minimum angular separation between two leptons is $dR_{\ell\ell} < 0.1$, where $dR_{\ell\ell} = \sqrt{(\Delta\phi_{\ell\ell})^2 + (\Delta\eta_{\ell\ell})^2}$.

Jets are reconstructed from particle-flow objects [79] using the anti-$k_t$ algorithm [80, 81] with radius parameter $R = 0.4$. The jet-energy scale is calibrated using simulation and further corrected with *in situ* methods [82]. Reconstructed jets are required to have $p_T > 30$ GeV and $|\eta| < 4.5$. A jet-vertex tagger [83] is applied to jets with $p_T < 60$ GeV and $|\eta| < 2.4$ to suppress jets that originate from pileup. In the forward region, for jets with $p_T < 50$ GeV and $2.5 < |\eta| < 4.5$, another tagger based on jet shapes and topological jet correlations [84] is used to suppress pileup jets.

### 5.2. Event selection and description

The selection of candidate events follows that described in [17]. Events with at least four leptons (electrons or muons) are used in this analysis. The $p_T$ thresholds for the three leading leptons are 20, 15 and 10 GeV, respectively. The four-lepton invariant mass is required to be above the on-shell $ZZ$ production threshold, $180 < m_{4\ell} < 2000$ GeV. Candidate lepton quadruplets are formed by selecting two opposite-charge, same-flavor dilepton pairs in each event. In the 4e and $4\mu$ channels, in which there are two possible pairings, the one that includes the lepton pair with mass closest to that of

**Table 3.** Definition of the observables to describe an event. The observables are defined relative to the ATLAS coordinate system. The vectors $\mathbf{q}_1$, $\mathbf{q}_2$, $\mathbf{q}_{11}$, $\mathbf{q}_{21}$, $\mathbf{n}_1$, $\mathbf{n}_2$, and $\mathbf{n}_{sc}$ are defined in section 5.2.

| Variable | Definition |
|---|---|
| $m_{4\ell}$ | quadruplet mass |
| $m_{Z_1}$ | $Z_1$ mass |
| $m_{Z_2}$ | $Z_2$ mass |
| $\cos\theta^*$ | cosine of the Higgs boson decay angle $[\mathbf{q}_1 \cdot \mathbf{n}_z/\lvert\mathbf{q}_1\rvert]$ |
| $\cos\theta_1$ | cosine of the $Z_1$ decay angle $[-(\mathbf{q}_2)\cdot\mathbf{q}_{11}/(\lvert\mathbf{q}_2\rvert\cdot\lvert\mathbf{q}_{11}\rvert)]$ |
| $\cos\theta_2$ | cosine of the $Z_2$ decay angle $[-(\mathbf{q}_1)\cdot\mathbf{q}_{21}/(\lvert\mathbf{q}_1\rvert\cdot\lvert\mathbf{q}_{21}\rvert)]$ |
| $\Phi_1$ | $Z_1$ decay plane angle $[\cos^{-1}(\mathbf{n}_1\cdot\mathbf{n}_{sc})\,(\mathbf{q}_1\cdot(\mathbf{n}_1\times\mathbf{n}_{sc})/(\lvert\mathbf{q}_1\rvert\cdot\lvert\mathbf{n}_1\times\mathbf{n}_{sc}\rvert)]$ |
| $\Phi$ | angle between $Z_1, Z_2$ decay planes $[\cos^{-1}(\mathbf{n}_1\cdot\mathbf{n}_2)\,(\mathbf{q}_1\cdot(\mathbf{n}_1\times\mathbf{n}_2)/(\lvert\mathbf{q}_1\rvert\cdot\lvert\mathbf{n}_1\times\mathbf{n}_2\rvert)]$ |
| $p_T^{4\ell}$ | quadruplet transverse momentum |
| $y^{4\ell}$ | quadruplet rapidity |
| $n_{\text{jets}}$ | number of jets in the event |
| $m_{jj}$ | leading dijet system mass |
| $\Delta\eta_{jj}$ | leading dijet system pseudorapidity |
| $\Delta\phi_{jj}$ | leading dijet system azimuthal angle difference |

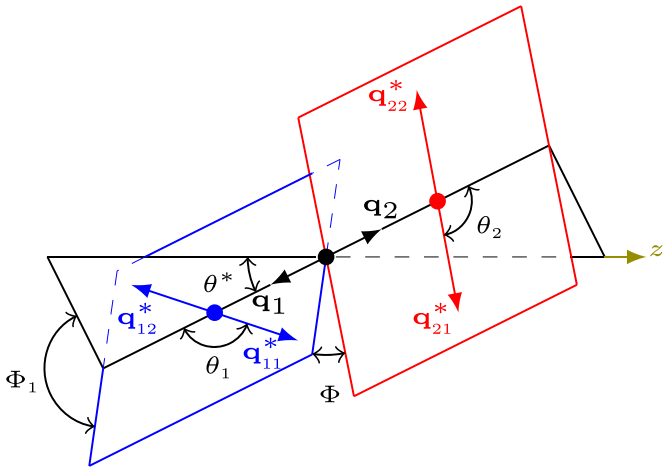


**Figure 4.** Representation of the angular observables used to describe the probability density ratio of each event. The three-momenta of the fermions ($\mathbf{q}_{11}^*$, $\mathbf{q}_{21}^*$) and anti-fermions ($\mathbf{q}_{12}^*$, $\mathbf{q}_{22}^*$) are shown in their parent rest-frames, and the three-momenta of the vector bosons ($\mathbf{q}_1$, $\mathbf{q}_2$) are shown in the quadruplet rest frame.

the $Z$ boson mass is chosen. In each quadruplet, the lepton pair with mass closest to the $Z$ boson mass, $m_{Z_1}$, is referred to as the leading pair and required to have $50 < m_{Z_1} < 106$ GeV. The sub-leading pair mass, $m_{Z_2}$, must satisfy $50 < m_{Z_2} < 115$ GeV when $m_{4\ell} > 190$ GeV. Due to the increased probability of one $Z$ boson being off-shell at lower values of $m_{4\ell}$, the lower threshold for $m_{Z_2}$ decreases linearly from 50 GeV at $m_{4\ell} = 190$ GeV to 45 GeV at $m_{4\ell} = 180$ GeV.

Events are described in the analysis by 14 observables, summarized in table 3. The 14 observables provide a complete description of the reconstructed final state phase space. The three-momentum of the fermion (anti-fermion) in the $Z_1$ decay is defined as $\mathbf{q}_{11}$ ($\mathbf{q}_{12}$). Similarly, the three-momentum of the fermion (anti-fermion) in the $Z_2$ decay is defined as $\mathbf{q}_{21}$ ($\mathbf{q}_{22}$). The three-momentum of $Z_1$ ($Z_2$) is defined as $\mathbf{q}_1$ ($\mathbf{q}_2$). All three-momenta are defined in the rest frame of the quadruplet. Jets are ordered in $p_T$ and their momenta are defined in the laboratory reference frame.

The observables in table 3 are the components of the vector $x$ in equation (3). The observables $m_{jj}$, $\eta_{jj}$, and $\phi_{jj}$ related to the leading dijet system, i.e. the two jets with highest $p_T$ in the event, are only well-defined for events with at least two jets. For events with fewer jets, the value of these observables are chosen as the median of the corresponding distribution for events with at least two jets. The observable $n_{\text{jets}}$ is used for classification of the non-interfering background in equation (7), where all events with more than two jets are described by $n_{\text{jets}} = 2$.

The normal vectors $\mathbf{n}_1$ and $\mathbf{n}_2$ to the $Z_1$ and $Z_2$ decay planes and the normal vector $\mathbf{n}_{sc}$ to the Higgs boson decay plane are defined as:

$$\mathbf{n}_1 = \frac{\mathbf{q}_{11}\times\mathbf{q}_{12}}{\lvert\mathbf{q}_{11}\times\mathbf{q}_{12}\rvert}, \qquad \mathbf{n}_2 = \frac{\mathbf{q}_{21}\times\mathbf{q}_{22}}{\lvert\mathbf{q}_{21}\times\mathbf{q}_{22}\rvert}, \qquad \mathbf{n}_{sc} = \frac{\mathbf{n}_z\times\mathbf{q}_1}{\lvert\mathbf{n}_z\times\mathbf{q}_1\rvert}, \tag{8}$$

where $\mathbf{n}_z$ is the unit vector in the $z$ direction. These vectors are used to build angles that are sensitive to the spin and parity of the quadruplet. Their geometrical visualization [85] is given in figure 4, where the three-momenta are shown in the rest frame of each particle's parent for clarity. Figure 5 shows the comparison between observed and expected background distributions for the $m_{4\ell}$ and $m_{jj}$ observables showing good agreement for two of the observables used in the analysis.

## 6. Neural simulation-based inference

Several analyses at the LHC use multinomial probability densities (histograms) of a single observable to describe each component $p_X(x)$ of the probability model used to interpret the data. A commonly used framework for histogram-based analyses in ATLAS is described in detail in [86] and was used in the previous result on the off-shell Higgs boson production [17]. In analyses with non-linear signal models, like the measurements of processes with large quantum interference, a single observable cannot optimally capture the information needed to measure all possible signal strength values and complete dimensional reduction cannot be achieved without information loss. In addition, the multinomial modeling treats all events inside a bin as indistinguishable, which leads to a loss in statistical power. These losses can be partially mitigated by using approximations to optimal observables [27], by increasing the dimensionality of the histograms, and by reducing the bin width. Recent measurements of the off-shell Higgs boson production in the $H^* \to ZZ \to 4\ell$ channel by the CMS Collaboration [32] have used all of these strategies to improve the significance of the result.

These mitigation strategies are limited by the finite number of simulated events and by the so-called curse of dimensionality. Practical considerations may reduce the accuracy of the multinomial approximation and reduce the power of

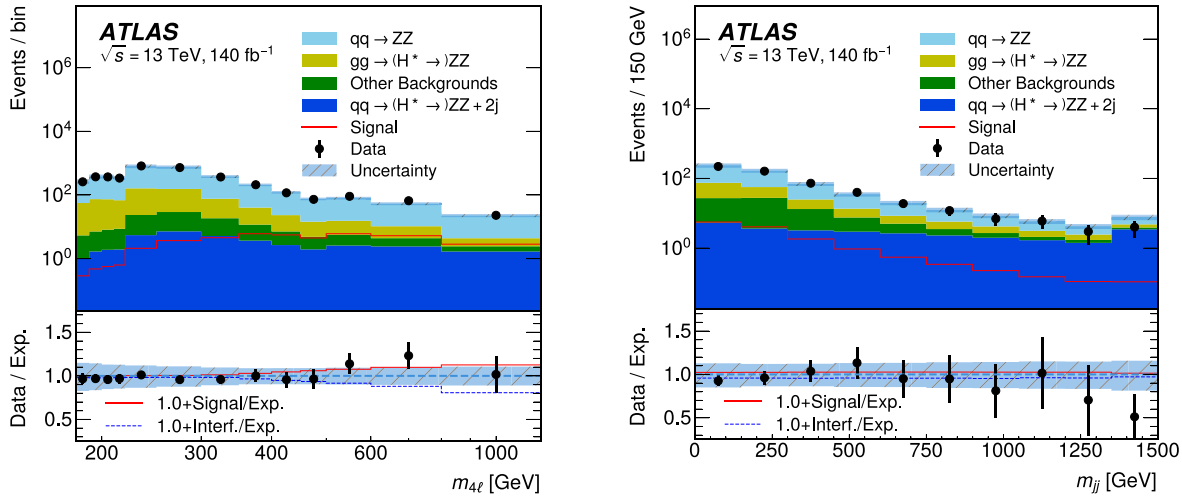


(a) (b)

**Figure 5.** Comparison between observed and expected distribution of two observables used to describe events: (a) the four-lepton invariant mass and the (b) invariant mass of the two leading jets showing good agreement for two of the observables used in this analysis. The expected distributions for $q\bar{q} \to ZZ$, ggF SBI ($gg \to (H^* \to)ZZ$), EW SBI$_1$ ($qq \to (H^* \to)ZZ + 2j$) and other backgrounds are shown as stacked histograms, and the expected signal (interference) is shown as a red solid (blue dashed) line. The background is estimated under the SM hypothesis (post-fit, $\mu_{\text{off-shell}} = 1$). The lower panels show the ratio of data to expectation. The hatched band shows the total systematic uncertainty in the expected distribution. The last bin contains overflow events.

the statistical inference, especially in regions with high signal significance (signal regions). Regions with low signal significance (control regions (CRs)), traditionally used for the description of backgrounds and systematic uncertainties, are less sensitive to these limitations.

NN approximations of probability densities and probability density ratios can outperform histogram approximations when high-dimensional parameter spaces are considered. The use of NNs for statistical inference is known as *NSBI* [27–30]. This analysis uses a particular version of NSBI adapted to the type of parameter inference done at the LHC to model events in the signal region. A self-contained description of the method is given below, and more details can be found in [31].

### 6.1. Signal and control regions

An initial multi-class classification NN is trained to split the events into signal and CRs using the observables defined in table 3. This NN has five hidden layers each with 1 000 neurons and a *swish* activation function [87]. The output layer has five neurons with a *softmax* $[e^{-x_i}/\sum_j e^{-x_j}]$ activation function. The NN is trained with a multi-class cross-entropy loss corresponding to the five processes used in the training: ggF S, ggF B, VBF, EW B, and $q\bar{q} \to ZZ$. The vector boson fusion (VBF) process is obtained from a dedicated MC sample that uses only the EW VBF diagram in figure 2(a). While this process does not provide a full description of the EW S production of off-shell Higgs bosons, it provides a sufficiently good approximation to define control and signal regions. The preselection discriminant $D_{\text{pre}}(x)$ is defined as:

$$D_{\text{pre}}(x) = \log \frac{s_{\text{pre}}^{\text{ggF S}}(x) + s_{\text{pre}}^{\text{VBF}}(x)}{s_{\text{pre}}^{\text{ggF B}}(x) + s_{\text{pre}}^{\text{EW B}}(x) + s_{\text{pre}}^{q\bar{q}ZZ}(x)}, \tag{9}$$

where $s(x)$ denotes the score function of the NN. The signal region (SR) is defined as events satisfying $D_{\text{pre}}(x) > -0.85$. Events failing this condition define the CR. The CR is largely dominated by $q\bar{q} \to ZZ$ events and can be used to constrain the parameters $\theta_{q\bar{q}ZZ}^{0j,1j,2j}$ in equation (7). Figure 6 shows a comparison between the observed and expected distribution of the observable $D_{\text{pre}}(x)$ used to define the SR and the CR indicating a good description of the acceptance times efficiency in each region. Figure 6(b) depicts a comparison of the observed and expected $n_{\text{jets}}$ distribution, showing a good description of the normalization obtained in each bin with the data-driven background normalization parameters.

In the CR, only the $n_{\text{jets}}$ observable is used to describe the probability model, while in the SR all 14 observables listed in table 3 are used to create an NSBI model. For the NSBI model, a probability density ratio is formed from each process X (where X is one of the processes in table 1) and a fixed reference process, $p_{\text{X}}(x)/p_{\text{ref}}(x)$, and each ratio is estimated with a separate NN. The reference process is chosen as a mixture of the ggF signal and EW SBI$_{10}$ processes:

$$\nu_{\text{ref}} p_{\text{ref}}(x) = \nu_{\text{S}}^{\text{ggF}} p_{\text{S}}^{\text{ggF}}(x) + \nu_{\text{SBI}_{10}}^{\text{EW}} p_{\text{SBI}_{10}}^{\text{EW}}(x), \tag{10}$$

and does not depend on any parameter. While machine learning methods exist that allow to directly estimate the probability densities $p_{\text{X}}(x)$ [88] in equation (3), the estimation of probability density ratios [89] is a simpler numerical problem and is used in this analysis. As shown in section 7, estimating these probability density ratios for the different hypotheses is sufficient for a frequentist statistical data analysis [90], as $p_{\text{ref}}(x)$ cancels out in the likelihood ratio test statistic. The choice of reference sample is driven by the phase space where the method is applied [31]. The density ratio $p_{\text{X}}(x)/p_{\text{ref}}(x)$ can only reliably be estimated when $p_{\text{ref}}(x) > 0$, which is ensured

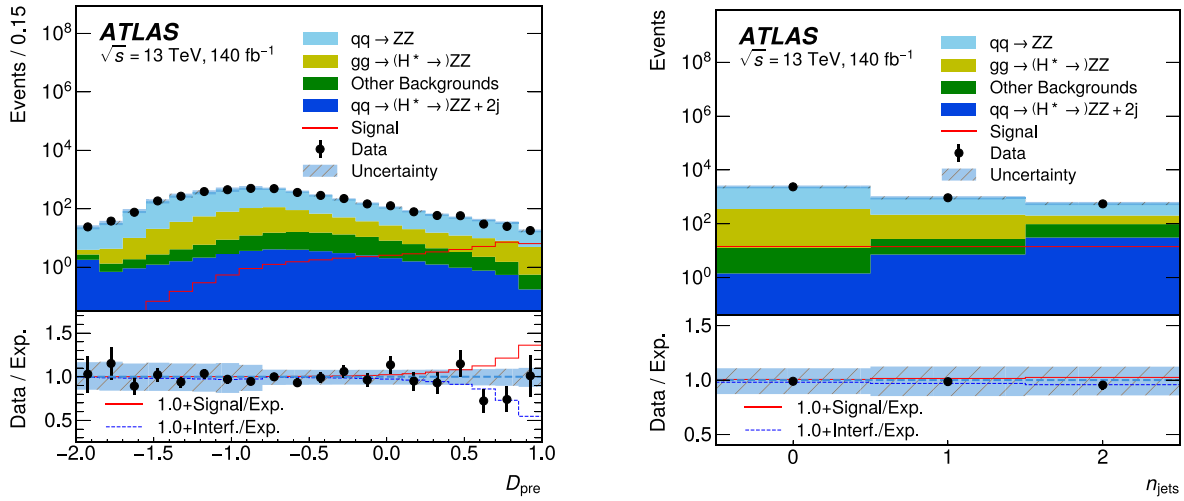


(a) (b)

**Figure 6.** (a) Comparison between observed and expected distribution of the preselection discriminant $D_{\text{pre}}(x)$ showing a good description of the acceptance times efficiency in each region. (b) Comparison between observed and expected distribution of $n_{\text{jets}}$ showing a good description of the normalization obtained in each bin with the data-driven background normalization parameters. The expected distributions for $q\bar{q} \to ZZ$, ggF SBI ($gg \to (H^* \to)ZZ$), EW SBI$_1$ ($qq \to (H^* \to)ZZ + 2j$) and other backgrounds are shown as stacked histograms, and the expected signal (interference) is shown as a solid red (dashed blue) line. The background is estimated under the SM hypothesis (post-fit, $\mu_{\text{off-shell}} = 1$). The lower panels show the ratio of data to expectation. The hatched band shows the total systematic uncertainty in the expected distribution. The last bin of panel (b) contains overflow events.

by the preselection condition $D_{\text{pre}}(x) > -0.85$ without significantly reducing the power of the analysis.

### 6.2. Probability density ratio estimation

The probability density ratios are estimated as functions of the 14 observables in table 3 by using fully-connected NNs, i.e. where all neurons in a layer are connected to the neurons in the next layer. The architecture of this NN is the same as the one used for the preselection discriminant, but additional steps are taken to improve the accuracy of the score, which are described below.

The events in the simulated sample for each process X are split into ten disjoint sets for use in ten-fold cross validation [91]. For each cross-validation set, the events in the other nine sets are used to train an ensemble of NNs, each with the structure described above. The ten-fold cross validation ensures that the NNs are never evaluated using events used in their training, which would otherwise generate over-confident estimates of the probability density ratios for rare events. An ensemble member is trained with 80% of the events in the training set of the cross-validation splitting, randomly sampled without replacement. The total number of ensemble members varies between 10 and 70 for each ten-fold cross-validation set, depending on the process X, and resulting in 100 to 700 NNs in total. The larger ensembles are required for processes X that are very different from the reference process. The estimate of a probability density ratio is taken as its ensemble mean. Using ensembles sampled without replacement helps to minimize both the bias and variance of the final result, and the ensembles are also used for an uncertainty estimate, as is explained below.

The NNs are trained to minimize the binary cross-entropy loss between the normalized simulated sample $p_{\text{X}}(x)$ , with truth label $s_{\text{truth}} \equiv 1$, and the normalized simulated sample $p_{\text{ref}}(x)$, with truth label $s_{\text{truth}} \equiv 0$. For balanced training samples ($\nu_{\text{X}} = \nu_{\text{ref}}$), the NN converges to the optimal classifier score function $s_{\text{X}}(x) = p_{\text{X}}(x)/(p_{\text{ref}}(x) + p_{\text{X}}(x))$ and the probability density ratio can be written as $p_{\text{X}}(x)/p_{\text{ref}}(x) = s_{\text{X}}(x)/(1 - s_{\text{X}}(x))$ [89, 91–93].

The batch size used for the gradient descent step of the training process is optimized separately for each process, but has to be kept sufficiently large to ensure that the NN extrapolates well and remains representative for other samples not used in the training. Larger batch sizes are also necessary when the training samples have a large fraction of negatively-weighted events to ensure convexity of the loss function. Events with negative weights come from simulations with higher-order corrections in perturbation theory and multijet merging with parton showers. An average batch size of 1 024 was used for the NNs in this analysis. The *NAdam* adaptive learning rate algorithm [94, 95] is used for all trainings. In each training, 10% of the available events are used for loss function validation. A summary of the NN structure and training is given in appendix A.

The NN-estimated probability density ratios $p_{\text{X}}(x)/p_{\text{ref}}(x)$ for each process X are used to construct the signal strength-dependent probability density ratio:

$$\frac{p\,(x|\mu,\theta)}{p_{\text{ref}}\,(x)} = \frac{1}{\nu\,(\mu,\theta)} \sum_{\text{processes X}} f_X\,(\mu,\theta)\;\nu_X\,\frac{p_{\text{X}}\,(x)}{p_{\text{ref}}\,(x)}, \qquad (11)$$

where $f_X(\mu,\theta)$ are the sample-dependent multipliers listed in table 1.

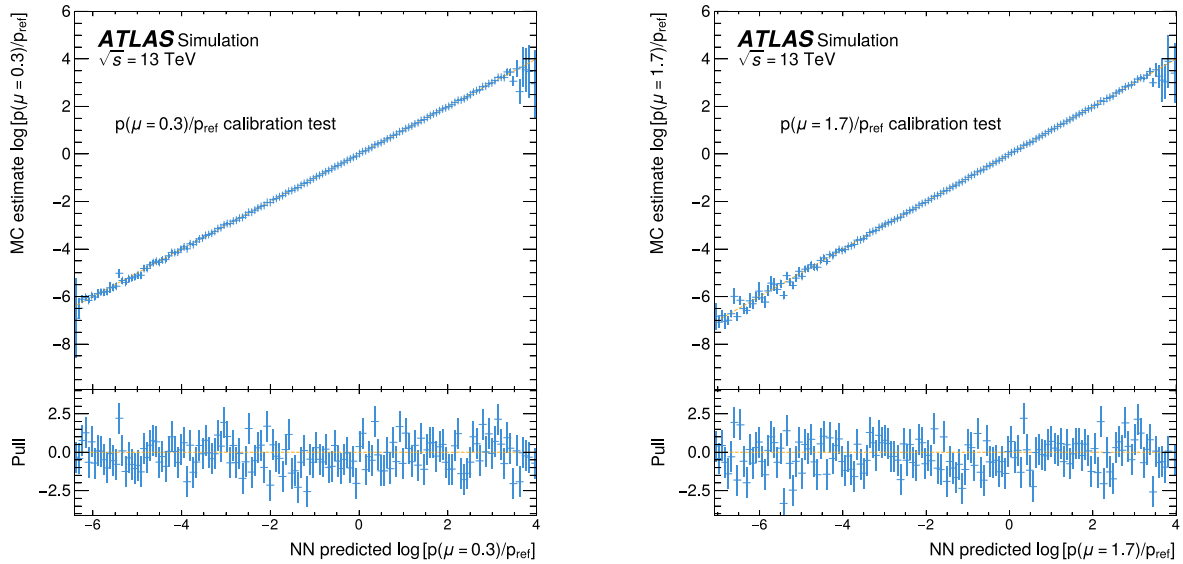


(a) (b)

**Figure 7.** Comparison between the NN-based and histogram-based estimate of the density ratio $p(x|\mu_{\text{off-shell}})/p_{\text{ref}}(x)$ for (a) $\mu_{\text{off-shell}} = 0.3$ and (b) $\mu_{\text{off-shell}} = 1.7$. The comparison is done as a function of $\log\left[p(x|\mu_{\text{off-shell}})/p_{\text{ref}}(x)\right]$ to separate the comparison for events that are very signal-like and reference-like. The lower panels show the pull, defined as the difference between the NN and MC-based estimate divided by the statistical uncertainty due to the finite number of MC events. The error bars indicate the uncertainty due to the finite number of simulated events in the histogram-based estimate of the density ratio.

The different hyperparameters described above, including the preselection threshold, the width and depth of each individual NN, and the size of the NN ensembles were optimized to obtain density ratio estimates as accurate as possible given the number of events in the simulated samples available for training. Several tests are performed to assess the accuracy of the NN training. A complete description of all tests performed can be found in [31], and only a summary is given here. Figure 7 compares the NN-based and histogram-based estimates of the density ratio $p(x|\mu_{\text{off-shell}})/p_{\text{ref}}(x)$ for two high-statistics Asimov samples[2] with signal strengths $\mu_{\text{off-shell}} = 0.3$ and 1.7. As can be seen with equation (3), these two samples validate the NN-based procedure in a regime that is dominated by the interference component ($\mu_{\text{off-shell}} < 1$), and in a regime that is dominated by the signal component ($\mu_{\text{off-shell}} > 1$), respectively. In both cases, the NNs show excellent probability calibration. Note that the result is obtained without a NN calibration layer [97].

If the NNs are unbiased, the probability density ratio $p(x|\mu_{\text{off-shell}})/p_{\text{ref}}(x)$ can be used to reweight distributions from one value of $\mu_{\text{off-shell}}$ to another, where the reweighting factor is obtained from the NN-based estimate of the probability density ratio using:

$$\frac{p\left(x|\mu_{\text{off-shell}}\right)}{p\left(x|\mu_{\text{off-shell}}=1\right)} = \left(\frac{p\left(x|\mu_{\text{off-shell}}\right)}{p_{\text{ref}}\left(x\right)}\right)\left(\frac{p\left(x|\mu_{\text{off-shell}}=1\right)}{p_{\text{ref}}\left(x\right)}\right)^{-1}. \quad (12)$$

Comparisons between distributions estimated directly from an Asimov sample with a known value of $\mu_{\text{off-shell}}$ with those obtained through reweighting of an Asimov sample with a different value of $\mu_{\text{off-shell}}$ allows to test for possible bias in different regions of phase space. This test is demonstrated in figure 8 where histograms of distributions of $D_{\text{pre}}(x)$ obtained from high-statistics Asimov samples with signal strengths $\mu_{\text{off-shell}} = 0.3$ and 1.7 are compared with the same distributions obtained through reweighting of a SM ($\mu_{\text{off-shell}} = 1.0$) Asimov sample. The results shown in figures 7 and 8 indicate that the NNs are trained with low bias and low variance. A separate multidimensional test is performed by training a second NN to discriminate between an Asimov sample with known $\mu_{\text{off-shell}}$ and another sample obtained from reweighting the reference sample with $p(x|\mu_{\text{off-shell}})/p_{\text{ref}}(x)$. No discriminating power is observed in this second NN, which indicates that it cannot distinguish between the original and reweighted samples, and that no significant biases in the estimate of the density ratios are present. The multidimensional test probes a limited range of the complete phase space and only confirms what thorough reweighting tests performed with many different observables already show.

[2] An Asimov dataset is one for which the application of any unbiased estimator for all parameters will provide the true values [96]. In unbinned analyses, an approximation of such a dataset can be constructed using a large number of simulated events with appropriate event weights.

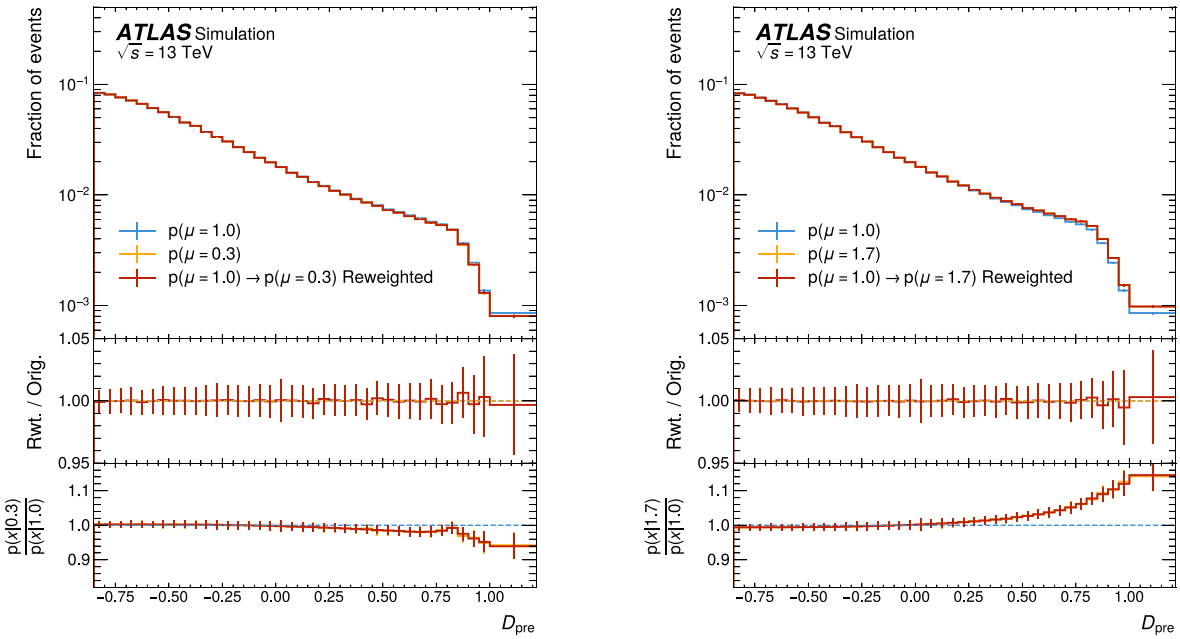


(a) (b)

**Figure 8.** Comparison between the $D_{\text{pre}}(x)$ normalized distribution obtained using an Asimov sample with (a) $\mu_{\text{off-shell}} = 0.3$ and (b) $\mu_{\text{off-shell}} = 1.7$, and the same distributions obtained through reweighting of a SM ($\mu_{\text{off-shell}} = 1.0$) Asimov sample. The ratio plots provide a comparison between the two estimates (middle panel) and between the distributions at the given value of $\mu_{\text{off-shell}}$ and the SM expectation (bottom panel).

### *6.3. Systematic uncertainties*

Systematic uncertainties include experimental uncertainties in the reconstructed objects and modeling uncertainties in the simulated samples. The systematic uncertainty model follows closely that reported in [17] and only a summary is presented here. Modeling uncertainties and uncertainties in the jet energy scale and resolution dominate the systematic uncertainty of the measurement. Jet-related observables used to describe the events provide important information for discrimination between hypotheses, especially for EW off-shell Higgs boson production. However, they also make the result sensitive to modeling of jet energy scale and resolution.

The uncertainty in the integrated luminosity for the full Run 2 dataset is 0.83% [48], obtained using the LUCID-2 detector [40] for the primary luminosity measurements. Experimental uncertainties include momentum scale and resolution uncertainties for muons, electrons, and jets. These uncertainties are estimated by using calibrations performed for each individual object and by comparing them with different simulation models. Uncertainties in the reconstruction, identification and trigger efficiency of electrons [50, 78] and muons [51, 77] are determined from tag-and-probe efficiency measurements using $Z \to \ell^+\ell^-$ and $J/\psi \to \ell^+\ell^-$ events. uncertainties in the jet energy scale are derived by combining information from test-beam data, LHC collision data and simulation [82]. Uncertainties in the jet energy resolution are estimated as a function of jet $p_{\text{T}}$ and rapidity using dijet events, based on a similar method as in [82].

Modeling uncertainties arise from the choice of PDF, missing higher-order corrections in both QCD and EW perturbative calculations, the merging of additional partons to the hard-scatter ME, and the description of the parton shower. The methods used to estimate modeling uncertainties are summarized in table 4.

The PDF uncertainties are evaluated using the NNPDF prescription with 100 replicas from the NNPDF3.0 set [57]. The uncertainties due to missing higher-order QCD corrections are estimated by varying the renormalization and factorization scales independently, by factors one-half and two.

For the $gg \to ZZ \to 4\ell$ processes, the renormalization and factorization scales variations are evaluated on the NLO/LO $K$-factors and propagated to the measurement as a function of $m_{ZZ}$ only [60]. The $gg \to ZZ \to 4\ell$ NLO scale variation is found to be approximately uniform throughout the phase space, with a 10% relative magnitude, and independent of the process (ggF S, ggF B, ggF SBI). The NLO $K$-factors and scale variations used for the $gg \to ZZ \to 4\ell$ processes do not contain the complete top-quark mass dependency, which has only been recently calculated [98]. Therefore, the $gg \to ZZ \to 4\ell$ uncertainties due to scale variations are increased by 50% for $m_{ZZ}$ in the $\bar{t}t$ threshold region, and doubled in the phase space containing a jet with $p_{\text{T}} > 150$ GeV [17].

For all other processes, the two variations of the renormalization and factorization scales with largest impact in the expected value $\nu_{\text{X}}$ were taken as representative of this uncertainty. An additional uncertainty in missing higher-order QCD corrections is estimated for the $gg \to ZZ \to 4\ell$ and $q\bar{q} \to ZZ \to 4\ell$

**Table 4.** Description of the different sources of modeling systematic uncertainties considered for each process and the method used to estimate it.

| Process | Uncertainty | Method |
|---|---|---|
| $q\bar{q} \to ZZ$ | Missing higher-order QCD | Renormalization and factorization scales |
| $q\bar{q} \to ZZ$ | Soft-gluon resummation | QSF resummation scale |
| $q\bar{q} \to ZZ$ | Jet merging | CKKW merging scale |
| $q\bar{q} \to ZZ$ | Parton shower | SHERPA showering scheme |
| $q\bar{q} \to ZZ$ | Missing higher-order EW | NLO/LO $K$-factor in regions of high recoil |
| $q\bar{q} \to ZZ$ | PDF | NNPDF MC replicas |
| EW $qq \to ZZ + 2j$ | Missing higher-order QCD | Renormalization and factorization scales |
| EW $qq \to ZZ + 2j$ | Parton Shower | A14 tune parameters, ISR and FSR scales |
| EW $qq \to ZZ + 2j$ | PDF | NNPDF MC replicas |
| $gg \to ZZ$ | Missing higher-order QCD | Renormalization and factorization scales |
| $gg \to ZZ$ | Soft-gluon resummation | QSF resummation scale |
| $gg \to ZZ$ | Jet merging | CKKW merging scale |
| $gg \to ZZ$ | Parton shower | SHERPA showering scheme |
| $gg \to ZZ$ | PDF | NNPDF MC replicas |

processes by varying the soft-gluon resummation scale (QSF) in SHERPA by half and twice the nominal value used in the simulation. The QSF scale variation is evaluated separately for each $gg \to ZZ \to 4\ell$ component (ggF S, ggF B, and ggF SBI) and can induce variations as large as 40% on the expected yield [59].

Jet merging uncertainties are evaluated by varying the matching scale (based on the Catani-Krauss-Kuhn-Webber CKKW prescription [99]) for the processes simulated with the SHERPA generator. Parton-shower uncertainties are evaluated by varying the SHERPA showering scheme [59]. For those processes simulated with the PYTHIA shower program, the uncertainty is assessed by varying the PYTHIA configurations, such as the parameter values of the A14 tune, the multi-parton models, and the initial and final-state radiation scales.

The uncertainties due to missing higher-order EW corrections are considered for the main $q\bar{q} \to ZZ \to 4\ell$ process. The largest missing higher-order component comprises mixed NLO QCD + NLO EW corrections, which are relevant in regions of phase space with large NLO QCD corrections. Following the procedure from [100], the full magnitude of the NLO EW correction is taken as uncertainty for events in which the quadruplet has large recoil. The same prescription was used in histogram-based analysis and further discussion can be found in [17]. These uncertainties are subleading when compared to the dominant modeling uncertainties related to missing higher-order corrections in $gg \to ZZ$, soft-gluon resummation in $gg \to ZZ$, and jet matching in $q\bar{q} \to ZZ$.

Systematic uncertainties are introduced in the measurement model by nuisance parameters (NPs) $\alpha_m$, which modify both the expected event rates $\nu_{\mathrm{X}}(\alpha_m) = G_{X,m}(\alpha_m)\nu_{\mathrm{X}}$ and the probability densities $p_{\mathrm{X}}(x|\alpha_m) = g_{X,m}(x|\alpha_m)p_{\mathrm{X}}(x)$. The different sources of systematic uncertainties are considered to be independent, and lead to the following probability model for each process X:

$$\nu_{\mathrm{X}}(\alpha)\, p_{\mathrm{X}}(x_i|\alpha) = \left[\prod_m G_{\mathrm{X},m}(\alpha_m)\right] \nu_{\mathrm{X}} \left[\prod_m g_{\mathrm{X},m}(x_i, \alpha_m)\right] p_{\mathrm{X}}(x_i)\,. \quad (13)$$

The values of the NPs are constrained by auxiliary measurements that are defined by two auxiliary observables (AOs): the central value $a_m$ and the uncertainty $\delta_{\alpha,m}$. The functions $G_{\mathrm{X},m}(\alpha_m)$ are polynomial-exponential interpolations of the expected number of events $\nu_{\mathrm{X}}$ based on simulated samples with NPs varied between $a_m + \delta_{\alpha,m}$ and $a_m - \delta_{\alpha,m}$ [90]. The same samples are used to describe the probability density ratios $g_{\mathrm{X},m}(x, \alpha_m = a_m \pm \delta_{\alpha,m})$ using NN estimates for the density ratios $p_{\mathrm{X}}(x|\alpha_m = a_m \pm \delta_{\alpha,m})/p_{\mathrm{X}}(x|\alpha_m = 0)$ [31]. In the CR, where no per-event density ratios are used, only per-bin $G$ functions are used. In the SR, the per-bin $G$ functions parametrize the normalization uncertainty, while the per-event $g$ functions parametrize the shape uncertainty as a function of the 14 observables used to describe the event.

For the theoretical modeling uncertainties of $gg \to ZZ \to 4\ell$ production, common NPs are introduced for the ggF S, ggF B, and ggF SBI processes. The same is done for the theoretical modeling uncertainties of EW $qq \to ZZ + 2j \to 4\ell + 2j$ production, where common NPs are used for EW $\mathrm{SBI}_1$, EW $\mathrm{SBI}_{10}$, and EW B. In the description of theoretical uncertainties in $gg \to ZZ \to 4\ell$, the normalization and shape components are described with different NPs. Since separate normalization parameters are introduced for the $q\bar{q} \to ZZ \to 4\ell$ processes with $n_{\mathrm{jets}} = 0, 1, \geqslant 2$, separate NPs are also used to describe the corresponding modeling systematic uncertainty for the three different processes.

Dedicated NPs are introduced to account for the uncertainty due to the finite number of simulated events in each process and to the natural stochasticity of the NN training. These uncertainties are evaluated by bootstrapping the ensemble members used to estimate the density ratios. Each bootstrapped ensemble is used to infer the signal strengths $\hat{\mu}$ using the maximum likelihood methods described in section 7. The standard deviation $\delta\hat{\mu}$ of the maximum likelihood estimators (MLEs) is used as a proxy for the uncertainty arising from the finite number of simulated events, with a correction factor to account for the partial overlap of events in each member of the ensemble [101]. The associated NP is introduced as

a spurious signal uncertainty [102] by introducing a new NP $\alpha_{\text{MCstat}}$ and shifting $\mu \to \mu + \alpha_{\text{MCstat}}\delta\hat{\mu}$.

## 7. Statistical analysis and results

Histograms of the scores $s_X(x)$ used to estimate the density ratios in the SR are shown in figure 9 for all processes in this analysis indicating a good modeling of the probability density ratios throughout the SR. A single histogram is shown for $s_{q\bar{q}ZZ}$ since a single NN ensemble is used for the three $q\bar{q}ZZ$ processes (with $n_{\text{jets}} = 0$, 1, and $\geqslant 2$). This is possible without loss of information because the observable that distinguishes the three processes ($n_{\text{jets}}$) is part of the vector $x$ that describes the event, and therefore:

$$\nu_{q\bar{q}ZZ}^{n_{\text{jets}}=i} \frac{p_{q\bar{q}ZZ}^{n_{\text{jets}}=i}(x)}{p_{\text{ref}}(x)} = \delta_{n_{\text{jets}},i}\, \nu_{q\bar{q}ZZ} \frac{p_{q\bar{q}ZZ}(x)}{p_{\text{ref}}(x)}, \tag{14}$$

where $\delta_{n_{\text{jets}},i}$ is the Kronecker delta.

The NN-based density ratios allows an unbinned analysis to be performed. The data are analyzed using the likelihood function $\lambda(\mu,\theta,\alpha)$:

$$\begin{aligned} -2\ln\lambda(\mu,\theta,\alpha) = &-2\sum_{\text{regions }(I)} \ln\left[\text{Pois}\left(N_I|\nu_I(\mu,\theta,\alpha)\right)\right] \\ &-2\sum_{\text{events }(i)} \ln\left[\frac{p(x_i|\mu,\theta,\alpha)}{p_{\text{ref}}(x_i)}\right] \\ &+\sum_{\text{systematics }(m)} (\alpha_m - a_m)^2 . \end{aligned} \tag{15}$$

The first term in the sum corresponds to the Poisson probability of observing a total of $N_I$ events in a region $I$ with $\nu_I(\mu,\theta,\alpha)$ expected events. The second term is the ratio of the probability density of the dataset $\{x_i\}$ for a hypothesis given by parameters $(\mu,\theta,\alpha)$ and the probability density of the same dataset for the fixed reference hypothesis. The last term in the sum represents Gaussian constraints for the NPs $\alpha_m$ from auxiliary measurements with value given by the AOs $a_m$. The values of the NPs and AOs are considered to be normalized by the value of the uncertainty of the corresponding auxiliary measurement, so that the width of the Gaussian density can always be taken as unity.

Four regions are considered in the sum of Poisson terms. The SR (defined as $D_{\text{pre}}(x) > -0.85$), and the CR (defined by $D_{\text{pre}}(x) \leqslant -0.85$) that is further divided into three $n_{\text{jets}}$ bins: 0, 1, and $\geqslant 2$ to provide enough constraining power for the $\theta_{q\bar{q}ZZ}^{\text{incl},1,2j}$ background normalization parameters, which are treated as unconstrained NPs, i.e. they have no corresponding auxiliary measurements that constrain them.

Only events in the SR are used in the sum over events, as defined in equation (15). To simplify the notation, all constrained and unconstrained NPs are collectively denoted by $\alpha$ hereafter. The test statistic used in this measurement is the profile log-likelihood ratio, traditionally used in LHC measurements [90]:

$$t_\mu = -2\ln\frac{\lambda\left(\mu,\hat{\hat{\alpha}}(\mu)\right)}{\lambda(\hat{\mu},\hat{\alpha})}, \tag{16}$$

where $(\hat{\mu},\hat{\alpha})$ are the parameters estimates that maximize the function $\lambda(\mu,\alpha)$ and $\hat{\hat{\alpha}}(\mu)$ is a parameter estimate that conditionally maximizes the function $\lambda(\mu,\alpha)$ for a given $\mu$:

$$(\hat{\mu},\hat{\alpha}) = \underset{\mu,\alpha}{\text{argmax}}\ \lambda(\mu,\alpha); \qquad \hat{\hat{\alpha}}(\mu) = \underset{\alpha}{\text{argmax}}\ \lambda(\mu,\alpha). \tag{17}$$

The term $\sum_{\text{events}} \ln(p_{\text{ref}}(x))$ in the denominator of equation (15) cancels in the ratio used to define the test statistic $t_\mu$ since it is independent of any parameter $(\mu,\alpha)$. Figure 10 shows the results of a closure test of the $t_{\mu_{\text{off-shell}}}$ test statistic: the value of the estimate $\hat{\mu}_{\text{off-shell}}$ for an Asimov sample with a true value of $\mu_{\text{off-shell}}$ for a wide range of $\mu_{\text{off-shell}}$ values. Closure is observed for all values of $\mu_{\text{off-shell}}$, within the statistical uncertainty of the simulation samples used. An additional test was performed replacing the $q\bar{q} \to ZZ$ SHERPA sample in the Asimov data by an alternative simulation done with POWHEG. The hard scattering ME in both samples is calculated at the same perturbative order in QCD, but the samples have different parton shower matching and simulation. Closure of the $\mu_{\text{off-shell}}$ MLE is also observed with the alternative Asimov sample.

A total of 127 NPs are used in the measurement, and no significant differences between the MLE estimates $\hat{\alpha}_m$ and the values of the auxiliary measurements $a_m$ are observed. The observed and expected values of the profile likelihood ratios $t_{\mu_{\text{off-shell}}}$ are shown in figure 11 as functions of $\mu_{\text{off-shell}}$ for a variety of scenarios, assuming $\mu_{\text{off-shell}} = \kappa_{g,\text{off-shell}}^2 \kappa_{V,\text{off-shell}}^2 = \kappa_{V,\text{off-shell}}^4$. Figure 11(a) compares the profile likelihood ratio for the histogram-based [17] and the NSBI-based analyses, and shows the improved constraints on $\mu_{\text{off-shell}}$ obtained with the latter. Additional comparisons with the histogram-based analysis are shown in appendix B. Figure 11(b) compares the profile likelihood ratio for the NSBI-based analysis to a variant where the NPs are fixed to the best-fit value $\hat{\alpha}$, reflecting only the statistical uncertainty on the data. The comparison indicates that systematic uncertainties are more important for tests of signal-dominated hypotheses ($\mu_{\text{off-shell}} > 1$) than for tests of interference-dominated hypotheses ($\mu_{\text{off-shell}} < 1$).

As is the case for the histogram-based analysis, the test statistic is not distributed as a $\chi^2$ probability density, due to the double minima created by the interference terms and due to the constraint $\mu_{\text{off-shell}} > 0$ imposed by the model of equation (3). Confidence intervals are built using the Neyman construction (NC) [103] instead of relying on the asymptotic approximation. In the NC, pseudo-experiments are built by performing a Poisson bootstrapping on the high-statistic reference sample [102, 104]. In each pseudo-experiment, the bootstrapped weight of an event $x_i$ with weight $w_i$ in the reference sample is sampled from a Poisson distribution with expected value $w_i(\nu(\mu,\hat{\alpha})/\nu_{\text{ref}})(p(x_i|\mu,\hat{\alpha})/p_{\text{ref}}(x))$. The value of the

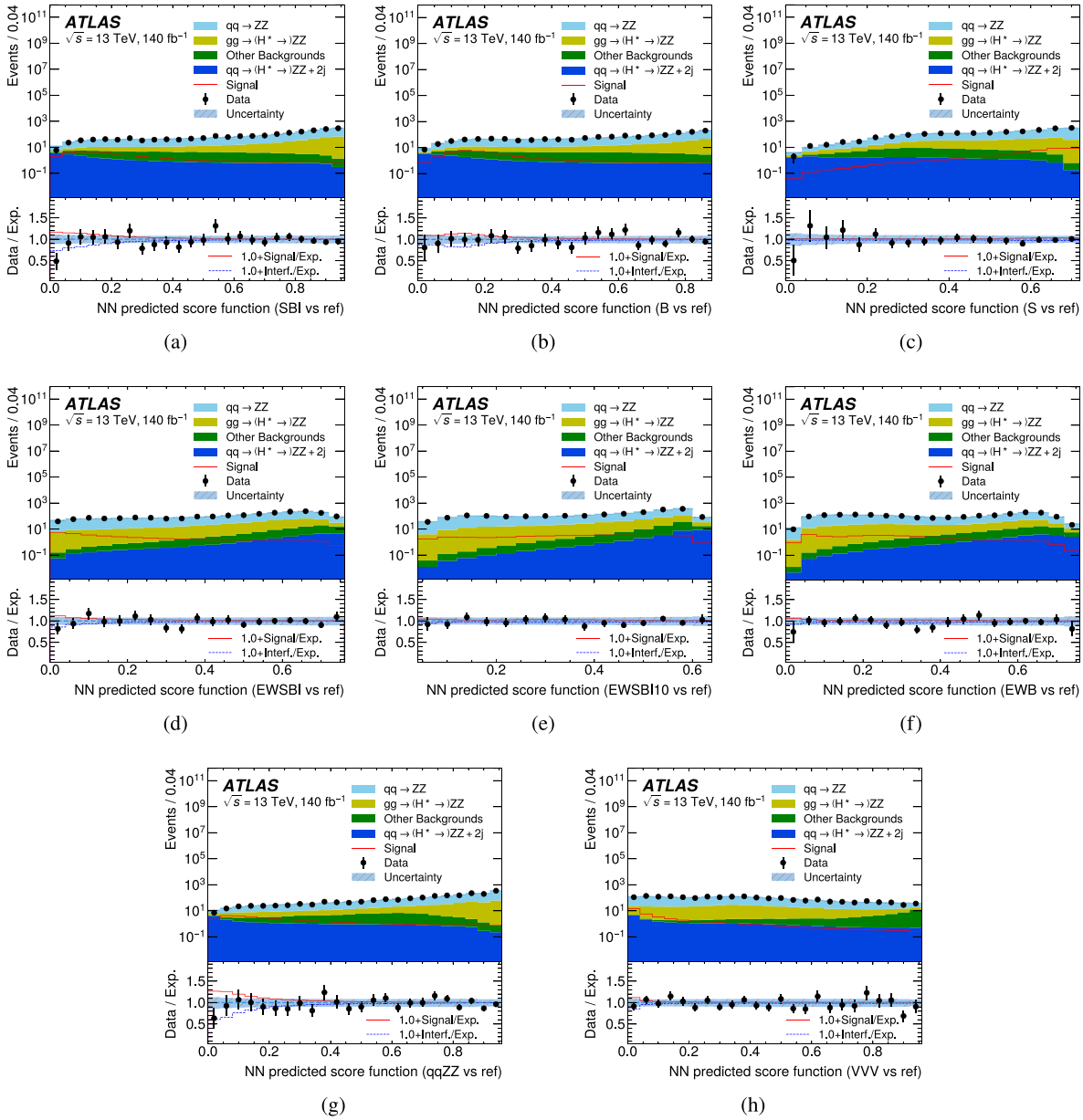


**Figure 9.** Comparison between data and expectation in the SR ($D_{\text{pre}}(x) > -0.85$) of the NN scores of the all major samples used to describe the probability density ratio of the reference process and (a) ggF SBI, (b) ggF S, (c) ggF B, (d) EW $\text{SBI}_1$, (e) EW $\text{SBI}_{10}$, (f) EW B, (g) $q\bar{q} \to ZZ$, and (h) *VVV*. The comparisons show a good modeling of the probability density ratios throughout the SR. The lower panels show the ratio of data to expectation. The expected SM distributions are shown as stacked histograms and the expected signal (interference) is shown as a solid red (dashed blue) line. The background is estimated under the SM hypothesis (post-fit, $\mu_{\text{off-shell}} = 1$). The hatched band shows the total systematic uncertainty in the expected distribution. The last bin contains overflow events.

AO $a_m$ associated with each constrained NP $\alpha_m$ is sampled from a Gaussian probability density $\text{Gaus}(a_m|\widehat{\alpha}_m, 1)$ [90].

Figure 12 shows the expected distribution of $t_{\mu_{\text{off-shell}}=0}$ for the SM hypothesis ($\mu^{\text{truth}}_{\text{off-shell}} = 1$) and the *no off-shell Higgs boson hypothesis* ($\mu^{\text{truth}}_{\text{off-shell}} = 0$). The black and dashed blue vertical lines indicate the observed and expected values of $t_{\mu_{\text{off-shell}}=0}$, respectively.The red dash-dotted curve in figure 12 shows the expected distribution of $t_{\mu_{\text{off-shell}}=0}$ assuming the SM hypothesis ($\mu^{\text{truth}}_{\text{off-shell}} = 1$). The $p$-value of the observed value of $t_{\mu_{\text{off-shell}}=0}$ under the SM hypothesis is 0.11, corresponding to one-sided significance of $1.2\sigma$. The green solid curve shows the shows the expected distribution of $t_{\mu_{\text{off-shell}}=0}$ assuming $\mu^{\text{truth}}_{\text{off-shell}} = 0$ (no off-shell Higgs boson hypothesis). The green dotted lines show the $p$-value thresholds corresponding to the one-sided significance of $1\sigma$ and $2\sigma$ under this hypothesis. The evidence for off-shell Higgs boson production has an observed (expected) significance of $2.5\sigma$ ($1.3\sigma$) using only the $H^* \to ZZ \to 4\ell$ decay channel. The evidence for off-shell Higgs boson hypothesis has a larger significance than the one observed (expected) in the previous histogram-based analysis [17] of the same dataset, which had a value of $0.8\sigma$ ($0.5\sigma$).

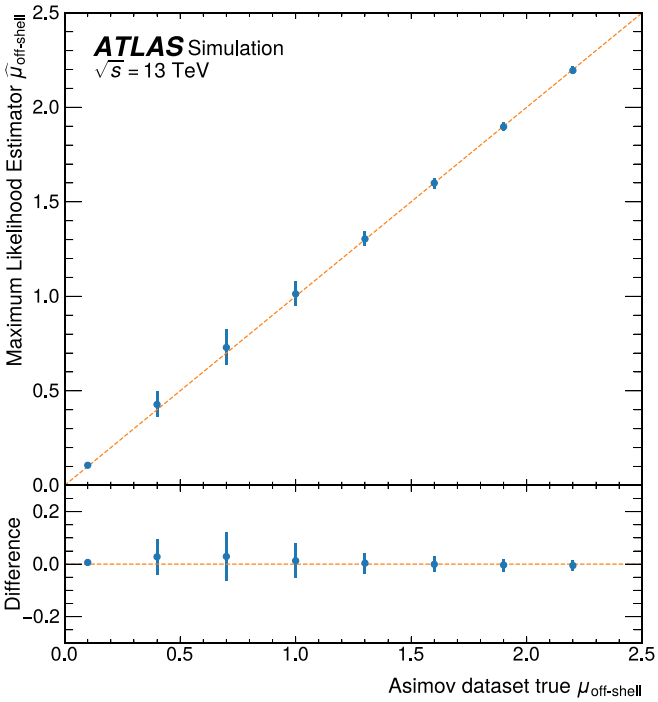


**Figure 10.** Maximum likelihood estimator $\hat{\mu}_{\text{off-shell}}$ for different Asimov pseudo-data with known value of $\mu^{\text{truth}}_{\text{off-shell}}$. The error bar shows the estimate of the uncertainty from the limited number of MC events in the Asimov dataset, which is introduced as a spurious signal uncertainty.

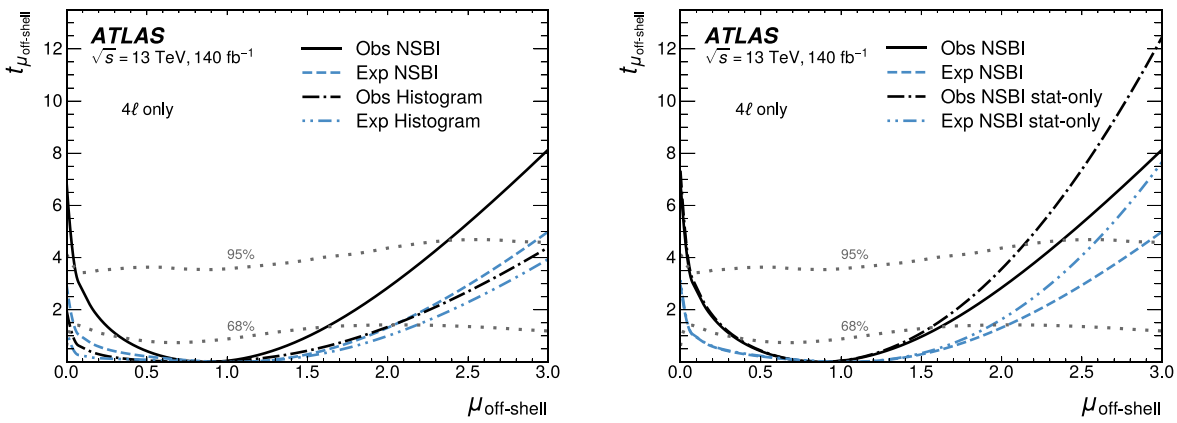


(a) (b)

**Figure 11.** (a) Values of the test statistic $t_{\mu_{\text{off-shell}}}$ assuming a single parameter of interest $\mu_{\text{off-shell}}$ obtained with an Asimov dataset (expected, dashed blue) and with data (observed, solid black) in the $H^* \to ZZ \to 4\ell$ decay channel. The values from the histogram-based analysis [17] are added in dash-dotted lines for comparison. The dotted gray lines show the 68% and 95% confidence belt, obtained from the Neyman construction. (b) Same values obtained with data (observed, solid black) and Asimov dataset (expected, dashed blue) compared with the *statistics-only* case with all NP fixed at their best-fit values $\hat{\alpha}$.

Figure 13(a) shows the distribution of the probability density ratio $p(x|\mu_{\text{off-shell}} = 0, \hat{\alpha})/p(x|\mu_{\text{off-shell}} = 1, \hat{\alpha})$, which is a optimal observable for $\mu_{\text{off-shell}} = 0$. The lower panel shows a comparison with the distribution from the best-fit hypothesis depicting the data behavior that leads to the observed exclusion of the no off-shell Higgs boson hypothesis. The difference between the observed and expected values of $t_{\mu_{\text{off-shell}}=0}$ indicates that there are regions of phase-space where the data are more interference-like than signal-like, as can be seen by the rightmost bins in figure 13(a) where the observed deficit of events is larger than expect. Given the small significance of the difference between expected and observed values of $t_{\mu_{\text{off-shell}}=0}$, it is difficult to isolate a specific region of phase-space with this behavior.

Figure 13(b) shows the distribution of the quadruplet mass $m_{4\ell}$ and, in the lower panel, the comparison with the best-fit hypothesis. This indicates that the quadruplet mass information alone would not be enough to obtain evidence of off-shell Higgs boson production in this channel and illustrates the importance of the ME-based analysis performed with the

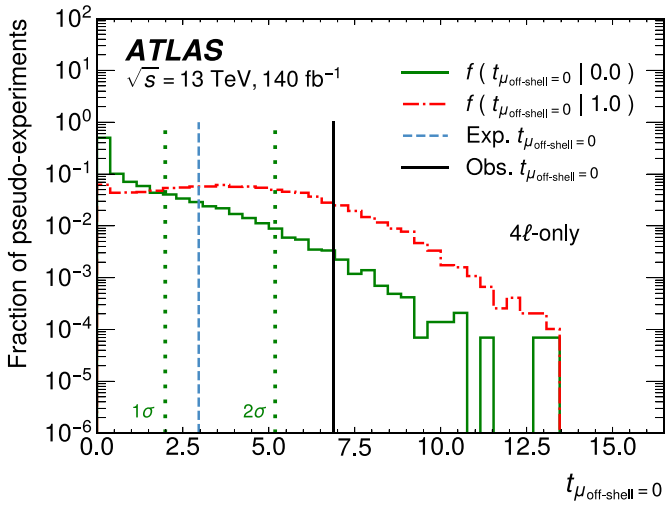


**Figure 12.** Expected distribution of $t_{\mu_{\text{off-shell}}=0}$ estimated with pseudo-experiments for the case of $\mu^{\text{truth}}_{\text{off-shell}} = 0$ (solid green, no off-shell Higgs boson production hypothesis) and $\mu^{\text{truth}}_{\text{off-shell}} = 1$ (dash-dotted red, SM hypothesis). The vertical solid black (dashed blue) line shows the observed (expected) value of $t_{\mu_{\text{off-shell}}=0}$. The dotted vertical green lines at $t_{\mu_{\text{off-shell}}=0} = 1.99$ and 5.18 represent the one-sided $1\sigma$ and $2\sigma$ significance thresholds, respectively, under the $\mu^{\text{truth}}_{\text{off-shell}} = 0$ hypothesis. These values differ slightly from the ones in the asymptotic approximation, in which the thresholds would be 1.97 and 5.19.

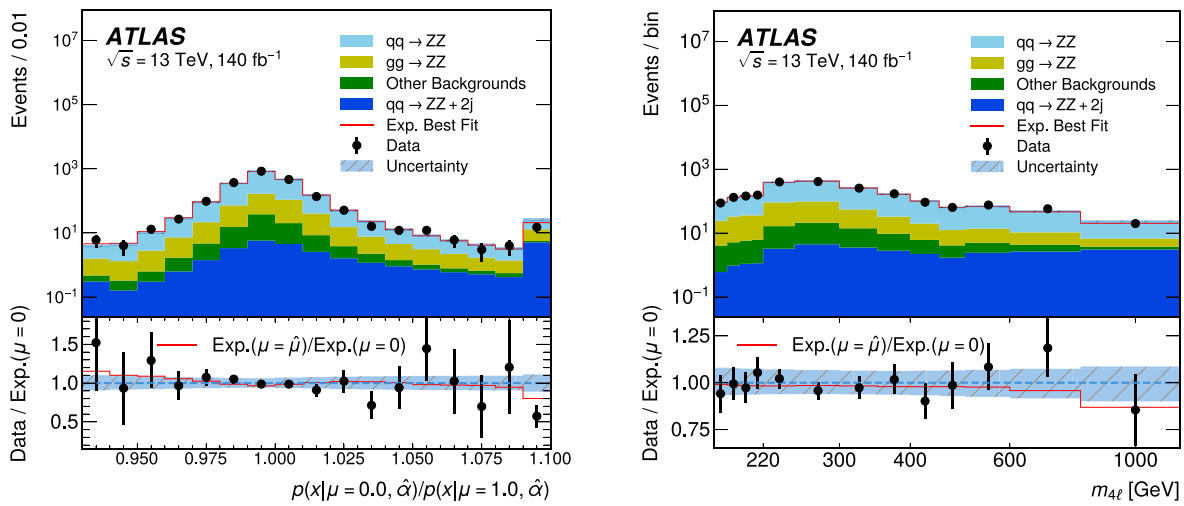


(a) (b)

**Figure 13.** Comparison between observed and the expected background distributions of (a) the optimal observable at $\mu_{\text{off-shell}} = 0$ and (b) the quadruplet mass $m_{4\ell}$. The solid red lines shows the expected distribution of the best-fit hypothesis $\widehat{\mu}$. The lower panel shows a comparison between the distribution of the background-only and best-fit hypotheses. The background is estimated under the SM hypothesis (post-fit, $\mu_{\text{off-shell}} = 1$). A comparison between the two distributions indicate that the optimal observable built with the NSBI method provides better evidence for off-shell Higgs boson production than only the $m_{4\ell}$ distribution. The hatched area corresponds to the total systematic uncertainty in the expected distributions. The first and last bins contain overflow events.

NSBI method. Further descriptions of the optimal observables can be found in appendix C.

Two methods are used to estimate the sensitivity of the measurement to different systematic uncertainties. The two methods differ in what is varied: either the NPs $\alpha_m$, or of the AOs $a_m$ associated with these NPs [105]. When using the variations of NPs, each parameter $\alpha_m$ is varied by its uncertainty and the conditional maximum likelihood estimate $\widehat{\widehat{\mu}}$ is re-derived with only that NP fixed. On the other hand, when varying AOs, each observable $a_m$ is set to $\pm 1$ and the unconditional maximum likelihood estimate $\widehat{\mu}$ is re-derived without fixing any NP. In both methods, the difference between the new and original estimate $\widehat{\mu}$ is taken as the propagated uncertainty.

The results of both methods are summarized in table 5. The propagated uncertainties are summed in quadrature within each group. The sum in quadrature does not take into account correlations between the different parameters $\widehat{\alpha}_m$ when using the method based on the variation of NPs. The same problem does not exist when varying AOs: the sum in quadrature can be made without loss of information and it can be used to provide a consistent decomposition of the total uncertainty into statistical and systematic uncertainties. In both methods,

**Table 5.** Absolute systematic uncertainties in the measurement of $\mu_{\text{off-shell}}$ in the $H \to ZZ \to 4\ell$ decay channel. Two methods of estimation are presented: based on the variation of nuisance parameters and on the variation of auxiliary observables. Uncertainties are given using the auxiliary observables methods since it allows variations to be summed in quadrature. The total uncertainty is independent of the method used to estimate systematic uncertainties.

| | Absolute impact on $\mu_{\text{off-shell}}$ | |
|---|---|---|
| Uncertainty source | Nuisance Parameter | Auxiliary Observable |
| Electron uncertainties | $(-0.05, +0.06)$ | $(-0.05, +0.06)$ |
| Muon uncertainties | $(-0.03, +0.03)$ | $(-0.02, +0.03)$ |
| Jet uncertainties | $(-0.10, +0.10)$ | $(-0.09, +0.11)$ |
| Luminosity | $(-0.01, +0.01)$ | $(-0.01, +0.01)$ |
| Total experimental | $(-0.12, +0.13)$ | $(-0.11, +0.12)$ |
| $q\bar{q} \to ZZ$ modeling | $(-0.06, +0.07)$ | $(-0.06, +0.07)$ |
| $gg \to ZZ$ modeling | $(-0.08, +0.13)$ | $(-0.07, +0.09)$ |
| EW $q\bar{q} \to ZZ + 2j$ modeling | $(-0.01, +0.01)$ | $(-0.01, +0.01)$ |
| Total modeling | $(-0.10, +0.15)$ | $(-0.09, +0.12)$ |
| Systematic uncertainty | $(-0.16, +0.19)$ | $(-0.14, +0.17)$ |
| Statistical uncertainty | $(-0.49, +0.72)$ | $(-0.50, +0.73)$ |
| Total uncertainty | $(-0.54, +0.75)$ | |

the statistical uncertainty is obtained by the square root of the difference of the total uncertainty squared and the systematic uncertainty squared.

The largest contributions to the measurement uncertainty are the statistical uncertainty on the data, the theoretical modeling uncertainties, and uncertainties on the jet energy scale and resolution. The contribution of MC statistical uncertainty to the total uncertainty is less than 0.01. The observed (expected) value of $\mu_{\text{off-shell}}$ at 68% CL is:

$$\mu_{\text{off-shell}} = 0.87^{+0.75}_{-0.54} \quad \left(1.00^{+1.04}_{-0.95}\right).$$

The fitted values of $\theta^{\text{incl}}_{q\bar{q}ZZ}$, $\theta^{1j}_{q\bar{q}ZZ}$, and $\theta^{2j}_{q\bar{q}ZZ}$ are $1.12 \pm 0.04$, $0.85 \pm 0.05$, and $0.90 \pm 0.07$, respectively. The result presented here has a reduced uncertainty when compared with the previous histogram-based analysis observed value at 68% CL of $0.79^{+1.21}_{-0.77}$ (expected $\mu_{\text{off-shell}} < 1.14$).

### 7.1. Combination with the analysis in the $2\ell 2\nu$ decay channel

The new result presented in this paper is combined with the most recent ATLAS off-shell Higgs boson production measurement in the $H^* \to ZZ \to 2\ell 2\nu$ decay channel [17]. The histogram-based $H^* \to ZZ \to 2\ell 2\nu$ analysis uses the binned transverse mass $m_{\text{T}}^{ZZ}$ distribution in three different SRs, in addition to the yield of four CRs enriched in $Z+$jets, non-resonant $e\mu$ events, and $q\bar{q} \to WZ$ events. The test statistic used for the combination is built from the log-likelihood ratio in equation (15), where now the sum over regions also includes the several $m_{\text{T}}^{ZZ}$ bins and CRs of the analysis in the $H^* \to ZZ \to 2\ell 2\nu$ decay channel.

The systematic uncertainty model used here is expanded to include constrained and unconstrained NPs exclusive to the analysis of the $H^* \to ZZ \to 2\ell 2\nu$ decay channels. Experimental and common theory uncertainties, i.e. pertaining to $gg \to ZZ$ and $q\bar{q} \to ZZ$ modeling, are modeled with common NPs that modify both likelihood components. Uncertainties related to missing higher-order EW corrections in the $q\bar{q} \to ZZ$ process, which were estimated with different methods in both analyses, are modeled with separate NPs for the $H^* \to ZZ \to 4\ell$ and $H^* \to ZZ \to 2\ell 2\nu$ analyses. However, the measured off-shell Higgs boson production is largely insensitive to this modeling choice. Common $q\bar{q} \to ZZ$ data-driven normalization parameters $\theta^{\text{incl}}_{q\bar{q}ZZ}$, $\theta^{1j}_{q\bar{q}ZZ}$, and $\theta^{2j}_{q\bar{q}ZZ}$ are used in the two channels since the phase space probed is similar within each $n_{\text{jets}}$ bin.

Figure 14(a) shows the test statistic values as a function of $\mu_{\text{off-shell}}$, for a joint likelihood model with a single common parameter of interest $\mu_{\text{off-shell}}$ ($\kappa^2_{g,\text{off-shell}}\kappa^2_{V,\text{off-shell}} = \kappa^4_{V,\text{off-shell}}$). Similar to the result using only the $ZZ \to 4\ell$ channel, the comparison indicates that systematic uncertainties are more important for tests of signal-dominated hypotheses ($\mu_{\text{off-shell}} \gg 1$) than for tests of interference-dominated hypotheses ($\mu_{\text{off-shell}} \ll 1$). Figure 14(b) shows the expected distribution of $t_{\mu_{\text{off-shell}}}$ for the SM hypothesis ($\mu^{\text{truth}}_{\text{off-shell}} = 1$) and the no off-shell Higgs boson hypothesis ($\mu^{\text{truth}}_{\text{off-shell}} = 0$) using the bootstrapping technique described above. The observed (expected) value of $\mu_{\text{off-shell}}$ at 68% CL is:

$$\mu_{\text{off-shell}} = 1.06^{+0.62}_{-0.45} \quad \left(1.00^{+0.83}_{-0.83}\right).$$

The result using uncertainties at 95% CL can be found in table 6. The evidence for off-shell Higgs boson production has an observed (expected) significance of $3.7\sigma$ ($2.4\sigma$).

Figure 15 shows the values of the test statistic $t_{\kappa_{g,\text{off-shell}}}$ and $t_{\kappa_{V,\text{off-shell}}}$ as a function of $\kappa_{g,\text{off-shell}}$ and $\kappa_{V,\text{off-shell}}$, respectively. In both cases, the $\kappa$ parameter not shown is profiled. The resulting confidence intervals in $\kappa_{g,\text{off-shell}}$ and $\kappa_{V,\text{off-shell}}$ provide a measurement of the Higgs boson couplings to gluons and vector bosons without any assumption on the Higgs boson total

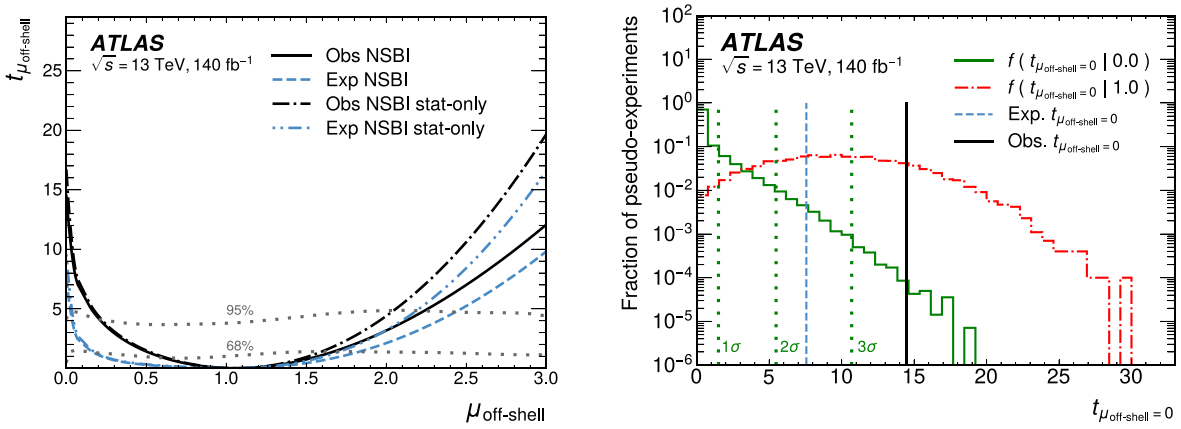


(a) (b)

**Figure 14.** (a) Values of the test statistic $t_{\mu_{\text{off-shell}}}$ assuming a single parameter of interest $t_{\mu_{\text{off-shell}}}$ obtained with an Asimov dataset (expected, dashed blue) and with data (observed, solid black) combining the $H^* \to ZZ \to 4\ell$ and $H^* \to ZZ \to 2\ell 2\nu$ decay channels. The dash-dotted curves show the *statistics-only* results where all NP are fixed to their best-fit values $\widehat{\alpha}$. The dotted gray lines show the 68% and 95% confidence belt, obtained from the Neyman construction. (b) Expected distribution of $t_{\mu_{\text{off-shell}}=0}$ estimated with pseudo-experiments for the case of $\mu^{\text{truth}}_{\text{off-shell}} = 0$ (solid green, no off-shell Higgs boson production hypothesis) and $\mu^{\text{truth}}_{\text{off-shell}} = 1$ (dashed-dotted red, SM hypothesis). The vertical solid black (dashed blue) line shows the observed (expected) value of $t_{\mu_{\text{off-shell}=0}}$. The vertical dotted green lines represent the $1\sigma$, $2\sigma$, an $3\sigma$ significance thresholds under the $\mu^{\text{truth}}_{\text{off-shell}} = 0$ hypothesis.

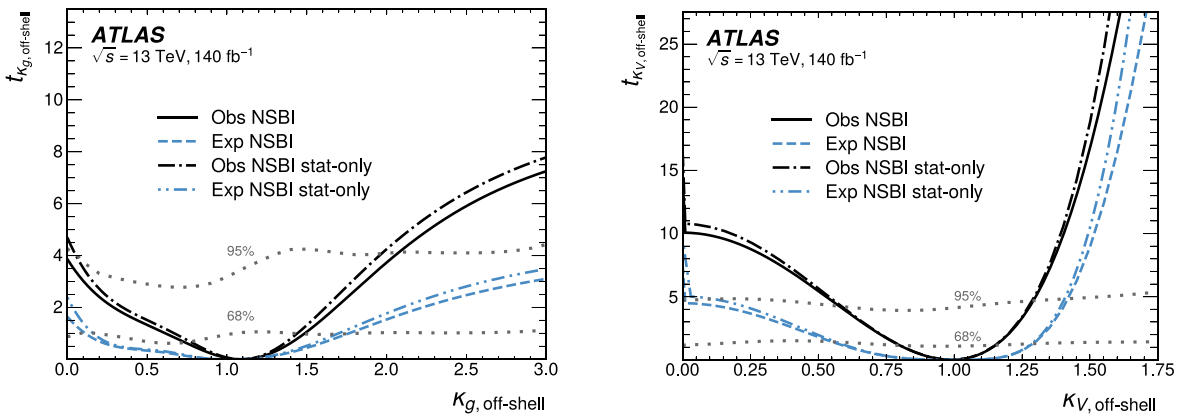


(a) (b)

**Figure 15.** Values of the (a) test statistic $t_{\kappa_{g,\text{off-shell}}}$ as a function of $\kappa_{g,\text{off-shell}}$ and (b) the test statistic $t_{\kappa_{V,\text{off-shell}}}$ as a function of $\kappa_{V,\text{off-shell}}$ obtained with an Asimov dataset (expected, dashed blue) and with data (observed, solid black). The dash-dotted curves show the *statistics-only* results where all NP are fixed to their best-fit values $\widehat{\alpha}$. The dotted gray lines show the 68% and 95% confidence belt, obtained from the Neyman construction. The $\kappa$ parameter not shown is profiled in both cases. The abrupt change at $\kappa_{V,\text{off-shell}} = 0$ comes from the strong $\kappa^4_{V,\text{off-shell}}$ dependency in the EW production of off-shell Higgs bosons.

width [8]. The observed (expected) values at 68% CL are:

$$\kappa_{g,\text{off-shell}} = 1.09^{+0.39}_{-0.35} \ \left(1.00^{+0.76}_{-0.89}\right),$$
$$\kappa_{V,\text{off-shell}} = 0.99^{+0.16}_{-0.19} \ \left(1.00^{+0.29}_{-0.45}\right).$$

### *7.2. Combination with on-shell 4ℓ analysis and Higgs boson width interpretation*

Measurements of the on-shell Higgs boson production [106] provide constraints on the signal strengths $\mu^{\text{ggF}}_{\text{on-shell}} = \kappa^2_{g,\text{on-shell}}\kappa^2_{V,\text{on-shell}}/\kappa_H$ and $\mu^{\text{EW}}_{\text{on-shell}} = \kappa^4_{V,\text{on-shell}}/\kappa_H$, where $\kappa_H = \Gamma_H/\Gamma^{\text{SM}}_H$ is the Higgs boson width normalized to the SM expectation.

Assuming that $\kappa^2_{g,\text{on-shell}}\kappa^2_{V,\text{on-shell}} = \kappa^4_{V,\text{on-shell}} = \kappa^2_{g,\text{off-shell}}\kappa^2_{V,\text{off-shell}} = \kappa^4_{V,\text{off-shell}}$, the off-shell Higgs boson production measurement can be combined with the on-shell $H \to ZZ \to 4\ell$ production measurement [106] to provide a measurement of the Higgs boson total width. The joint likelihood model for this measurement extends equation (15) with a common $H \to ZZ$ coupling modifier $\theta_{HZZ}$ and the modifier $\kappa_H$ to the Higgs boson width:

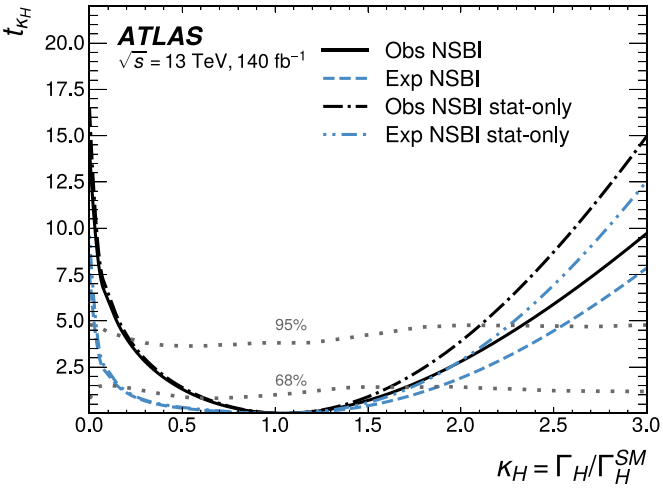


**Figure 16.** Values of the test statistic $t_{\kappa_H}$ as a function of $\kappa_H = \Gamma_H/\Gamma_H^{\mathrm{SM}}$ obtained with an Asimov dataset (expected, dotted black) and with data (observed, solid black). The dash-dotted curves show the *statistics-only* results where all NP are fixed to their best-fit values $\widehat{\alpha}$. The dotted gray lines show the 68% and 95% confidence belt, obtained from the Neyman construction.

$$
\begin{aligned}
&-2\ln\lambda\left(\kappa_H,\theta_{HZZ},\theta,\alpha\right)\\
&\quad=-2\sum_{\substack{\text{on-shell } 4\ell\\ \text{regions } (I)}}\ln\left[\mathrm{Pois}\left(N_I|\nu_I\left(\theta_{HZZ}/\kappa_H,\alpha\right)\right)\right]\\
&\qquad-2\sum_{\substack{\text{off-shell}\\ \text{regions } (I)}}\ln\left[\mathrm{Pois}\left(N_I|\nu_I\left(\theta_{HZZ},\theta,\alpha\right)\right)\right]\\
&\qquad-2\sum_{\substack{\text{off-shell } 4\ell\\ \text{SR events } (i)}}\ln\left[\frac{p\left(x_i|\theta_{HZZ},\theta,\alpha\right)}{p_{\mathrm{ref}}\left(x_i\right)}\right]\\
&\qquad+\sum_{\text{systematics } (m)}\left(\alpha_m-a_m\right)^2,
\end{aligned}
\tag{18}
$$

where $\theta_{HZZ} = \kappa^2_{g,\text{on-shell}}\kappa^2_{V,\text{on-shell}} = \kappa^4_{V,\text{on-shell}} = \kappa^2_{g,\text{off-shell}}\kappa^2_{V,\text{off-shell}} = \kappa^4_{V,\text{off-shell}}$. This assumption follows the one used in [17], but the sensitivity could be weakened by allowing $\kappa_V$ and $\kappa_g$ to vary independently and account for BSM contributions. The NP model for common experimental uncertainties follows the approach described in section 7.1. Events from on-shell Higgs boson processes in the off-shell background sample are also scaled as $\theta_{HZZ}/\kappa_H$. Theoretical modeling uncertainties in the on-shell and off-shell measurements are modeled with separate parameters, given the distinctness of the phase-space regions, but the measured Higgs boson width is largely insensitive to this modeling choice. Background normalization factors are also modeled separately.

Figure 16 shows the test statistic values as a function of $\kappa_H$ when profiling $\theta_{HZZ}$. The observed (expected) value of $\kappa_H$ and $\Gamma_H$ at 68% CL are:

$$
\begin{aligned}
\kappa_H &= 1.05^{+0.65}_{-0.46}\ \left(1.00^{+0.86}_{-0.84}\right),\\
\Gamma_H &= 4.3^{+2.7}_{-1.9}\ \left(4.1^{+3.5}_{-3.4}\right)\ \text{MeV}.
\end{aligned}
$$

The result using uncertainties at 95% CL can be found in table 6.

A similar combined measurement strategy can be used to constrain $R_{gg} = \kappa^2_{g,\text{on-shell}}/\kappa^2_{g,\text{off-shell}}$ and $R_{VV} = \kappa^2_{V,\text{on-shell}}/\kappa^2_{V,\text{off-shell}}$. The value of the two test statistics as a function of $R_{gg}$ and $R_{VV}$ are shown in figure 17. The observed (expected) values at 68% CL are:

$$
\begin{aligned}
R_{gg} &= 1.19^{+0.89}_{-0.66}\ \left(1.00^{+0.92}_{-0.98}\right),\\
R_{VV} &= 0.95^{+0.44}_{-0.35}\ \left(1.00^{+0.70}_{-0.69}\right),
\end{aligned}
$$

profiling the other $R$ parameter and setting $\kappa_H$ to unity. Table 6 summarizes all the results presented in this paper.

## 8. Conclusion

A measurement of the off-shell Higgs boson production in the $H^* \to ZZ \to 4\ell$ decay channel is presented. The measurement uses 140 fb$^{-1}$ of integrated luminosity collected at $\sqrt{s} =$ 13 TeV during the Run 2 of the LHC by the ATLAS detector. The data are analyzed with a NSBI strategy in which NNs are used to estimate a per-event contribution to the likelihood ratio between different hypotheses. This result is combined with the most recent measurement of the off-shell Higgs boson production in the $H^* \to ZZ \to 2\ell 2\nu$ decay channel. The observed (expected) value of the off-shell Higgs boson signal strength is $1.06^{+0.62}_{-0.45}$ $(1.00^{+0.83}_{-0.83})$ at 68% CL. The evidence for off-shell Higgs boson production has an observed (expected) significance of $3.7\sigma$ $(2.4\sigma)$. The off-shell Higgs boson production measurement in the $H^* \to ZZ$ decay channel is combined with the on-shell Higgs boson production measurement in the same channel to obtain a constraint on the Higgs boson total width. The observed (expected) value of the Higgs boson total width is $\Gamma_H = 4.3^{+2.7}_{-1.9}(4.1^{+3.5}_{-3.4})$ MeV at 68% CL, improved relative to the ATLAS previous result of $\Gamma_H = 4.4^{+3.1}_{-2.3}(4.1^{+3.8}_{-3.8})$ MeV using the same dataset.

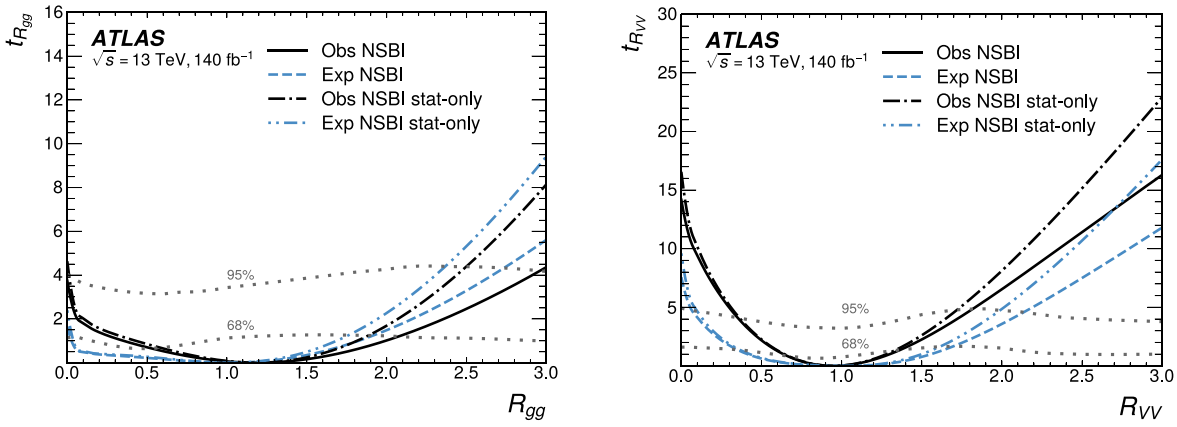


(a) (b)

**Figure 17.** Values of (a) the test statistic $t_{R_{gg}}$ as a function of $R_{gg} = \kappa^2_{g,\text{on-shell}}/\kappa^2_{g,\text{off-shell}}$ and of (b) the test statistic $t_{R_{VV}}$ as a function of $R_{VV} = \kappa^2_{V,\text{on-shell}}/\kappa^2_{V,\text{off-shell}}$ obtained with an Asimov dataset (expected, dashed blue) and with data (observed, solid black). The values obtained when all NP are fixed to their best-fit values $\widehat{\alpha}$, corresponding to the *statistics-only* case, are shown in dash-dotted lines for comparison. The dotted gray lines show the 68% and 95% confidence belt, obtained from the Neyman construction. In both figures, the $R$ parameter not shown is profiled and $\kappa_H$ is fixed to 1.

**Table 6.** Summary of the results for $\kappa_{g,\text{off-shell}}$, $\kappa_{V,\text{off-shell}}$, and $\mu_{\text{off-shell}}$ combining the measurement of the off-shell Higgs boson production analysis in the $H \to ZZ \to 4\ell$ decay channel presented in this paper with the analysis in the $H \to ZZ \to 2\ell 2\nu$ decay channel from [17]. The results for $\Gamma_H$, $R_{gg}$ and $R_{VV}$ are obtained combining the off-shell production measurement with the on-shell analysis from [106]. All results are presented with their 68% CL and 95% CL intervals. No expected 95% CL interval for $\kappa_{g,\text{off-shell}}$ is obtained because the Asimov sample is unable to break the degeneracy between $\kappa_{g,\text{off-shell}}$ and $\kappa_{V,\text{off-shell}}$ in ggF production. All results use the full Run 2 dataset with 140 fb$^{-1}$ of integrated luminosity.

| | | 68% CL interval | | 95% CL interval | |
|---|---|---|---|---|---|
| Parameter | Value | Observed | Expected | Observed | Expected |
| $\mu_{\text{off-shell}}$ | 1.06 | [0.61, 1.67] | [0.17, 1.83] | [0.21, 2.24] | [0.01, 2.42] |
| $\kappa_{g,\text{off-shell}}$ | 1.09 | [0.74, 1.48] | [0.11, 1.76] | $< 2.08$ | — |
| $\kappa_{V,\text{off-shell}}$ | 0.99 | [0.80, 1.15] | [0.55, 1.29] | [0.58, 1.30] | [0.01, 1.42] |
| $\Gamma_H$ [MeV] | 4.29 | [2.41, 6.95] | [0.66, 7.61] | [0.76, 9.66] | [0.12, 10.50] |
| $R_{gg}$ | 1.19 | [0.53, 2.07] | [0.02, 1.92] | $< 2.96$ | $< 2.73$ |
| $R_{VV}$ | 0.95 | [0.61, 1.39] | [0.31, 1.70] | [0.30, 1.86] | [0.06, 2.14] |

## Data availability statement

The public release of data supporting the findings of this article will follow the CERN Open Data Policy [107]. The values from relevant plots and tables associated with this article are stored in HEPData at https://www.hepdata.net/record/156805.

## Acknowledgment

We thank CERN for the very successful operation of the LHC and its injectors, as well as the support staff at CERN and at our institutions worldwide without whom ATLAS could not be operated efficiently.

The crucial computing support from all WLCG partners is acknowledged gratefully, in particular from CERN, the ATLAS Tier-1 facilities at TRIUMF/SFU (Canada), NDGF (Denmark, Norway, Sweden), CC-IN2P3 (France), KIT/GridKA (Germany), INFN-CNAF (Italy), NL-T1 (Netherlands), PIC (Spain), RAL (UK) and BNL (USA), the Tier-2 facilities worldwide and large non-WLCG resource providers. Major contributors of computing resources are listed in [108].

We gratefully acknowledge the support of ANPCyT, Argentina; YerPhI, Armenia; ARC, Australia; BMWFW and FWF, Austria; ANAS, Azerbaijan; CNPq and FAPESP, Brazil; NSERC, NRC and CFI, Canada; CERN; ANID, Chile; CAS, MOST and NSFC, China; Minciencias, Colombia; MEYS CR, Czech Republic; DNRF and DNSRC, Denmark; IN2P3-CNRS and CEA-DRF/IRFU, France; SRNSFG, Georgia; BMBF, HGF and MPG, Germany; GSRI, Greece; RGC and Hong Kong SAR, China; ICHEP and Academy of Sciences and Humanities, Israel; INFN, Italy; MEXT and JSPS, Japan; CNRST, Morocco; NWO, Netherlands; RCN, Norway; MNiSW, Poland; FCT, Portugal; MNE/IFA, Romania; MSTDI, Serbia; MSSR, Slovakia; ARIS and MVZI, Slovenia; DSI/NRF, South Africa; MICIU/AEI, Spain; SRC and Wallenberg Foundation, Sweden; SERI, SNSF and Cantons of Bern and Geneva, Switzerland; NSTC, Taipei; TENMAK, Türkiye; STFC/UKRI, United Kingdom; DOE and NSF, United States of America.

Individual groups and members have received support from BCKDF, CANARIE, CRC and DRAC, Canada; CERN-CZ, FORTE and PRIMUS, Czech Republic; COST, ERC, ERDF, Horizon 2020, ICSC-NextGenerationEU and Marie Skłodowska-Curie Actions, European Union; Investissements d'Avenir Labex, Investissements d'Avenir Idex and ANR, France; DFG and AvH Foundation, Germany; Herakleitos, Thales and Aristeia programmes co-financed by EU-ESF and the Greek NSRF, Greece; BSF-NSF and MINERVA, Israel; NCN and NAWA, Poland; La Caixa Banking Foundation, CERCA Programme Generalitat de Catalunya and PROMETEO and GenT Programmes Generalitat Valenciana, Spain; Göran Gustafssons Stiftelse, Sweden; The Royal Society and Leverhulme Trust, United Kingdom.

In addition, individual members wish to acknowledge support from Armenia: Yerevan Physics Institute (FAPERJ); CERN: European Organization for Nuclear Research (CERN DOCT); Chile: Agencia Nacional de Investigación y Desarrollo (FONDECYT 1230812, FONDECYT 1230987, FONDECYT 1240864); China: Chinese Ministry of Science and Technology (MOST-2023YFA1605700, MOST-2023YFA1609300), National Natural Science Foundation of China (NSFC - 12175119, NSFC 12275265, NSFC-12075060); Czech Republic: Czech Science Foundation (GACR—24-11373S), Ministry of Education Youth and Sports (ERC-CZ-LL2327, FORTE CZ.02.01.01/00/22_008/0004632), PRIMUS Research Programme (PRIMUS/21/SCI/017); EU: H2020 European Research Council (ERC—101002463); European Union: European Research Council (ERC - 948254, ERC 101089007, ERC, BARD, 101116429), Horizon 2020 Framework Programme (MUCCA—CHIST-ERA-19-XAI-00), European Union, Future Artificial Intelligence Research (FAIR-NextGenerationEU PE00000013), Italian Center for High Performance Computing, Big Data and Quantum Computing (ICSC, NextGenerationEU); France: Agence Nationale de la Recherche (ANR-20-CE31-0013, ANR-21-CE31-0013, ANR-21-CE31-0022, ANR-22-EDIR-0002); Germany: Baden-Württemberg Stiftung (BW Stiftung-Postdoc Eliteprogramme), Deutsche Forschungsgemeinschaft (DFG—469666862, DFG—CR 312/5-2); Italy: Istituto Nazionale di Fisica Nucleare (ICSC, NextGenerationEU), Ministero dell'Università e della Ricerca (NextGenEU PRIN20223N7F8K M4C2.1.1); Japan: Japan Society for the Promotion of Science (JSPS KAKENHI JP22H01227, JSPS KAKENHI JP22H04944, JSPS KAKENHI JP22KK0227, JSPS KAKENHI JP23KK0245); Norway: Research Council of Norway (RCN-314472); Poland: Ministry of Science and Higher Education (IDUB AGH, POB8, D4 no 9722), Polish National Agency for Academic Exchange (PPN/PPO/2020/1/00002/U/00001), Polish National Science Centre (NCN 2021/42/E/ST2/00350, NCN OPUS 2023/51/B/ST2/02507, NCN OPUS nr 2022/47/B/ST2/03059, NCN UMO-2019/34/E/ST2/00393, NCN & H2020 MSCA 945339, UMO-2020/37/B/ST2/01043, UMO-2021/40/C/ST2/00187, UMO-2022/47/O/ST2/00148, UMO-2023/49/B/ST2/04085, UMO-2023/51/B/ST2/00920); Portugal: Foundation for Science and Technology (FCT); Spain: Generalitat Valenciana (Artemisa, FEDER, IDIFEDER/2018/048), Ministry of Science and Innovation (MCIN & NextGenEU PCI2022-135018-2, MICIN & FEDER PID2021-125273NB, RYC2019-028510-I, RYC2020-030254-I, RYC2021-031273-I, RYC2022-038164-I); Sweden: Carl Trygger Foundation (Carl Trygger Foundation CTS 22:2312), Swedish Research Council (Swedish Research Council 2023-04654, VR 2018-00482, VR 2021-03651, VR 2022-03845, VR 2022-04683, VR 2023-03403), Knut and Alice Wallenberg Foundation (KAW 2018.0458, KAW 2019.0447, KAW 2022.0358); Switzerland: Swiss National Science Foundation (SNSF—PCEFP2_194658); United Kingdom: Leverhulme Trust (Leverhulme Trust RPG-2020-004), Royal Society (NIF-R1-231091); United States of America: U.S. Department of Energy (ECA DE-AC02-76SF00515), Neubauer Family Foundation.

This work started as part of the ATLAS Google Cloud Platform project [109]. Later stages of the work utilized computing resources at Southern Methodist University's O'Donnell Data Science and Research Computing Institute and computing resources at the University of Massachusetts Amherst Research Computing.

## The ATLAS Collaboration

G Aad[104], E Aakvaag[17], B Abbott[123], S Abdelhameed[119a], K Abeling[56], N J Abicht[50], S H Abidi[30], M Aboelela[46], A Aboulhorma[36e], H Abramowicz[155], Y Abulaiti[120], B S Acharya[70a,70b,o], A Ackermann[64a], C Adam Bourdarios[4], L Adamczyk[87a], S V Addepalli[147], M J Addison[103], J Adelman[118], A Adiguzel[22c], T Adye[137], A A Affolder[139], Y Afik[41], M N Agaras[13], A Aggarwal[102], C Agheorghiesei[28c], F Ahmadov[40,ae], S Ahuja[97], X Ai[63e], G Aielli[77a,77b], A Aikot[168], M Ait Tamlihat[36e], B Aitbenchikh[36a], M Akbiyik[102], T P A Åkesson[100], A V Akimov[149], D Akiyama[173], N N Akolkar[25], S Aktas[22a], G L Alberghi[24b], J Albert[170], P Albicocco[54], G L Albouy[61], S Alderweireldt[53], Z L Alegria[124], M Aleksa[37], I N Aleksandrov[40], C Alexa[28b], T Alexopoulos[10], F Alfonsi[24b], M Algren[57], M Alhroob[172], B Ali[135], H M J Ali[93,x], S Ali[32], S W Alibocus[94], M Aliev[34c], G Alimonti[72a], W Alkakhi[56], C Allaire[67], B M M Allbrooke[150], J S Allen[103], J F Allen[53], P P Allport[21], A Aloisio[73a,73b], F Alonso[92], C Alpigiani[142], Z M K Alsolami[93], A Alvarez Fernandez[102], M Alves Cardoso[57], M G Alviggi[73a,73b], M Aly[103], Y Amaral Coutinho[84b], A Ambler[106], C Amelung[37], M Amerl[103], C G Ames[111], D Amidei[108], B Amini[55], K Amirie[159], A Amirkhanov[40], S P Amor Dos Santos[133a], K R Amos[168], D Amperiadou[156], S An[85], V Ananiev[128], C Anastopoulos[143], T Andeen[11], J K Anders[94], A C Anderson[60], A Andreazza[72a,72b], S Angelidakis[9], A Angerami[43], A V Anisenkov[40], A Annovi[75a],

C Antel[57], E Antipov[149], M Antonelli[54], F Anulli[76a], M Aoki[85], T Aoki[157], M A Aparo[150], L Aperio Bella[49], C Appelt[155], A Apyan[27], S J Arbiol Val[88], C Arcangeletti[54], A T H Arce[52], J-F Arguin[110], S Argyropoulos[156], J-H Arling[49], O Arnaez[4], H Arnold[149], G Artoni[76a,76b], H Asada[113], K Asai[121], S Asai[157], N A Asbah[37], R A Ashby Pickering[172], A M Aslam[97], K Assamagan[30], R Astalos[29a], K S V Astrand[100], S Atashi[163], R J Atkin[34a], H Atmani[36f], P A Atmasiddha[131], K Augsten[135], A D Auriol[42], V A Austrup[103], G Avolio[37], K Axiotis[57], G Azuelos[110,aj], D Babal[29b], H Bachacou[138], K Bachas[156,s], A Bachiu[35], E Bachmann[51], M J Backes[64a], A Badea[41], T M Baer[108], P Bagnaia[76a,76b], M Bahmani[19], D Bahner[55], K Bai[126], J T Baines[137], L Baines[96], O K Baker[177], E Bakos[16], D Bakshi Gupta[8], L E Balabram Filho[84b], V Balakrishnan[123], R Balasubramanian[4], E M Baldin[39], P Balek[87a], E Ballabene[24b,24a], F Balli[138], L M Baltes[64a], W K Balunas[33], J Balz[102], I Bamwidhi[119b], E Banas[88], M Bandieramonte[132], A Bandyopadhyay[25], S Bansal[25], L Barak[155], M Barakat[49], E L Barberio[107], D Barberis[58b,58a], M Barbero[104], M Z Barel[117], T Barillari[112], M-S Barisits[37], T Barklow[147], P Baron[125], D A Baron Moreno[103], A Baroncelli[63a], A J Barr[129], J D Barr[98], F Barreiro[101], J Barreiro Guimarães da Costa[14], M G Barros Teixeira[133a], S Barsov[39], F Bartels[64a], R Bartoldus[147], A E Barton[93], P Bartos[29a], A Basan[102], M Baselga[50], S Bashiri[88], A Bassalat[67,b], M J Basso[160a], S Bataju[46], R Bate[169], R L Bates[60], S Batlamous[101], M Battaglia[139], D Battulga[19], M Bauce[76a,76b], M Bauer[80], P Bauer[25], L T Bayer[49], L T Bazzano Hurrell[31], J B Beacham[112], T Beau[130], J Y Beaucamp[92], P H Beauchemin[162], P Bechtle[25], H P Beck[20,r], K Becker[172], A J Beddall[83], V A Bednyakov[40], C P Bee[149], L J Beemster[16], M Begalli[84d], M Begel[30], J K Behr[49], J F Beirer[37], F Beisiegel[25], M Belfkir[119b], G Bella[155], L Bellagamba[24b], A Bellerive[35], P Bellos[21], K Beloborodov[39], D Benchekroun[36a], F Bendebba[36a], Y Benhammou[155], K C Benkendorfer[62], L Beresford[49], M Beretta[54], E Bergeaas Kuutmann[166], N Berger[4], B Bergmann[135], J Beringer[18a], G Bernardi[5], C Bernius[147], F U Bernlochner[25], F Bernon[37], A Berrocal Guardia[13], T Berry[97], P Berta[136], A Berthold[51], S Bethke[112], A Betti[76a,76b], A J Bevan[96], N K Bhalla[55], S Bharthuar[112], S Bhatta[149], D S Bhattacharya[171], P Bhattarai[147], Z M Bhatti[120], K D Bhide[55], V S Bhopatkar[124], R M Bianchi[132], G Bianco[24b,24a], O Biebel[111], M Biglietti[78a], C S Billingsley[46], Y Bimgdi[36f], M Bindi[56], A Bingham[176], A Bingul[22b], C Bini[76a,76b], G A Bird[33], M Birman[174], M Biros[136], S Biryukov[150], T Bisanz[50], E Bisceglie[45b,45a], J P Biswal[137], D Biswas[145], I Bloch[49], A Blue[60], U Blumenschein[96], J Blumenthal[102], V S Bobrovnikov[40], M Boehler[55], B Boehm[171], D Bogavac[37], A G Bogdanchikov[39], L S Boggia[130], V Boisvert[97], P Bokan[37], T Bold[87a], M Bomben[5], M Bona[96], M Boonekamp[138], A G Borbély[60], I S Bordulev[39], G Borissov[93], D Bortoletto[129], D Boscherini[24b], M Bosman[13], K Bouaouda[36a], N Bouchhar[168], L Boudet[4], J Boudreau[132], E V Bouhova-Thacker[93], D Boumediene[42], R Bouquet[58b,58a], A Boveia[122], J Boyd[37], D Boye[30], I R Boyko[40], L Bozianu[57], J Bracinik[21], N Brahimi[4], G Brandt[176], O Brandt[33], B Brau[105], J E Brau[126], R Brener[174], L Brenner[117], R Brenner[166], S Bressler[174], G Brianti[79a,79b], D Britton[60], D Britzger[112], I Brock[25], R Brock[109], G Brooijmans[43], A J Brooks[69], E M Brooks[160b], E Brost[30], L M Brown[170,160a], L E Bruce[62], T L Bruckler[129], P A Bruckman de Renstrom[88], B Brüers[49], A Bruni[24b], G Bruni[24b], D Brunner[48a,48b], M Bruschi[24b], N Bruscino[76a,76b], T Buanes[17], Q Buat[142], D Buchin[112], A G Buckley[60], O Bulekov[39], B A Bullard[147], S Burdin[94], C D Burgard[50], A M Burger[37], B Burghgrave[8], O Burlayenko[55], J Burleson[167], J T P Burr[33], J C Burzynski[146], E L Busch[43], V Büscher[102], P J Bussey[60], J M Butler[26], C M Buttar[60], J M Butterworth[98], W Buttinger[137], C J Buxo Vazquez[109], A R Buzykaev[40], S Cabrera Urbán[168], L Cadamuro[67], D Caforio[59], H Cai[132], Y Cai[24b,114c,24a], Y Cai[114a], V M M Cairo[37], O Cakir[3a], N Calace[37], P Calafiura[18a], G Calderini[130], P Calfayan[35], G Callea[60], L P Caloba[84b], D Calvet[42], S Calvet[42], R Camacho Toro[130], S Camarda[37], D Camarero Munoz[27], P Camarri[77a,77b], M T Camerlingo[73a,73b], D Cameron[37], C Camincher[170], M Campanelli[98], A Camplani[44], V Canale[73a,73b], A C Canbay[3a], E Canonero[97], J Cantero[168], Y Cao[167], F Capocasa[27], M Capua[45b,45a], A Carbone[72a,72b], R Cardarelli[77a], J C J Cardenas[8], M P Cardiff[27], G Carducci[45b,45a], T Carli[37], G Carlino[73a], J I Carlotto[13], B T Carlson[132,t], E M Carlson[170], J Carmignani[94], L Carminati[72a,72b], A Carnelli[138], M Carnesale[37], S Caron[116], E Carquin[140f], I B Carr[107], S Carrá[72a], G Carratta[24b,24a], A M Carroll[126], M P Casado[13,i], M Caspar[49], F L Castillo[4], L Castillo Garcia[13], V Castillo Gimenez[168], N F Castro[133a,133e], A Catinaccio[37], J R Catmore[128], T Cavaliere[4], V Cavaliere[30], L J Caviedes Betancourt[23b], Y C Cekmecelioglu[49], E Celebi[83], S Cella[37], V Cepaitis[57], K Cerny[125], A S Cerqueira[84a], A Cerri[75a,75b], L Cerrito[77a,77b], F Cerutti[18a], B Cervato[145], A Cervelli[24b], G Cesarini[54], S A Cetin[83], P M Chabrillat[130], J Chan[18a], W Y Chan[157], J D Chapman[33], E Chapon[138], B Chargeishvili[153b], D G Charlton[21], C Chauhan[136],

Y Che[114a], S Chekanov[6], S V Chekulaev[160a], G A Chelkov[40,a], B Chen[155], B Chen[170], H Chen[114a], H Chen[30], J Chen[63c], J Chen[146], M Chen[129], S Chen[89], S J Chen[114a], X Chen[63c], X Chen[15,ai], C L Cheng[175], H C Cheng[65a], S Cheong[147], A Cheplakov[40], E Cheremushkina[49], E Cherepanova[117], R Cherkaoui El Moursli[36e], E Cheu[7], K Cheung[66], L Chevalier[138], V Chiarella[54], G Chiarelli[75a], N Chiedde[104], G Chiodini[71a], A S Chisholm[21], A Chitan[28b], M Chitishvili[168], M V Chizhov[40,u], K Choi[11], Y Chou[142], E Y S Chow[116], K L Chu[174], M C Chu[65a], X Chu[14,114c], Z Chubinidze[54], J Chudoba[134], J J Chwastowski[88], D Cieri[112], K M Ciesla[87a], V Cindro[95], A Ciocio[18a], F Cirotto[73a,73b], Z H Citron[174], M Citterio[72a], D A Ciubotaru[28b], A Clark[57], P J Clark[53], N Clarke Hall[98], C Clarry[159], S E Clawson[49], C Clement[48a,48b], Y Coadou[104], M Cobal[70a,70c], A Coccaro[58b], R F Coelho Barrue[133a], R Coelho Lopes De Sa[105], S Coelli[72a], L S Colangeli[159], B Cole[43], P Collado Soto[101], J Collot[61], P Conde Muiño[133a,133g], M P Connell[34c], S H Connell[34c], E I Conroy[129], F Conventi[73a,ak], H G Cooke[21], A M Cooper-Sarkar[129], F A Corchia[24b,24a], A Cordeiro Oudot Choi[130], L D Corpe[42], M Corradi[76a,76b], F Corriveau[106,ac], A Cortes-Gonzalez[19], M J Costa[168], F Costanza[4], D Costanzo[143], B M Cote[122], J Couthures[4], G Cowan[97], K Cranmer[175], L Cremer[50], D Cremonini[24b,24a], S Crépé-Renaudin[61], F Crescioli[130], M Cristinziani[145], M Cristoforetti[79a,79b], V Croft[117], J E Crosby[124], G Crosetti[45b,45a], A Cueto[101], H Cui[98], Z Cui[7], W R Cunningham[60], F Curcio[168], J R Curran[53], P Czodrowski[37], M J Da Cunha Sargedas De Sousa[58b,58a], J V Da Fonseca Pinto[84b], C Da Via[103], W Dabrowski[87a], T Dado[37], S Dahbi[152], T Dai[108], D Dal Santo[20], C Dallapiccola[105], M Dam[44], G D'amen[30], V D'Amico[111], J Damp[102], J R Dandoy[35], D Dannheim[37], M Danninger[146], V Dao[149], G Darbo[58b], S J Das[30], F Dattola[49], S D'Auria[72a,72b], A D'Avanzo[73a,73b], T Davidek[136], I Dawson[96], H A Day-hall[135], K De[8], C De Almeida Rossi[159], R De Asmundis[73a], N De Biase[49], S De Castro[24b,24a], N De Groot[116], P de Jong[117], H De la Torre[118], A De Maria[114a], A De Salvo[76a], U De Sanctis[77a,77b], F De Santis[71a,71b], A De Santo[150], J B De Vivie De Regie[61], J Debevc[95], D V Dedovich[40], J Degens[94], A M Deiana[46], J Del Peso[101], L Delagrange[130], F Deliot[138], C M Delitzsch[50], M Della Pietra[73a,73b], D Della Volpe[57], A Dell'Acqua[37], L Dell'Asta[72a,72b], M Delmastro[4], C C Delogu[102], P A Delsart[61], S Demers[177], M Demichev[40], S P Denisov[39], H Denizli[22a,m], L D'Eramo[42], D Derendarz[88], F Derue[130], P Dervan[94], K Desch[25], C Deutsch[25], F A Di Bello[58b,58a], A Di Ciaccio[77a,77b], L Di Ciaccio[4], A Di Domenico[76a,76b], C Di Donato[73a,73b], A Di Girolamo[37], G Di Gregorio[37], A Di Luca[79a,79b], B Di Micco[78a,78b], R Di Nardo[78a,78b], K F Di Petrillo[41], M Diamantopoulou[35], F A Dias[117], T Dias Do Vale[146], M A Diaz[140a,140b], A R Didenko[40], M Didenko[168], E B Diehl[108], S Díez Cornell[49], C Diez Pardos[145], C Dimitriadi[148], A Dimitrievska[21], A Dimri[149], J Dingfelder[25], T Dingley[129], I-M Dinu[28b], S J Dittmeier[64b], F Dittus[37], M Divisek[136], B Dixit[94], F Djama[104], T Djobava[153b], C Doglioni[103,100], A Dohnalova[29a], Z Dolezal[136], K Domijan[87a], K M Dona[41], M Donadelli[84d], B Dong[109], J Donini[42], A D'Onofrio[73a,73b], M D'Onofrio[94], J Dopke[137], A Doria[73a], N Dos Santos Fernandes[133a], P Dougan[103], M T Dova[92], A T Doyle[60], M A Draguet[129], M P Drescher[56], E Dreyer[174], I Drivas-koulouris[10], M Drnevich[120], M Drozdova[57], D Du[63a], T A du Pree[117], F Dubinin[39], M Dubovsky[29a], E Duchovni[174], G Duckeck[111], O A Ducu[28b], D Duda[53], A Dudarev[37], E R Duden[27], M D'uffizi[103], L Duflot[67], M Dührssen[37], I Duminica[28g], A E Dumitriu[28b], M Dunford[64a], S Dungs[50], K Dunne[48a,48b], A Duperrin[104], H Duran Yildiz[3a], M Düren[59], A Durglishvili[153b], D Duvnjak[35], B L Dwyer[118], G I Dyckes[18a], M Dyndal[87a], B S Dziedzic[37], Z O Earnshaw[150], G H Eberwein[129], B Eckerova[29a], S Eggebrecht[56], E Egidio Purcino De Souza[84e], G Eigen[17], K Einsweiler[18a], T Ekelof[166], P A Ekman[100], S El Farkh[36b], Y El Ghazali[63a], H El Jarrari[37], A El Moussaouy[36a], V Ellajosyula[166], M Ellert[166], F Ellinghaus[176], N Ellis[37], J Elmsheuser[30], M Elsawy[119a], M Elsing[37], D Emeliyanov[137], Y Enari[85], I Ene[18a], S Epari[13], D Ernani Martins Neto[88], M Errenst[176], M Escalier[67], C Escobar[168], E Etzion[155], G Evans[133a,133b], H Evans[69], L S Evans[97], A Ezhilov[39], S Ezzarqtouni[36a], F Fabbri[24b,24a], L Fabbri[24b,24a], G Facini[98], V Fadeyev[139], R M Fakhrutdinov[39], D Fakoudis[102], S Falciano[76a], L F Falda Ulhoa Coelho[133a], F Fallavollita[112], G Falsetti[45b,45a], J Faltova[136], C Fan[167], K Y Fan[65b], Y Fan[14], Y Fang[14,114c], M Fanti[72a,72b], M Faraj[70a,70b], Z Farazpay[99], A Farbin[8], A Farilla[78a], T Farooque[109], J N Farr[177], S M Farrington[137,53], F Fassi[36e], D Fassouliotis[9], L Fayard[67], P Federic[136], P Federicova[134], O L Fedin[39,a], M Feickert[175], L Feligioni[104], D E Fellers[126], C Feng[63b], Z Feng[117], M J Fenton[163], L Ferencz[49], P Fernandez Martinez[68], M J V Fernoux[104], J Ferrando[93], A Ferrari[166], P Ferrari[117,116], R Ferrari[74a], D Ferrere[57], C Ferretti[108], M P Fewell[1], D Fiacco[76a,76b], F Fiedler[102], P Fiedler[135], S Filimonov[39], A Filipčič[95], E K Filmer[160a], F Filthaut[116],

M C N Fiolhais[133a,133c,c], L Fiorini[168], W C Fisher[109], T Fitschen[103], P M Fitzhugh[138], I Fleck[145], P Fleischmann[108], T Flick[176], M Flores[34d,ag], L R Flores Castillo[65a], L Flores Sanz De Acedo[37], F M Follega[79a,79b], N Fomin[33], J H Foo[159], A Formica[138], A C Forti[103], E Fortin[37], A W Fortman[18a], L Fountas[9,k], D Fournier[67], H Fox[93], P Francavilla[75a,75b], S Francescato[62], S Franchellucci[57], M Franchini[24b,24a], S Franchino[64a], D Francis[37], L Franco[116], V Franco Lima[37], L Franconi[49], M Franklin[62], G Frattari[27], Y Y Frid[155], J Friend[60], N Fritzsche[37], A Froch[57], D Froidevaux[37], J A Frost[129], Y Fu[109], S Fuenzalida Garrido[140f], M Fujimoto[104], K Y Fung[65a], E Furtado De Simas Filho[84e], M Furukawa[157], J Fuster[168], A Gaa[56], A Gabrielli[24b,24a], A Gabrielli[159], P Gadow[37], G Gagliardi[58b,58a], L G Gagnon[18a], S Gaid[165], S Galantzan[155], J Gallagher[1], E J Gallas[129], A L Gallen[166], B J Gallop[137], K K Gan[122], S Ganguly[157], Y Gao[53], A Garabaglu[142], F M Garay Walls[140a,140b], B Garcia[30], C García[168], A Garcia Alonso[117], A G Garcia Caffaro[177], J E García Navarro[168], M Garcia-Sciveres[18a], G L Gardner[131], R W Gardner[41], N Garelli[162], R B Garg[147], J M Gargan[53], C A Garner[159], C M Garvey[34a], V K Gassmann[162], G Gaudio[74a], V Gautam[13], P Gauzzi[76a,76b], J Gavranovic[95], I L Gavrilenko[39], A Gavrilyuk[39], C Gay[169], G Gaycken[126], E N Gazis[10], A Gekow[122], C Gemme[58b], M H Genest[61], A D Gentry[115], S George[97], W F George[21], T Geralis[47], A A Gerwin[123], P Gessinger-Befurt[37], M E Geyik[176], M Ghani[172], K Ghorbanian[96], A Ghosal[145], A Ghosh[163], A Ghosh[7], B Giacobbe[24b], S Giagu[76a,76b], T Giani[117], A Giannini[63a], S M Gibson[97], M Gignac[139], D T Gil[87b], A K Gilbert[87a], B J Gilbert[43], D Gillberg[35], G Gilles[117], L Ginabat[130], D M Gingrich[2,aj], M P Giordani[70a,70c], P F Giraud[138], G Giugliarelli[70a,70c], D Giugni[72a], F Giuli[77a,77b], I Gkialas[9,k], L K Gladilin[39], C Glasman[101], G Glemža[49], M Glisic[126], I Gnesi[45b], Y Go[30], M Goblirsch-Kolb[37], B Gocke[50], D Godin[110], B Gokturk[22a], S Goldfarb[107], T Golling[57], M G D Gololo[34c], D Golubkov[39], J P Gombas[109], A Gomes[133a,133b], G Gomes Da Silva[145], A J Gomez Delegido[168], R Gonçalo[133a], L Gonella[21], A Gongadze[153c], F Gonnella[21], J L Gonski[147], R Y González Andana[53], S González de la Hoz[168], R Gonzalez Lopez[94], C Gonzalez Renteria[18a], M V Gonzalez Rodrigues[49], R Gonzalez Suarez[166], S Gonzalez-Sevilla[57], L Goossens[37], B Gorini[37], E Gorini[71a,71b], A Gorišek[95], T C Gosart[131], A T Goshaw[52], M I Gostkin[40], S Goswami[124], C A Gottardo[37], S A Gotz[111], M Gouighri[36b], A G Goussiou[142], N Govender[34c], R P Grabarczyk[129], I Grabowska-Bold[87a], K Graham[35], E Gramstad[128], S Grancagnolo[71a,71b], C M Grant[1,138], P M Gravila[28f], F G Gravili[71a,71b], H M Gray[18a], M Greco[112], M J Green[1], C Grefe[25], A S Grefsrud[17], I M Gregor[49], K T Greif[163], P Grenier[147], S G Grewe[112], A A Grillo[139], K Grimm[32], S Grinstein[13,y], J-F Grivaz[67], E Gross[174], J Grosse-Knetter[56], L Guan[108], G Guerrieri[37], R Gugel[102], J A M Guhit[108], A Guida[19], E Guilloton[172], S Guindon[37], F Guo[14,114c], J Guo[63c], L Guo[49], L Guo[114b,w], Y Guo[108], A Gupta[50], R Gupta[132], S Gurbuz[25], S S Gurdasani[49], G Gustavino[76a,76b], P Gutierrez[123], L F Gutierrez Zagazeta[131], M Gutsche[51], C Gutschow[98], C Gwenlan[129], C B Gwilliam[94], E S Haaland[128], A Haas[120], M Habedank[60], C Haber[18a], H K Hadavand[8], A Haddad[42], A Hadef[51], A I Hagan[93], J J Hahn[145], E H Haines[98], M Haleem[171], J Haley[124], G D Hallewell[104], L Halser[20], K Hamano[170], M Hamer[25], E J Hampshire[97], J Han[63b], L Han[114a], L Han[63a], S Han[18a], K Hanagaki[85], M Hance[139], D A Hangal[43], H Hanif[146], M D Hank[131], J B Hansen[44], P H Hansen[44], D Harada[57], T Harenberg[176], S Harkusha[178], M L Harris[105], Y T Harris[25], J Harrison[13], N M Harrison[122], P F Harrison[172], N M Hartman[112], N M Hartmann[111], R Z Hasan[97,137], Y Hasegawa[144], F Haslbeck[129], S Hassan[17], R Hauser[109], C M Hawkes[21], R J Hawkings[37], Y Hayashi[157], D Hayden[109], C Hayes[108], R L Hayes[117], C P Hays[129], J M Hays[96], H S Hayward[94], F He[63a], M He[14,114c], Y He[49], Y He[98], N B Heatley[96], V Hedberg[100], A L Heggelund[128], C Heidegger[55], K K Heidegger[55], J Heilman[35], S Heim[49], T Heim[18a], J G Heinlein[131], J J Heinrich[126], L Heinrich[112,ah], J Hejbal[134], A Held[175], S Hellesund[17], C M Helling[169], S Hellman[48a,48b], L Henkelmann[33], A M Henriques Correia[37], H Herde[100], Y Hernández Jiménez[149], L M Herrmann[25], T Herrmann[51], G Herten[55], R Hertenberger[111], L Hervas[37], M E Hesping[102], N P Hessey[160a], J Hessler[112], M Hidaoui[36b], N Hidic[136], E Hill[159], S J Hillier[21], J R Hinds[109], F Hinterkeuser[25], M Hirose[127], S Hirose[161], D Hirschbuehl[176], T G Hitchings[103], B Hiti[95], J Hobbs[149], R Hobincu[28e], N Hod[174], M C Hodgkinson[143], B H Hodkinson[129], A Hoecker[37], D D Hofer[108], J Hofer[168], M Holzbock[37], L B A H Hommels[33], B P Honan[103], J J Hong[69], J Hong[63c], T M Hong[132], B H Hooberman[167], W H Hopkins[6], M C Hoppesch[167], Y Horii[113], M E Horstmann[112], S Hou[152], M R Housenga[167], A S Howard[95], J Howarth[60], J Hoya[6], M Hrabovsky[125], T Hryn'ova[4], P J Hsu[66], S-C Hsu[142], T Hsu[67], M Hu[18a], Q Hu[63a], S Huang[33], X Huang[14,114c], Y Huang[136], Y Huang[114b], Y Huang[102], Y Huang[14], Z Huang[103], Z Hubacek[135], M Huebner[25], F Huegging[25], T B Huffman[129],

M Hufnagel Maranha De Faria[84a], C A Hugli[49], M Huhtinen[37], S K Huiberts[17], R Hulsken[106], C E Hultquist[18a], N Huseynov[12,g], J Huston[109], J Huth[62], R Hyneman[7], G Iacobucci[57], G Iakovidis[30], L Iconomidou-Fayard[67], J P Iddon[37], P Iengo[73a,73b], R Iguchi[157], Y Iiyama[157], T Iizawa[129], Y Ikegami[85], D Iliadis[156], N Ilic[159], H Imam[84c], G Inacio Goncalves[84d], S A Infante Cabanas[140c], T Ingebretsen Carlson[48a,48b], J M Inglis[96], G Introzzi[74a,74b], M Iodice[78a], V Ippolito[76a,76b], R K Irwin[94], M Ishino[157], W Islam[175], C Issever[19], S Istin[22a,ao], H Ito[173], R Iuppa[79a,79b], A Ivina[174], V Izzo[73a], P Jacka[134], P Jackson[1], P Jain[49], K Jakobs[55], T Jakoubek[174], J Jamieson[60], W Jang[157], M Javurkova[105], P Jawahar[103], L Jeanty[126], J Jejelava[153a,af], P Jenni[55,f], C E Jessiman[35], C Jia[63b], H Jia[169], J Jia[149], X Jia[14,114c], Z Jia[114a], C Jiang[53], Q Jiang[65b], S Jiggins[49], J Jimenez Pena[13], S Jin[114a], A Jinaru[28b], O Jinnouchi[141], P Johansson[143], K A Johns[7], J W Johnson[139], F A Jolly[49], D M Jones[150], E Jones[49], K S Jones[8], P Jones[33], R W L Jones[93], T J Jones[94], H L Joos[56,37], R Joshi[122], J Jovicevic[16], X Ju[18a], J J Junggeburth[37], T Junkermann[64a], A Juste Rozas[13,y], M K Juzek[88], S Kabana[140e], A Kaczmarska[88], M Kado[112], H Kagan[122], M Kagan[147], A Kahn[131], C Kahra[102], T Kaji[157], E Kajomovitz[154], N Kakati[174], I Kalaitzidou[55], N J Kang[139], D Kar[34g], K Karava[129], E Karentzos[25], O Karkout[117], S N Karpov[40], Z M Karpova[40], V Kartvelishvili[93], A N Karyukhin[39], E Kasimi[156], J Katzy[49], S Kaur[35], K Kawade[144], M P Kawale[123], C Kawamoto[89], T Kawamoto[63a], E F Kay[37], F I Kaya[162], S Kazakos[109], V F Kazanin[39], Y Ke[149], J M Keaveney[34a], R Keeler[170], G V Kehris[62], J S Keller[35], J J Kempster[150], O Kepka[134], J Kerr[160b], B P Kerridge[137], B P Kerševan[95], L Keszeghova[29a], R A Khan[132], A Khanov[124], A G Kharlamov[39], T Kharlamova[39], E E Khoda[142], M Kholodenko[133a], T J Khoo[19], G Khoriauli[171], J Khubua[153b,†], Y A R Khwaira[130], B Kibirige[34g], D Kim[6], D W Kim[48a,48b], Y K Kim[41], N Kimura[98], M K Kingston[56], A Kirchhoff[56], C Kirfel[25], F Kirfel[25], J Kirk[137], A E Kiryunin[112], S Kita[161], C Kitsaki[10], O Kivernyk[25], M Klassen[162], C Klein[35], L Klein[171], M H Klein[46], S B Klein[57], U Klein[94], A Klimentov[30], T Klioutchnikova[37], P Kluit[117], S Kluth[112], E Kneringer[80], T M Knight[159], A Knue[50], M Kobel[51], D Kobylianskii[174], S F Koch[129], M Kocian[147], P Kodyš[136], D M Koeck[126], P T Koenig[25], T Koffas[35], O Kolay[51], I Koletsou[4], T Komarek[88], K Köneke[56], A X Y Kong[1], T Kono[121], N Konstantinidis[98], P Kontaxakis[57], B Konya[100], R Kopeliansky[43], S Koperny[87a], K Korcyl[88], K Kordas[156,e], A Korn[98], S Korn[56], I Korolkov[13], N Korotkova[39], B Kortman[117], O Kortner[112], S Kortner[112], W H Kostecka[118], V V Kostyukhin[145], A Kotsokechagia[37], A Kotwal[52], A Koulouris[37], A Kourkoumeli-Charalampidi[74a,74b], C Kourkoumelis[9], E Kourlitis[112], O Kovanda[126], R Kowalewski[170], W Kozanecki[126], A S Kozhin[39], V A Kramarenko[39], G Kramberger[95], P Kramer[25], M W Krasny[130], A Krasznahorkay[105], A C Kraus[118], J W Kraus[176], J A Kremer[49], T Kresse[51], L Kretschmann[176], J Kretzschmar[94], K Kreul[19], P Krieger[159], K Krizka[21], K Kroeninger[50], H Kroha[112], J Kroll[134], J Kroll[131], K S Krowpman[109], U Kruchonak[40], H Krüger[25], N Krumnack[82], M C Kruse[52], O Kuchinskaia[39], S Kuday[3a], S Kuehn[37], R Kuesters[55], T Kuhl[49], V Kukhtin[40], Y Kulchitsky[40], S Kuleshov[140d,140b], M Kumar[34g], N Kumari[49], P Kumari[160b], A Kupco[134], T Kupfer[50], A Kupich[39], O Kuprash[55], H Kurashige[86], L L Kurchaninov[160a], O Kurdysh[4], Y A Kurochkin[38], A Kurova[39], M Kuze[141], A K Kvam[105], J Kvita[125], N G Kyriacou[108], L A O Laatu[104], C Lacasta[168], F Lacava[76a,76b], H Lacker[19], D Lacour[130], N N Lad[98], E Ladygin[40], A Lafarge[42], B Laforge[130], T Lagouri[177], F Z Lahbabi[36a], S Lai[56], J E Lambert[170], S Lammers[69], W Lampl[7], C Lampoudis[156,e], G Lamprinoudis[102], A N Lancaster[118], E Lançon[30], U Landgraf[55], M P J Landon[96], V S Lang[55], O K B Langrekken[128], A J Lankford[163], F Lanni[37], K Lantzsch[25], A Lanza[74a], M Lanzac Berrocal[168], J F Laporte[138], T Lari[72a], F Lasagni Manghi[24b], M Lassnig[37], V Latonova[134], S D Lawlor[143], Z Lawrence[103], R Lazaridou[172], M Lazzaroni[72a,72b], H D M Le[109], E M Le Boulicaut[177], L T Le Pottier[18a], B Leban[24b,24a], M LeBlanc[103], F Ledroit-Guillon[61], S C Lee[152], T F Lee[94], L L Leeuw[34c,am], M Lefebvre[170], C Leggett[18a], G Lehmann Miotto[37], M Leigh[57], W A Leight[105], W Leinonen[116], A Leisos[156,v], M A L Leite[84c], C E Leitgeb[19], R Leitner[136], K J C Leney[46], T Lenz[25], S Leone[75a], C Leonidopoulos[53], A Leopold[148], J H Lepage Bourbonnais[35], R Les[109], C G Lester[33], M Levchenko[39], J Levêque[4], L J Levinson[174], G Levrini[24b,24a], M P Lewicki[88], C Lewis[142], D J Lewis[4], L Lewitt[143], A Li[30], B Li[63b], C Li[108], C-Q Li[112], H Li[63a], H Li[63b], H Li[103], H Li[15], H Li[63a], H Li[63b], J Li[63c], K Li[14], L Li[63c], R Li[177], S Li[14,114c], S Li[63d,63c,d], T Li[5], X Li[106], Z Li[157], Z Li[14,114c], Z Li[63a], S Liang[14,114c], Z Liang[14], M Liberatore[138], B Liberti[77a], K Lie[65c], J Lieber Marin[84e], H Lien[69], H Lin[108], L Linden[111], R E Lindley[7], J H Lindon[2], J Ling[62], E Lipeles[131], A Lipniacka[17], A Lister[169], J D Little[69], B Liu[14], B X Liu[114b], D Liu[63d,63c], E H L Liu[21], J K K Liu[33], K Liu[63d], K Liu[63d,63c], M Liu[63a], M Y Liu[63a], P Liu[14], Q Liu[63d,142,63c], X Liu[63a], X Liu[63b], Y Liu[114b,114c], Y L Liu[63b], Y W Liu[63a], S L Lloyd[96], E M Lobodzinska[49], P Loch[7], E Lodhi[159], T Lohse[19], K Lohwasser[143],

E Loiacono[49], J D Lomas[21], J D Long[43], I Longarini[163], R Longo[167], A Lopez Solis[49], N A Lopez-canelas[7], N Lorenzo Martinez[4], A M Lory[111], M Losada[119a], G Löschcke Centeno[150], O Loseva[39], X Lou[48a,48b], X Lou[14,114c], A Lounis[67], G C Louppe[j], P A Love[93], G Lu[14,114c], M Lu[67], S Lu[131], Y J Lu[152], H J Lubatti[142], C Luci[76a,76b], F L Lucio Alves[114a], F Luehring[69], B S Lunday[131], O Lundberg[148], B Lund-Jensen[148,†], N A Luongo[6], M S Lutz[37], A B Lux[26], D Lynn[30], R Lysak[134], E Lytken[100], V Lyubushkin[40], T Lyubushkina[40], M M Lyukova[149], M Firdaus M Soberi[53], H Ma[30], K Ma[63a], L L Ma[63b], W Ma[63a], Y Ma[124], J C MacDonald[102], P C Machado De Abreu Farias[84e], R Madar[42], T Madula[98], J Maeda[86], T Maeno[30], P T Mafa[34c,l], H Maguire[143], V Maiboroda[138], A Maio[133a,133b,133d], K Maj[87a], O Majersky[49], S Majewski[126], R Makhmanazarov[39], N Makovec[67], V Maksimovic[16], B Malaescu[130], Pa Malecki[88], V P Maleev[39], F Malek[61,q], M Mali[95], D Malito[97], U Mallik[81,†], S Maltezos[10], S Malyukov[40], J Mamuzic[13], G Mancini[54], M N Mancini[27], G Manco[74a,74b], J P Mandalia[96], S S Mandarry[150], I Mandić[95], L Manhaes de Andrade Filho[84a], I M Maniatis[174], J Manjarres Ramos[91], D C Mankad[174], A Mann[111], S Manzoni[37], L Mao[63c], X Mapekula[34c], A Marantis[156,v], G Marchiori[5], M Marcisovsky[134], C Marcon[72a], M Marinescu[21], S Marium[49], M Marjanovic[123], A Markhoos[55], M Markovitch[67], M K Maroun[105], E J Marshall[93], Z Marshall[18a], S Marti-Garcia[168], J Martin[98], T A Martin[137], V J Martin[53], B Martin dit Latour[17], L Martinelli[76a,76b], M Martinez[13,y], P Martinez Agullo[168], V I Martinez Outschoorn[105], P Martinez Suarez[13], S Martin-Haugh[137], G Martinovicova[136], V S Martoiu[28b], A C Martyniuk[98], A Marzin[37], D Mascione[79a,79b], L Masetti[102], J Masik[103], A L Maslennikov[40], S L Mason[43], P Massarotti[73a,73b], P Mastrandrea[75a,75b], A Mastroberardino[45b,45a], T Masubuchi[127], T T Mathew[126], J Matousek[136], D M Mattern[50], J Maurer[28b], T Maurin[60], A J Maury[67], B Maček[95], D A Maximov[39], A E May[103], E Mayer[42], R Mazini[34g], I Maznas[118], M Mazza[109], S M Mazza[139], E Mazzeo[72a,72b], J P Mc Gowan[170], S P Mc Kee[108], C A Mc Lean[6], C C McCracken[169], E F McDonald[107], A E McDougall[117], L F Mcelhinney[93], J A Mcfayden[150], R P McGovern[131], R P Mckenzie[34g], T C Mclachlan[49], D J Mclaughlin[98], S J McMahon[137], C M Mcpartland[94], R A McPherson[170,ac], S Mehlhase[111], A Mehta[94], D Melini[168], B R Mellado Garcia[34g], A H Melo[56], F Meloni[49], A M Mendes Jacques Da Costa[103], H Y Meng[159], L Meng[93], S Menke[112], M Mentink[37], E Meoni[45b,45a], G Mercado[118], S Merianos[156], C Merlassino[70a,70c], C Meroni[72a,72b], J Metcalfe[6], A S Mete[6], E Meuser[102], C Meyer[69], J-P Meyer[138], R P Middleton[137], L Mijović[53], G Mikenberg[174], M Mikestikova[134], M Mikuž[95], H Mildner[102], A Milic[37], D W Miller[41], E H Miller[147], L S Miller[35], A Milov[174], D A Milstead[48a,48b], T Min[114a], A A Minaenko[39], I A Minashvili[153b], A I Mincer[120], B Mindur[87a], M Mineev[40], Y Mino[89], L M Mir[13], M Miralles Lopez[60], M Mironova[18a], M C Missio[116], A Mitra[172], V A Mitsou[168], Y Mitsumori[113], O Miu[159], P S Miyagawa[96], T Mkrtchyan[64a], M Mlinarevic[98], T Mlinarevic[98], M Mlynarikova[37], S Mobius[20], P Mogg[111], M H Mohamed Farook[115], A F Mohammed[14,114c], S Mohapatra[43], S Mohiuddin[124], G Mokgatitswane[34g], L Moleri[174], B Mondal[145], S Mondal[135], K Mönig[49], E Monnier[104], L Monsonis Romero[168], J Montejo Berlingen[13], A Montella[48a,48b], M Montella[122], F Montereali[78a,78b], F Monticelli[92], S Monzani[70a,70c], A Morancho Tarda[44], N Morange[67], A L Moreira De Carvalho[49], M Moreno Llácer[168], C Moreno Martinez[57], J M Moreno Perez[23b], P Morettini[58b], S Morgenstern[37], M Morii[62], M Morinaga[157], M Moritsu[90], F Morodei[76a,76b], P Moschovakos[37], B Moser[129], M Mosidze[153b], T Moskalets[46], P Moskvitina[116], J Moss[32,n], P Moszkowicz[87a], A Moussa[36d], Y Moyal[174], E J W Moyse[105], O Mtintsilana[34g], S Muanza[104], J Mueller[132], R Müller[37], G A Mullier[166], A J Mullin[33], J J Mullin[52], A E Mulski[62], D P Mungo[159], D Munoz Perez[168], F J Munoz Sanchez[103], M Murin[103], W J Murray[172,137], M Muškinja[95], C Mwewa[30], A G Myagkov[39,a], A J Myers[8], G Myers[108], M Myska[135], B P Nachman[18a], K Nagai[129], K Nagano[85], R Nagasaka[157], J L Nagle[30,al], E Nagy[104], A M Nairz[37], Y Nakahama[85], K Nakamura[85], K Nakkalil[5], H Nanjo[127], E A Narayanan[46], Y Narukawa[157], I Naryshkin[39], L Nasella[72a,72b], S Nasri[119b], C Nass[25], G Navarro[23a], J Navarro-Gonzalez[168], A Nayaz[19], P Y Nechaeva[39], S Nechaeva[24b,24a], F Nechansky[134], L Nedic[129], T J Neep[21], A Negri[74a,74b], M Negrini[24b], C Nellist[117], C Nelson[106], K Nelson[108], S Nemecek[134], M Nessi[37,h], M S Neubauer[167], F Neuhaus[102], J Newell[94], P R Newman[21], Y W Y Ng[167], B Ngair[119a], H D N Nguyen[110], R B Nickerson[129], R Nicolaidou[138], J Nielsen[139], M Niemeyer[56], J Niermann[37], N Nikiforou[37], V Nikolaenko[39,a], I Nikolic-Audit[130], P Nilsson[30], I Ninca[49], G Ninio[155], A Nisati[76a], N Nishu[2], R Nisius[112], N Nitika[70a,70c], J-E Nitschke[51], E K Nkadimeng[34g], T Nobe[157], T Nommensen[151], M B Norfolk[143], B J Norman[35], M Noury[36a], J Novak[95], T Novak[95], R Novotny[115], L Nozka[125], K Ntekas[163], N M J Nunes De Moura Junior[84b], J Ocariz[130], A Ochi[86], I Ochoa[133a], S Oerdek[49,z], J T Offermann[41], A Ogrodnik[136], A Oh[103], C C Ohm[148], H Oide[85], R Oishi[157], M L Ojeda[37],

Y Okumura[157], L F Oleiro Seabra[133a], I Oleksiyuk[57], S A Olivares Pino[140d], G Oliveira Correa[13], D Oliveira Damazio[30], J L Oliver[163], Ö O Öncel[55], A P O'Neill[20], A Onofre[133a,133e], P U E Onyisi[11], M J Oreglia[41], D Orestano[78a,78b], R S Orr[159], L M Osojnak[131], Y Osumi[113], G Otero y Garzon[31], H Otono[90], G J Ottino[18a], M Ouchrif[36d], F Ould-Saada[128], T Ovsiannikova[142], M Owen[60], R E Owen[137], V E Ozcan[22a], F Ozturk[88], N Ozturk[8], S Ozturk[83], H A Pacey[129], K Pachal[160a], A Pacheco Pages[13], C Padilla Aranda[13], G Padovano[76a,76b], S Pagan Griso[18a], G Palacino[69], A Palazzo[71a,71b], J Pampel[25], J Pan[177], T Pan[65a], D K Panchal[11], C E Pandini[117], J G Panduro Vazquez[137], H D Pandya[1], H Pang[138], P Pani[49], G Panizzo[70a,70c], L Panwar[130], L Paolozzi[57], S Parajuli[167], A Paramonov[6], C Paraskevopoulos[54], D Paredes Hernandez[65b], A Pareti[74a,74b], K R Park[43], T H Park[112], F Parodi[58b,58a], J A Parsons[43], U Parzefall[55], B Pascual Dias[42], L Pascual Dominguez[101], E Pasqualucci[76a], S Passaggio[58b], F Pastore[97], P Patel[88], U M Patel[52], J R Pater[103], T Pauly[37], F Pauwels[136], C I Pazos[162], M Pedersen[128], R Pedro[133a], S V Peleganchuk[39], O Penc[37], E A Pender[53], S Peng[15], G D Penn[177], K E Penski[111], M Penzin[39], B S Peralva[84d], A P Pereira Peixoto[142], L Pereira Sanchez[147], D V Perepelitsa[30,al], G Perera[105], E Perez Codina[160a], M Perganti[10], H Pernegger[37], S Perrella[76a,76b], O Perrin[42], K Peters[49], R F Y Peters[103], B A Petersen[37], T C Petersen[44], E Petit[104], V Petousis[135], C Petridou[156,e], T Petru[136], A Petrukhin[145], M Pettee[18a], A Petukhov[83], K Petukhova[37], R Pezoa[140f], L Pezzotti[24b,24a], G Pezzullo[177], L Pfaffenbichler[37], A J Pfleger[37], T M Pham[175], T Pham[107], P W Phillips[137], G Piacquadio[149], E Pianori[18a], F Piazza[126], R Piegaia[31], D Pietreanu[28b], A D Pilkington[103], M Pinamonti[70a,70c], J L Pinfold[2], B C Pinheiro Pereira[133a], J Pinol Bel[13], A E Pinto Pinoargote[138], L Pintucci[70a,70c], K M Piper[150], A Pirttikoski[57], D A Pizzi[35], L Pizzimento[65b], M-A Pleier[30], V Pleskot[136], E Plotnikova[40], G Poddar[96], R Poettgen[100], L Poggioli[130], S Polacek[136], G Polesello[74a], A Poley[146,160a], A Polini[24b], C S Pollard[172], Z B Pollock[122], E Pompa Pacchi[123], N I Pond[98], D Ponomarenko[69], L Pontecorvo[37], S Popa[28a], G A Popeneciu[28d], A Poreba[37], D M Portillo Quintero[160a], S Pospisil[135], M A Postill[143], P Postolache[28c], K Potamianos[172], P A Potepa[87a], I N Potrap[40], C J Potter[33], H Potti[151], J Poveda[168], M E Pozo Astigarraga[37], A Prades Ibanez[77a,77b], J Pretel[170], D Price[103], M Primavera[71a], L Primomo[70a,70c], M A Principe Martin[101], R Privara[125], T Procter[60], M L Proffitt[142], N Proklova[131], K Prokofiev[65c], G Proto[112], J Proudfoot[6], M Przybycien[87a], W W Przygoda[87b], A Psallidas[47], J E Puddefoot[143], D Pudzha[55], D Pyatiizbyantseva[116], J Qian[108], R Qian[109], D Qichen[103], Y Qin[13], T Qiu[53], A Quadt[56], M Queitsch-Maitland[103], G Quetant[57], R P Quinn[169], G Rabanal Bolanos[62], D Rafanoharana[55], F Raffaeli[77a,77b], F Ragusa[72a,72b], J L Rainbolt[41], J A Raine[57], S Rajagopalan[30], E Ramakoti[39], L Rambelli[58b,58a], I A Ramirez-Berend[35], K Ran[49,114c], D S Rankin[131], N P Rapheeha[34g], H Rasheed[28b], V Raskina[130], D F Rassloff[64a], A Rastogi[18a], S Rave[102], S Ravera[58b,58a], B Ravina[37], I Ravinovich[174], M Raymond[37], A L Read[128], N P Readioff[143], D M Rebuzzi[74a,74b], A S Reed[112], K Reeves[27], J A Reidelsturz[176], D Reikher[126], A Rej[50], C Rembser[37], H Ren[63a], M Renda[28b], F Renner[49], A G Rennie[163], A L Rescia[49], S Resconi[72a], M Ressegotti[58b,58a], S Rettie[37], W F Rettie[35], J G Reyes Rivera[109], E Reynolds[18a], O L Rezanova[40], P Reznicek[136], H Riani[36d], N Ribaric[52], E Ricci[79a,79b], R Richter[112], S Richter[48a,48b], E Richter-Was[87b], M Ridel[130], S Ridouani[36d], P Rieck[120], P Riedler[37], E M Riefel[48a,48b], J O Rieger[117], M Rijssenbeek[149], M Rimoldi[37], L Rinaldi[24b,24a], P Rincke[56], G Ripellino[166], I Riu[13], J C Rivera Vergara[170], F Rizatdinova[124], E Rizvi[96], B R Roberts[18a], S S Roberts[139], D Robinson[33], M Robles Manzano[102], A Robson[60], A Rocchi[77a,77b], C Roda[75a,75b], S Rodriguez Bosca[37], Y Rodriguez Garcia[23a], A M Rodríguez Vera[118], S Roe[37], J T Roemer[37], O Røhne[128], R A Rojas[37], C P A Roland[130], J Roloff[30], A Romaniouk[80], E Romano[74a,74b], M Romano[24b], A C Romero Hernandez[167], N Rompotis[94], L Roos[130], S Rosati[76a], B J Rosser[41], E Rossi[129], E Rossi[73a,73b], L P Rossi[62], L Rossini[55], R Rosten[122], M Rotaru[28b], B Rottler[55], D Rousseau[67], D Rousso[49], S Roy-Garand[159], A Rozanov[104], Z M A Rozario[60], Y Rozen[154], A Rubio Jimenez[168], V H Ruelas Rivera[19], T A Ruggeri[1], A Ruggiero[129], A Ruiz-Martinez[168], A Rummler[37], Z Rurikova[55], N A Rusakovich[40], H L Russell[170], G Russo[76a,76b], J P Rutherfoord[7], S Rutherford Colmenares[33], M Rybar[136], E B Rye[128], A Ryzhov[46], J A Sabater Iglesias[57], H F-W Sadrozinski[139], F Safai Tehrani[76a], S Saha[1], M Sahinsoy[83], A Saibel[168], B T Saifuddin[123], M Saimpert[138], M Saito[157], T Saito[157], A Sala[72a,72b], D Salamani[37], A Salnikov[147], J Salt[168], A Salvador Salas[155], D Salvatore[45b,45a], F Salvatore[150], A Salzburger[37], D Sammel[55], E Sampson[93], D Sampsonidis[156,e], D Sampsonidou[126], J Sánchez[168], V Sanchez Sebastian[168], H Sandaker[128], C O Sander[49], J A Sandesara[105], M Sandhoff[176], C Sandoval[23b], L Sanfilippo[64a], D P C Sankey[137], T Sano[89], A Sansoni[54], L Santi[37], C Santoni[42], H Santos[133a,133b], A Santra[174], E Sanzani[24b,24a],

K A Saoucha[165], J G Saraiva[133a,133d], J Sardain[7], O Sasaki[85], K Sato[161], C Sauer[37], E Sauvan[4], P Savard[159,aj], R Sawada[157], C Sawyer[137], L Sawyer[99], C Sbarra[24b], A Sbrizzi[24b,24a], T Scanlon[98], J Schaarschmidt[142], U Schäfer[102], A C Schaffer[67,46], D Schaile[111], R D Schamberger[149], C Scharf[19], M M Schefer[20], V A Schegelsky[39], D Scheirich[136], M Schernau[140e], C Scheulen[57], C Schiavi[58b,58a], M Schioppa[45b,45a], B Schlag[147], S Schlenker[37], J Schmeing[176], M A Schmidt[176], K Schmieden[102], C Schmitt[102], N Schmitt[102], S Schmitt[49], L Schoeffel[138], A Schoening[64b], P G Scholer[35], E Schopf[145], M Schott[25], S Schramm[57], T Schroer[57], H-C Schultz-Coulon[64a], M Schumacher[55], B A Schumm[139], Ph Schune[138], H R Schwartz[139], A Schwartzman[147], T A Schwarz[108], Ph Schwemling[138], R Schwienhorst[109], F G Sciacca[20], A Sciandra[30], G Sciolla[27], F Scuri[75a], C D Sebastiani[37], K Sedlaczek[118], S C Seidel[115], A Seiden[139], B D Seidlitz[43], C Seitz[49], J M Seixas[84b], G Sekhniaidze[73a], L Selem[61], N Semprini-Cesari[24b,24a], A Semushin[178,39], D Sengupta[57], V Senthilkumar[168], L Serin[67], M Sessa[77a,77b], H Severini[123], F Sforza[58b,58a], A Sfyrla[57], Q Sha[14], E Shabalina[56], H Shaddix[118], A H Shah[33], R Shaheen[148], J D Shahinian[131], D Shaked Renous[174], M Shamim[37], L Y Shan[14], M Shapiro[18a], A Sharma[37], A S Sharma[169], P Sharma[30], P B Shatalov[39], K Shaw[150], S M Shaw[103], Q Shen[63c], D J Sheppard[146], P Sherwood[98], L Shi[98], X Shi[14], S Shimizu[85], C O Shimmin[177], I P J Shipsey[129,†], S Shirabe[90], M Shiyakova[40,aa], M J Shochet[41], D R Shope[128], B Shrestha[123], S Shrestha[122,an], I Shreyber[39], M J Shroff[170], P Sicho[134], A M Sickles[167], E Sideras Haddad[34g,164], A C Sidley[117], A Sidoti[24b], F Siegert[51], Dj Sijacki[16], F Sili[92], J M Silva[53], I Silva Ferreira[84b], M V Silva Oliveira[30], S B Silverstein[48a], S Simion[67], R Simoniello[37], E L Simpson[103], H Simpson[150], L R Simpson[108], S Simsek[83], S Sindhu[56], P Sinervo[159], S N Singh[27], S Singh[30], S Sinha[49], S Sinha[103], M Sioli[24b,24a], K Sioulas[9], I Siral[37], E Sitnikova[49], J Sjölin[48a,48b], A Skaf[56], E Skorda[21], P Skubic[123], M Slawinska[88], I Slazyk[17], V Smakhtin[174], B H Smart[137], S Yu Smirnov[140b], Y Smirnov[39], L N Smirnova[39,a], O Smirnova[100], A C Smith[43], D R Smith[163], E A Smith[41], J L Smith[103], M B Smith[35], R Smith[147], H Smitmanns[102], M Smizanska[93], K Smolek[135], A A Snesarev[40], H L Snoek[117], S Snyder[30], R Sobie[170,ac], A Soffer[155], C A Solans Sanchez[37], E Yu Soldatov[39], U Soldevila[168], A A Solodkov[34g], S Solomon[27], A Soloshenko[40], K Solovieva[55], O V Solovyanov[42], P Sommer[51], A Sonay[13], W Y Song[160b], A Sopczak[135], A L Sopio[53], F Sopkova[29b], J D Sorenson[115], I R Sotarriva Alvarez[141], V Sothilingam[64a], O J Soto Sandoval[140c,140b], S Sottocornola[69], R Soualah[165], Z Soumaimi[36e], D South[49], N Soybelman[174], S Spagnolo[71a,71b], M Spalla[112], D Sperlich[55], B Spisso[73a,73b], D P Spiteri[60], M Spousta[136], E J Staats[35], R Stamen[64a], E Stanecka[88], W Stanek-Maslouska[49], M V Stange[51], B Stanislaus[18a], M M Stanitzki[49], B Stapf[49], E A Starchenko[39], G H Stark[139], J Stark[91], P Staroba[134], P Starovoitov[165], R Staszewski[88], G Stavropoulos[47], A Stefl[37], P Steinberg[30], B Stelzer[146,160a], H J Stelzer[132], O Stelzer-Chilton[160a], H Stenzel[59], T J Stevenson[150], G A Stewart[37], J R Stewart[124], M C Stockton[37], G Stoicea[28b], M Stolarski[133a], S Stonjek[112], A Straessner[51], J Strandberg[148], S Strandberg[48a,48b], M Stratmann[176], M Strauss[123], T Strebler[104], P Strizenec[29b], R Ströhmer[171], D M Strom[126], R Stroynowski[46], A Strubig[48a,48b], S A Stucci[30], B Stugu[17], J Stupak[123], N A Styles[49], D Su[147], S Su[63a], W Su[63d], X Su[63a], D Suchy[29a], K Sugizaki[131], V V Sulin[39], M J Sullivan[94], D M S Sultan[129], L Sultanaliyeva[39], S Sultansoy[3b], S Sun[175], W Sun[14], O Sunneborn Gudnadottir[166], N Sur[104], M R Sutton[150], H Suzuki[161], M Svatos[134], M Swiatlowski[160a], T Swirski[171], I Sykora[29a], M Sykora[136], T Sykora[136], D Ta[102], K Tackmann[49,z], A Taffard[163], R Tafirout[160a], J S Tafoya Vargas[67], Y Takubo[85], M Talby[104], A A Talyshev[39], K C Tam[65b], N M Tamir[155], A Tanaka[157], J Tanaka[157], R Tanaka[67], M Tanasini[149], Z Tao[169], S Tapia Araya[140f], S Tapprogge[102], A Tarek Abouelfadl Mohamed[109], S Tarem[154], K Tariq[14], G Tarna[28b], G F Tartarelli[72a], M J Tartarin[91], P Tas[136], M Tasevsky[134], E Tassi[45b,45a], A C Tate[167], G Tateno[157], Y Tayalati[36e,ab], G N Taylor[107], W Taylor[160b], A S Tegetmeier[91], P Teixeira-Dias[97], J J Teoh[159], K Terashi[157], J Terron[101], S Terzo[13], M Testa[54], R J Teuscher[159,ac], A Thaler[80], O Theiner[57], T Theveneaux-Pelzer[104], O Thielmann[176], D W Thomas[97], J P Thomas[21], E A Thompson[18a], P D Thompson[21], E Thomson[131], R E Thornberry[46], C Tian[63a], Y Tian[57], V Tikhomirov[39,a], Yu A Tikhonov[39], S Timoshenko[39], D Timoshyn[136], E X L Ting[1], P Tipton[177], A Tishelman-Charny[30], S H Tlou[34g], K Todome[141], S Todorova-Nova[136], S Todt[51], L Toffolin[70a,70c], M Togawa[85], J Tojo[90], S Tokár[29a], O Toldaiev[69], G Tolkachev[104], M Tomoto[85,113], L Tompkins[147,p], E Torrence[126], H Torres[91], E Torró Pastor[168], M Toscani[31], C Tosciri[41], M Tost[11], D R Tovey[143], T Trefzger[171], A Tricoli[30], I M Trigger[160a], S Trincaz-Duvoid[130], D A Trischuk[27], A Tropina[40], L Truong[34c], M Trzebinski[88], A Trzupek[88], F Tsai[149], M Tsai[108], A Tsiamis[156], P V Tsiareshka[40], S Tsigaridas[160a], A Tsirigotis[156,v], V Tsiskaridze[159], E G Tskhadadze[153a], M Tsopoulou[156], Y Tsujikawa[89], I I Tsukerman[39], V Tsulaia[18a], S Tsuno[85],

K Tsuri[121], D Tsybychev[149], Y Tu[65b], A Tudorache[28b], V Tudorache[28b], S Turchikhin[58b,58a], I Turk Cakir[3a], R Turra[72a], T Turtuvshin[40,ad], P M Tuts[43], S Tzamarias[156,e], E Tzovara[102], F Ukegawa[161], P A Ulloa Poblete[140c,140b], E N Umaka[30], G Unal[37], A Undrus[30], G Unel[163], J Urban[29b], P Urrejola[140a], G Usai[8], R Ushioda[158], M Usman[110], F Ustuner[53], Z Uysal[83], V Vacek[135], B Vachon[106], T Vafeiadis[37], A Vaitkus[98], C Valderanis[111], E Valdes Santurio[48a,48b], M Valente[160a], S Valentinetti[24b,24a], A Valero[168], E Valiente Moreno[168], A Vallier[91], J A Valls Ferrer[168], D R Van Arneman[117], T R Van Daalen[142], A Van Der Graaf[50], H Z Van Der Schyf[34g], P Van Gemmeren[6], M Van Rijnbach[37], S Van Stroud[98], I Van Vulpen[117], P Vana[136], M Vanadia[77a,77b], U M Vande Voorde[148], W Vandelli[37], E R Vandewall[124], D Vannicola[155], L Vannoli[54], R Vari[76a], E W Varnes[7], C Varni[18b], D Varouchas[67], L Varriale[168], K E Varvell[151], M E Vasile[28b], L Vaslin[85], A Vasyukov[40], L M Vaughan[124], R Vavricka[136], T Vazquez Schroeder[13], J Veatch[32], V Vecchio[103], M J Veen[105], I Veliscek[30], L M Veloce[159], F Veloso[133a,133c], S Veneziano[76a], A Ventura[71a,71b], S Ventura Gonzalez[138], A Verbytskyi[112], M Verducci[75a,75b], C Vergis[96], M Verissimo De Araujo[84b], W Verkerke[117], J C Vermeulen[117], C Vernieri[147], M Vessella[163], M C Vetterli[146,aj], A Vgenopoulos[102], N Viaux Maira[140f], T Vickey[143], O E Vickey Boeriu[143], G H A Viehhauser[129], L Vigani[64b], M Vigl[112], M Villa[24b,24a], M Villaplana Perez[168], E M Villhauer[53], E Vilucchi[54], M G Vincter[35], A Visibile[117], C Vittori[37], I Vivarelli[24b,24a], E Voevodina[112], F Vogel[111], J C Voigt[51], P Vokac[135], Yu Volkotrub[87b], E Von Toerne[25], B Vormwald[37], K Vorobev[39], M Vos[168], K Voss[145], M Vozak[37], L Vozdecky[123], N Vranjes[16], M Vranjes Milosavljevic[16], M Vreeswijk[117], N K Vu[63d,63c], R Vuillermet[37], O Vujinovic[102], I Vukotic[41], I K Vyas[35], S Wada[161], C Wagner[147], J M Wagner[18a], W Wagner[176], S Wahdan[176], H Wahlberg[92], C H Waits[123], J Walder[137], R Walker[111], W Walkowiak[145], A Wall[131], E J Wallin[100], T Wamorkar[18a], A Z Wang[139], C Wang[102], C Wang[11], H Wang[18a], J Wang[65c], P Wang[103], P Wang[98], R Wang[62], R Wang[6], S M Wang[152], S Wang[14], T Wang[63a], W T Wang[81], W Wang[14], X Wang[167], X Wang[63c], Y Wang[114a], Y Wang[63a], Z Wang[108], Z Wang[63d,52,63c], Z Wang[108], C Wanotayaroj[85], A Warburton[106], R J Ward[21], A L Warnerbring[145], N Warrack[60], S Waterhouse[97], A T Watson[21], H Watson[53], M F Watson[21], E Watton[60], G Watts[142], B M Waugh[98], J M Webb[55], C Weber[30], H A Weber[19], M S Weber[20], S M Weber[64a], C Wei[63a], Y Wei[55], A R Weidberg[129], E J Weik[120], J Weingarten[50], C Weiser[55], C J Wells[49], T Wenaus[30], B Wendland[50], T Wengler[37], N S Wenke[112], N Wermes[25], M Wessels[64a], A M Wharton[93], A S White[62], A White[8], M J White[1], D Whiteson[163], L Wickremasinghe[127], W Wiedenmann[175], M Wielers[137], C Wiglesworth[44], D J Wilbern[123], H G Wilkens[37], J J H Wilkinson[33], D M Williams[43], H H Williams[131], S Williams[33], S Willocq[105], B J Wilson[103], D J Wilson[103], P J Windischhofer[41], F I Winkel[31], F Winklmeier[126], B T Winter[55], M Wittgen[147], M Wobisch[99], T Wojtkowski[61], Z Wolffs[117], J Wollrath[37], M W Wolter[88], H Wolters[133a,133c], M C Wong[139], E L Woodward[43], S D Worm[49], B K Wosiek[88], K W Woźniak[88], S Wozniewski[56], K Wraight[60], C Wu[21], M Wu[114b], M Wu[116], S L Wu[175], X Wu[57], X Wu[63a], Y Wu[63a], Z Wu[4], J Wuerzinger[112,ah], T R Wyatt[103], B M Wynne[53], S Xella[44], L Xia[114a], M Xia[15], M Xie[63a], A Xiong[126], J Xiong[18a], D Xu[14], H Xu[63a], L Xu[63a], R Xu[131], T Xu[108], Y Xu[142], Z Xu[53], Z Xu[114a], B Yabsley[151], S Yacoob[34a], Y Yamaguchi[85], E Yamashita[157], H Yamauchi[161], T Yamazaki[18a], Y Yamazaki[86], S Yan[60], Z Yan[105], H J Yang[63c,63d], H T Yang[63a], S Yang[63a], T Yang[65c], X Yang[37], X Yang[14], Y Yang[46], Y Yang[63a], W-M Yao[18a], H Ye[56], J Ye[14], S Ye[30], X Ye[63a], Y Yeh[98], I Yeletskikh[40], B Yeo[18b], M R Yexley[98], T P Yildirim[129], P Yin[43], K Yorita[173], S Younas[28b], C J S Young[37], C Young[147], N D Young[126], Y Yu[63a], J Yuan[14,114c], M Yuan[108], R Yuan[63d,63c], L Yue[98], M Zaazoua[63a], B Zabinski[88], I Zahir[36a], Z K Zak[88], T Zakareishvili[168], S Zambito[57], J A Zamora Saa[140d,140b], J Zang[157], D Zanzi[55], R Zanzottera[72a,72b], O Zaplatilek[135], C Zeitnitz[176], H Zeng[14], J C Zeng[167], D T Zenger Jr[27], O Zenin[39], T Ženiš[29a], S Zenz[96], S Zerradi[36a], D Zerwas[67], M Zhai[14,114c], D F Zhang[143], J Zhang[63b], J Zhang[6], K Zhang[14,114c], L Zhang[63a], L Zhang[114a], P Zhang[14,114c], R Zhang[175], S Zhang[91], T Zhang[157], X Zhang[63c], Y Zhang[142], Y Zhang[98], Y Zhang[63a], Y Zhang[114a], Z Zhang[18a], Z Zhang[63b], Z Zhang[67], H Zhao[142], T Zhao[63b], Y Zhao[35], Z Zhao[63a], Z Zhao[63a], A Zhemchugov[40], J Zheng[114a], K Zheng[167], X Zheng[63a], Z Zheng[147], D Zhong[167], B Zhou[108], H Zhou[7], N Zhou[63c], Y Zhou[15], Y Zhou[114a], Y Zhou[7], C G Zhu[63b], J Zhu[108], X Zhu[63d], Y Zhu[63c], Y Zhu[63a], X Zhuang[14], K Zhukov[69], N I Zimine[40], J Zinsser[64b], M Ziolkowski[145], L Živković[16], A Zoccoli[24b,24a], K Zoch[62], T G Zorbas[143], O Zormpa[47], W Zou[43], L Zwalinski[37]

[1] Department of Physics, University of Adelaide, Adelaide, Australia
[2] Department of Physics, University of Alberta, Edmonton, AB, Canada

[3] [(a)]Department of Physics, Ankara University, Ankara, Türkiye; [(b)]Division of Physics, TOBB University of Economics and Technology, Ankara, Türkiye
[4] LAPP, Université Savoie Mont Blanc, CNRS/IN2P3, Annecy, France
[5] APC, Université Paris Cité, CNRS/IN2P3, Paris, France
[6] High Energy Physics Division, Argonne National Laboratory, Argonne, IL, United States of America
[7] Department of Physics, University of Arizona, Tucson, AZ, United States of America
[8] Department of Physics, University of Texas at Arlington, Arlington, TX, United States of America
[9] Physics Department, National and Kapodistrian University of Athens, Athens, Greece
[10] Physics Department, National Technical University of Athens, Zografou, Greece
[11] Department of Physics, University of Texas at Austin, Austin, TX, United States of America
[12] Institute of Physics, Azerbaijan Academy of Sciences, Baku, Azerbaijan
[13] Institut de Física d'Altes Energies (IFAE), Barcelona Institute of Science and Technology, Barcelona, Spain
[14] Institute of High Energy Physics, Chinese Academy of Sciences, Beijing, People's Republic of China
[15] Physics Department, Tsinghua University, Beijing, People's Republic of China
[16] Institute of Physics, University of Belgrade, Belgrade, Serbia
[17] Department for Physics and Technology, University of Bergen, Bergen, Norway
[18] [(a)]Physics Division, Lawrence Berkeley National Laboratory, Berkeley, CA, United States of America; [(b)]University of California, Berkeley, CA, United States of America
[19] Institut für Physik, Humboldt Universität zu Berlin, Berlin, Germany
[20] Albert Einstein Center for Fundamental Physics and Laboratory for High Energy Physics, University of Bern, Bern, Switzerland
[21] School of Physics and Astronomy, University of Birmingham, Birmingham, United Kingdom
[22] [(a)]Department of Physics, Bogazici University, Istanbul, Türkiye; [(b)]Department of Physics Engineering, Gaziantep University, Gaziantep, Türkiye; [(c)]Department of Physics, Istanbul University, Istanbul, Türkiye
[23] [(a)]Facultad de Ciencias y Centro de Investigaciónes, Universidad Antonio Nariño, Bogotá, Colombia; [(b)]Departamento de Física, Universidad Nacional de Colombia, Bogotá, Colombia
[24] [(a)]Dipartimento di Fisica e Astronomia A. Righi, Università di Bologna, Bologna, Italy; [(b)]INFN Sezione di Bologna, Italy
[25] Physikalisches Institut, Universität Bonn, Bonn, Germany
[26] Department of Physics, Boston University, Boston, MA, United States of America
[27] Department of Physics, Brandeis University, Waltham, MA, United States of America
[28] [(a)]Transilvania University of Brasov, Brasov, Romania; [(b)]Horia Hulubei National Institute of Physics and Nuclear Engineering, Bucharest, Romania; [(c)]Department of Physics, Alexandru Ioan Cuza University of Iasi, Iasi, Romania; [(d)]National Institute for Research and Development of Isotopic and Molecular Technologies, Physics Department, Cluj-Napoca, Romania; [(e)]National University of Science and Technology Politechnica, Bucharest, Romania; [(f)]West University in Timisoara, Timisoara, Romania; [(g)]Faculty of Physics, University of Bucharest, Bucharest, Romania
[29] [(a)]Faculty of Mathematics, Physics and Informatics, Comenius University, Bratislava, Slovakia; [(b)]Department of Subnuclear Physics, Institute of Experimental Physics of the Slovak Academy of Sciences, Kosice, Slovakia
[30] Physics Department, Brookhaven National Laboratory, Upton, NY, United States of America
[31] Universidad de Buenos Aires, Facultad de Ciencias Exactas y Naturales, Departamento de Física, y CONICET, Instituto de Física de Buenos Aires (IFIBA), Buenos Aires, Argentina
[32] California State University, CA, United States of America
[33] Cavendish Laboratory, University of Cambridge, Cambridge, United Kingdom
[34] [(a)]Department of Physics, University of Cape Town, Cape Town, South Africa; [(b)]iThemba Labs, Western Cape, South Africa; [(c)]Department of Mechanical Engineering Science, University of Johannesburg, Johannesburg, South Africa; [(d)]National Institute of Physics, University of the Philippines Diliman (Philippines), South Africa; [(e)]University of South Africa, Department of Physics, Pretoria, South Africa; [(f)]University of Zululand, KwaDlangezwa, South Africa; [(g)]School of Physics, University of the Witwatersrand, Johannesburg, South Africa
[35] Department of Physics, Carleton University, Ottawa, ON, Canada
[36] [(a)]Faculté des Sciences Ain Chock, Université Hassan II de Casablanca, Morocco; [(b)]Faculté des Sciences, Université Ibn-Tofail, Kénitra, Morocco; [(c)]Faculté des Sciences Semlalia, Université Cadi Ayyad, LPHEA-Marrakech, Morocco; [(d)]LPMR, Faculté des Sciences, Université Mohamed Premier, Oujda, Morocco; [(e)]Faculté des sciences, Université Mohammed V, Rabat, Morocco; [(f)]Institute of Applied Physics, Mohammed VI Polytechnic University, Ben Guerir, Morocco
[37] CERN, Geneva, Switzerland
[38] Affiliated with an institute formerly covered by a cooperation agreement with CERN
[39] Affiliated with an institute covered by a cooperation agreement with CERN
[40] Affiliated with an international laboratory covered by a cooperation agreement with CERN
[41] Enrico Fermi Institute, University of Chicago, Chicago, IL, United States of America
[42] LPC, Université Clermont Auvergne, CNRS/IN2P3, Clermont-Ferrand, France
[43] Nevis Laboratory, Columbia University, Irvington, NY, United States of America

[44] Niels Bohr Institute, University of Copenhagen, Copenhagen, Denmark
[45] [(a)]Dipartimento di Fisica, Università della Calabria, Rende, Italy; [(b)]INFN Gruppo Collegato di Cosenza, Laboratori Nazionali di Frascati, Italy
[46] Physics Department, Southern Methodist University, Dallas, TX, United States of America
[47] National Centre for Scientific Research "Demokritos", Agia Paraskevi, Greece
[48] [(a)]Department of Physics, Stockholm University, Sweden; [(b)]Oskar Klein Centre, Stockholm, Sweden
[49] Deutsches Elektronen-Synchrotron DESY, Hamburg and Zeuthen, Germany
[50] Fakultät Physik , Technische Universität Dortmund, Dortmund, Germany
[51] Institut für Kern- und Teilchenphysik, Technische Universität Dresden, Dresden, Germany
[52] Department of Physics, Duke University, Durham, NC, United States of America
[53] SUPA—School of Physics and Astronomy, University of Edinburgh, Edinburgh, United Kingdom
[54] INFN e Laboratori Nazionali di Frascati, Frascati, Italy
[55] Physikalisches Institut, Albert-Ludwigs-Universität Freiburg, Freiburg, Germany
[56] II. Physikalisches Institut, Georg-August-Universität Göttingen, Göttingen, Germany
[57] Département de Physique Nucléaire et Corpusculaire, Université de Genève, Genève, Switzerland
[58] [(a)]Dipartimento di Fisica, Università di Genova, Genova, Italy; [(b)]INFN Sezione di Genova, Italy
[59] II. Physikalisches Institut, Justus-Liebig-Universität Giessen, Giessen, Germany
[60] SUPA—School of Physics and Astronomy, University of Glasgow, Glasgow, United Kingdom
[61] LPSC, Université Grenoble Alpes, CNRS/IN2P3, Grenoble INP, Grenoble, France
[62] Laboratory for Particle Physics and Cosmology, Harvard University, Cambridge, MA, United States of America
[63] [(a)]Department of Modern Physics and State Key Laboratory of Particle Detection and Electronics, University of Science and Technology of China, Hefei, People's Republic of China; [(b)]Institute of Frontier and Interdisciplinary Science and Key Laboratory of Particle Physics and Particle Irradiation (MOE), Shandong University, Qingdao, People's Republic of China; [(c)]State Key Laboratory of Dark Matter Physics, School of Physics and Astronomy, Shanghai Jiao Tong University, Key Laboratory for Particle Astrophysics and Cosmology (MOE), SKLPPC, Shanghai, People's Republic of China; [(d)]State Key Laboratory of Dark Matter Physics, Tsung-Dao Lee Institute, Shanghai Jiao Tong University, Shanghai, People's Republic of China; [(e)]School of Physics, Zhengzhou University, People's Republic of China
[64] [(a)]Kirchhoff-Institut für Physik, Ruprecht-Karls-Universität Heidelberg, Heidelberg, Germany; [(b)]Physikalisches Institut, Ruprecht-Karls-Universität Heidelberg, Heidelberg, Germany
[65] [(a)]Department of Physics, Chinese University of Hong Kong, Shatin, N.T., Hong Kong, People's Republic of China; [(b)]Department of Physics, University of Hong Kong, Hong Kong, People's Republic of China; [(c)]Department of Physics and Institute for Advanced Study, Hong Kong University of Science and Technology, Clear Water Bay, Kowloon, Hong Kong, People's Republic of China
[66] Department of Physics, National Tsing Hua University, Hsinchu, Taiwan
[67] IJCLab, Université Paris-Saclay, CNRS/IN2P3, 91 405 Orsay, France
[68] Centro Nacional de Microelectrónica (IMB-CNM-CSIC), Barcelona, Spain
[69] Department of Physics, Indiana University, Bloomington, IN, United States of America
[70] [(a)]INFN Gruppo Collegato di Udine, Sezione di Trieste, Udine, Italy; [(b)]ICTP, Trieste, Italy; [(c)]Dipartimento Politecnico di Ingegneria e Architettura, Università di Udine, Udine, Italy
[71] [(a)]INFN Sezione di Lecce, Italy; [(b)]Dipartimento di Matematica e Fisica, Università del Salento, Lecce, Italy
[72] [(a)]INFN Sezione di Milano, Italy; [(b)]Dipartimento di Fisica, Università di Milano, Milano, Italy
[73] [(a)]INFN Sezione di Napoli, Italy; [(b)]Dipartimento di Fisica, Università di Napoli, Napoli, Italy
[74] [(a)]INFN Sezione di Pavia, Italy; [(b)]Dipartimento di Fisica, Università di Pavia, Pavia, Italy
[75] [(a)]INFN Sezione di Pisa, Italy; [(b)]Dipartimento di Fisica E. Fermi, Università di Pisa, Pisa, Italy
[76] [(a)]INFN Sezione di Roma, Italy; [(b)]Dipartimento di Fisica, Sapienza Università di Roma, Roma, Italy
[77] [(a)]INFN Sezione di Roma Tor Vergata, Italy; [(b)]Dipartimento di Fisica, Università di Roma Tor Vergata, Roma, Italy
[78] [(a)]INFN Sezione di Roma Tre, Italy; [(b)]Dipartimento di Matematica e Fisica, Università Roma Tre, Roma, Italy
[79] [(a)]INFN-TIFPA, Italy; [(b)]Università degli Studi di Trento, Trento, Italy
[80] Universität Innsbruck, Department of Astro and Particle Physics, Innsbruck, Austria
[81] University of Iowa, Iowa City, IA, United States of America
[82] Department of Physics and Astronomy, Iowa State University, Ames, IA, United States of America
[83] Istinye University, Sariyer, Istanbul, Türkiye
[84] [(a)]Departamento de Engenharia Elétrica, Universidade Federal de Juiz de Fora (UFJF), Juiz de Fora, Brazil; [(b)]Universidade Federal do Rio De Janeiro COPPE/EE/IF, Rio de Janeiro, Brazil; [(c)]Instituto de Física, Universidade de São Paulo, São Paulo, Brazil; [(d)]Rio de Janeiro State University, Rio de Janeiro, Brazil; [(e)]Federal University of Bahia, Bahia, Brazil
[85] KEK, High Energy Accelerator Research Organization, Tsukuba, Japan
[86] Graduate School of Science, Kobe University, Kobe, Japan
[87] [(a)]AGH University of Krakow, Faculty of Physics and Applied Computer Science, Krakow, Poland; [(b)]Marian

Smoluchowski Institute of Physics, Jagiellonian University, Krakow, Poland
[88] Institute of Nuclear Physics Polish Academy of Sciences, Krakow, Poland
[89] Faculty of Science, Kyoto University, Kyoto, Japan
[90] Research Center for Advanced Particle Physics and Department of Physics, Kyushu University, Fukuoka, Japan
[91] L2IT, Université de Toulouse, CNRS/IN2P3, UPS, Toulouse, France
[92] Instituto de Física La Plata, Universidad Nacional de La Plata and CONICET, La Plata, Argentina
[93] Physics Department, Lancaster University, Lancaster, United Kingdom
[94] Oliver Lodge Laboratory, University of Liverpool, Liverpool, United Kingdom
[95] Department of Experimental Particle Physics, Jožef Stefan Institute and Department of Physics, University of Ljubljana, Ljubljana, Slovenia
[96] Department of Physics and Astronomy, Queen Mary University of London, London, United Kingdom
[97] Department of Physics, Royal Holloway University of London, Egham, United Kingdom
[98] Department of Physics and Astronomy, University College London, London, United Kingdom
[99] Louisiana Tech University, Ruston, LA, United States of America
[100] Fysiska institutionen, Lunds universitet, Lund, Sweden
[101] Departamento de Física Teorica C-15 and CIAFF, Universidad Autónoma de Madrid, Madrid, Spain
[102] Institut für Physik, Universität Mainz, Mainz, Germany
[103] School of Physics and Astronomy, University of Manchester, Manchester, United Kingdom
[104] CPPM, Aix-Marseille Université, CNRS/IN2P3, Marseille, France
[105] Department of Physics, University of Massachusetts, Amherst, MA, United States of America
[106] Department of Physics, McGill University, Montreal, QC, Canada
[107] School of Physics, University of Melbourne, Victoria, Australia
[108] Department of Physics, University of Michigan, Ann Arbor, MI, United States of America
[109] Department of Physics and Astronomy, Michigan State University, East Lansing, MI, United States of America
[110] Group of Particle Physics, University of Montreal, Montreal, QC, Canada
[111] Fakultät für Physik, Ludwig-Maximilians-Universität München, München, Germany
[112] Max-Planck-Institut für Physik (Werner-Heisenberg-Institut), München, Germany
[113] Graduate School of Science and Kobayashi-Maskawa Institute, Nagoya University, Nagoya, Japan
[114] [(a)]Department of Physics, Nanjing University, Nanjing, People's Republic of China; [(b)]School of Science, Shenzhen Campus of Sun Yat-sen University, People's Republic of China; [(c)]University of Chinese Academy of Science (UCAS), Beijing, People's Republic of China
[115] Department of Physics and Astronomy, University of New Mexico, Albuquerque, NM, United States of America
[116] Institute for Mathematics, Astrophysics and Particle Physics, Radboud University/Nikhef, Nijmegen, Netherlands
[117] Nikhef National Institute for Subatomic Physics and University of Amsterdam, Amsterdam, Netherlands
[118] Department of Physics, Northern Illinois University, DeKalb, IL, United States of America
[119] [(a)]New York University Abu Dhabi, Abu Dhabi, United Arab Emirates; [(b)]United Arab Emirates University, Al Ain, United Arab Emirates
[120] Department of Physics, New York University, New York, NY, United States of America
[121] Ochanomizu University, Otsuka, Bunkyo-ku, Tokyo, Japan
[122] Ohio State University, Columbus, OH, United States of America
[123] Homer L. Dodge Department of Physics and Astronomy, University of Oklahoma, Norman, OK, United States of America
[124] Department of Physics, Oklahoma State University, Stillwater, OK, United States of America
[125] Palacký University, Joint Laboratory of Optics, Olomouc, Czech Republic
[126] Institute for Fundamental Science, University of Oregon, Eugene, OR, United States of America
[127] Graduate School of Science, Osaka University, Osaka, Japan
[128] Department of Physics, University of Oslo, Oslo, Norway
[129] Department of Physics, Oxford University, Oxford, United Kingdom
[130] LPNHE, Sorbonne Université, Université Paris Cité, CNRS/IN2P3, Paris, France
[131] Department of Physics, University of Pennsylvania, Philadelphia, PA, United States of America
[132] Department of Physics and Astronomy, University of Pittsburgh, Pittsburgh, PA, United States of America
[133] [(a)]Laboratório de Instrumentação e Física Experimental de Partículas—LIP, Lisboa, Portugal; [(b)]Departamento de Física, Faculdade de Ciências, Universidade de Lisboa, Lisboa, Portugal; [(c)]Departamento de Física, Universidade de Coimbra, Coimbra, Portugal; [(d)]Centro de Física Nuclear da Universidade de Lisboa, Lisboa, Portugal; [(e)]Departamento de Física, Escola de Ciências, Universidade do Minho, Braga, Portugal; [(f)]Departamento de Física Teórica y del Cosmos, Universidad de Granada, Granada (Spain), Portugal; [(g)]Departamento de Física, Instituto Superior Técnico, Universidade de Lisboa, Lisboa, Portugal
[134] Institute of Physics of the Czech Academy of Sciences, Prague, Czech Republic
[135] Czech Technical University in Prague, Prague, Czech Republic
[136] Charles University, Faculty of Mathematics and Physics, Prague, Czech Republic
[137] Particle Physics Department, Rutherford Appleton Laboratory, Didcot, United Kingdom
[138] IRFU, CEA, Université Paris-Saclay, Gif-sur-Yvette, France

[139] Santa Cruz Institute for Particle Physics, University of California Santa Cruz, Santa Cruz, CA, United States of America
[140] [(a)]Departamento de Física, Pontificia Universidad Católica de Chile, Santiago, Chile; [(b)]Millennium Institute for Subatomic physics at high energy frontier (SAPHIR), Santiago, Chile; [(c)]Instituto de Investigación Multidisciplinario en Ciencia y Tecnología, y Departamento de Física, Universidad de La Serena, Chile; [(d)]Universidad Andres Bello, Department of Physics, Santiago, Chile; [(e)]Instituto de Alta Investigación, Universidad de Tarapacá, Arica, Chile; [(f)]Departamento de Física, Universidad Técnica Federico Santa María, Valparaíso, Chile
[141] Department of Physics, Institute of Science, Tokyo, Japan
[142] Department of Physics, University of Washington, Seattle, WA, United States of America
[143] Department of Physics and Astronomy, University of Sheffield, Sheffield, United Kingdom
[144] Department of Physics, Shinshu University, Nagano, Japan
[145] Department Physik, Universität Siegen, Siegen, Germany
[146] Department of Physics, Simon Fraser University, Burnaby, BC, Canada
[147] SLAC National Accelerator Laboratory, Stanford, CA, United States of America
[148] Department of Physics, Royal Institute of Technology, Stockholm, Sweden
[149] Departments of Physics and Astronomy, Stony Brook University, Stony Brook, NY, United States of America
[150] Department of Physics and Astronomy, University of Sussex, Brighton, United Kingdom
[151] School of Physics, University of Sydney, Sydney, Australia
[152] Institute of Physics, Academia Sinica, Taipei, Taiwan
[153] [(a)]E. Andronikashvili Institute of Physics, Iv. Javakhishvili Tbilisi State University, Tbilisi, Georgia; [(b)]High Energy Physics Institute, Tbilisi State University, Tbilisi, Georgia; [(c)]University of Georgia, Tbilisi, Georgia
[154] Department of Physics, Technion, Israel Institute of Technology, Haifa, Israel
[155] Raymond and Beverly Sackler School of Physics and Astronomy, Tel Aviv University, Tel Aviv, Israel
[156] Department of Physics, Aristotle University of Thessaloniki, Thessaloniki, Greece
[157] International Center for Elementary Particle Physics and Department of Physics, University of Tokyo, Tokyo, Japan
[158] Graduate School of Science and Technology, Tokyo Metropolitan University, Tokyo, Japan
[159] Department of Physics, University of Toronto, Toronto, ON, Canada
[160] [(a)]TRIUMF, Vancouver, BC, Canada; [(b)]Department of Physics and Astronomy, York University, Toronto, ON, Canada
[161] Division of Physics and Tomonaga Center for the History of the Universe, Faculty of Pure and Applied Sciences, University of Tsukuba, Tsukuba, Japan
[162] Department of Physics and Astronomy, Tufts University, Medford, MA, United States of America
[163] Department of Physics and Astronomy, University of California Irvine, Irvine, CA, United States of America
[164] University of West Attica, Athens, Greece
[165] University of Sharjah, Sharjah, United Arab Emirates
[166] Department of Physics and Astronomy, University of Uppsala, Uppsala, Sweden
[167] Department of Physics, University of Illinois, Urbana, IL, United States of America
[168] Instituto de Física Corpuscular (IFIC), Centro Mixto Universidad de Valencia—CSIC, Valencia, Spain
[169] Department of Physics, University of British Columbia, Vancouver, BC, Canada
[170] Department of Physics and Astronomy, University of Victoria, Victoria, BC, Canada
[171] Fakultät für Physik und Astronomie, Julius-Maximilians-Universität Würzburg, Würzburg, Germany
[172] Department of Physics, University of Warwick, Coventry, United Kingdom
[173] Waseda University, Tokyo, Japan
[174] Department of Particle Physics and Astrophysics, Weizmann Institute of Science, Rehovot, Israel
[175] Department of Physics, University of Wisconsin, Madison, WI, United States of America
[176] Fakultät für Mathematik und Naturwissenschaften, Fachgruppe Physik, Bergische Universität Wuppertal, Wuppertal, Germany
[177] Department of Physics, Yale University, New Haven, CT, United States of America
[178] Yerevan Physics Institute, Yerevan, Armenia
[a] Also Affiliated with an institute covered by a cooperation agreement with CERN
[b] Also at An-Najah National University, Nablus, Palestine
[c] Also at Borough of Manhattan Community College, City University of New York, New York, NY, United States of America
[d] Also at Center for High Energy Physics, Peking University, People's Republic of China
[e] Also at Center for Interdisciplinary Research and Innovation (CIRI-AUTH), Thessaloniki, Greece
[f] Also at CERN, Geneva, Switzerland
[g] Also at CMD-AC UNEC Research Center, Azerbaijan State University of Economics (UNEC), Azerbaijan
[h] Also at Département de Physique Nucléaire et Corpusculaire, Université de Genève, Genève, Switzerland
[i] Also at Departament de Fisica de la Universitat Autonoma de Barcelona, Barcelona, Spain
[j] Associated at Department of Electrical Engineering and Computer Science, Université de Liège, Liège, Belgium
[k] Also at Department of Financial and Management Engineering, University of the Aegean, Chios, Greece
[l] Also at Department of Mathematical Sciences, University of South Africa, Johannesburg, South Africa
[m] Also at Department of Physics, Bolu Abant Izzet Baysal University, Bolu, Türkiye
[n] Also at Department of Physics, California State University, Sacramento, United States of America

[o] Also at Department of Physics, King's College London, London, United Kingdom
[p] Also at Department of Physics, Stanford University, Stanford, CA, United States of America
[q] Also at Department of Physics, Stellenbosch University, South Africa
[r] Also at Department of Physics, University of Fribourg, Fribourg, Switzerland
[s] Also at Department of Physics, University of Thessaly, Greece
[t] Also at Department of Physics, Westmont College, Santa Barbara, United States of America
[u] Also at Faculty of Physics, Sofia University, 'St. Kliment Ohridski', Sofia, Bulgaria
[v] Also at Hellenic Open University, Patras, Greece
[w] Also at Henan University, People's Republic of China
[x] Also at Imam Mohammad Ibn Saud Islamic University, Saudi Arabia
[y] Also at Institucio Catalana de Recerca i Estudis Avancats, ICREA, Barcelona, Spain
[z] Also at Institut für Experimentalphysik, Universität Hamburg, Hamburg, Germany
[aa] Also at Institute for Nuclear Research and Nuclear Energy (INRNE) of the Bulgarian Academy of Sciences, Sofia, Bulgaria
[ab] Also at Institute of Applied Physics, Mohammed VI Polytechnic University, Ben Guerir, Morocco
[ac] Also at Institute of Particle Physics (IPP), Canada
[ad] Also at Institute of Physics and Technology, Mongolian Academy of Sciences, Ulaanbaatar, Mongolia
[ae] Also at Institute of Physics, Azerbaijan Academy of Sciences, Baku, Azerbaijan
[af] Also at Institute of Theoretical Physics, Ilia State University, Tbilisi, Georgia
[ag] Also at National Institute of Physics, University of the Philippines Diliman (Philippines), Philippines
[ah] Also at Technical University of Munich, Munich, Germany
[ai] Also at The Collaborative Innovation Center of Quantum Matter (CICQM), Beijing, People's Republic of China
[aj] Also at TRIUMF, Vancouver, BC, Canada
[ak] Also at Università di Napoli Parthenope, Napoli, Italy
[al] Also at University of Colorado Boulder, Department of Physics, Colorado, United States of America
[am] Also at University of the Western Cape, South Africa
[an] Also at Washington College, Chestertown, MD, United States of America
[ao] Also at Yeditepe University, Physics Department, Istanbul, Türkiye
[†] Deceased.

## References

[1] ATLAS Collaboration 2012 Observation of a new particle in the search for the Standard Model Higgs boson with the ATLAS detector at the LHC *Phys. Lett. B* **716** 1
[2] CMS Collaboration 2012 Observation of a new boson at a mass of 125 GeV with the CMS experiment at the LHC *Phys. Lett. B* **716** 30
[3] ATLAS Collaboration 2015 Study of the spin and parity of the Higgs boson in diboson decays with the ATLAS detector *Eur. Phys. J. C* **75** 476
ATLAS Collaboration 2016 *Eur. Phys. J. C* **76** 152 (erratum)
[4] CMS Collaboration 2015 Constraints on the spin-parity and anomalous HVV couplings of the Higgs boson in proton collisions at 7 and 8 TeV *Phys. Rev. D* **92** 012004
[5] ATLAS Collaboration 2023 Combined Measurement of the Higgs Boson Mass from the $H \to \gamma\gamma$ and $H \to ZZ^* \to 4\ell$ Decay Channels with the ATLAS Detector Using $\sqrt{s} = 7, 8,$ and 13 TeV *pp* Collision Data *Phys. Rev. Lett.* **131** 251802
[6] CMS Collaboration 2020 A measurement of the Higgs boson mass in the diphoton decay channel *Phys. Lett. B* **805** 135425
[7] CMS Collaboration 2024 Measurement of the Higgs boson mass and width using the four-lepton final state in proton-proton collisions at $\sqrt{s} = 13$ TeV (arXiv:2409.13663 [hep-ex])
[8] ATLAS Collaboration 2022 A detailed map of Higgs boson interactions by the ATLAS experiment ten years after the discovery *Nature* 607 52–59
ATLAS Collaboration 2022 *Nature* **612** E24 (erratum)
[9] CMS Collaboration 2022 A portrait of the Higgs boson by the CMS experiment ten years after the discovery *Nature* **607** 60–68
CMS Collaboration 2023 *Nature* **623** E4 (erratum)
[10] Florian D *et al* 2017 Handbook of LHC Higgs cross sections: 4. Deciphering the nature of the Higgs sector (arXiv:1610.07922 [hep-ph])
[11] ATLAS Collaboration 2015 Limits on the Higgs boson lifetime and width from its decay to four charged leptons *Phys. Rev. D* **92** 072010
[12] Kauer N and Passarino G 2012 Inadequacy of zero-width approximation for a light Higgs boson signal *J. High Energy Phys.* JHEP08(2012)116
[13] Caola F and Melnikov K 2013 Constraining the Higgs boson width with ZZ production at the LHC *Phys. Rev. D* **88** 054024
[14] Campbell J M, Ellis R K and Williams C 2014 Bounding the Higgs width at the LHC using full analytic results for $gg \to e^-e^+\mu^-\mu^+$ *J. High Energy Phys.* JHEP04(2014)060
[15] ATLAS Collaboration 2015 Constraints on the off-shell Higgs boson signal strength in the high-mass *ZZ* and *WW* final states with the ATLAS detector *Eur. Phys. J. C* **75** 335
[16] ATLAS Collaboration 2024 Constraint on the total width of the Higgs boson from Higgs boson and four-top-quark measurements in *pp* collisions at $\sqrt{s} = 13$ TeV with the ATLAS detector *Phys. Lett. B* **861** 139277
[17] ATLAS Collaboration 2023 Evidence of off-shell Higgs boson production from *ZZ* leptonic decay channels and constraints on its total width with the ATLAS detector *Phys. Lett. B* **846** 138223
ATLAS Collaboration 2024 *Phys. Lett. B* **854** 138734 (erratum)
ATLAS Collaboration 2025 *Phys. Lett. B* **865** 139449 (erratum)
[18] ATLAS Collaboration 2022 Measurement of the Higgs boson width and evidence of its off-shell contributions to *ZZ* production *Nat. Phys.* **18** 1329–34
[19] Campbell J M, Ellis R K and Williams C 2014 Bounding the Higgs width at the LHC: Complementary results from $H \to WW$ *Phys. Rev. D* **89** 053011
[20] Gonçalves D, Han T and Mukhopadhyay S 2018 Off-Shell Higgs Probe of Naturalness *Phys. Rev. Lett.* **120** 111801
Gonçalves D, Han T and Mukhopadhyay S 2018 *Phys. Rev. Lett.* **121** 079902 (erratum)

[21] Weinberg S 1980 Effective Gauge theories *Phys. Lett. B* **91** 51–55

[22] Coleman S, Wess J and Zumino B 1969 Structure of phenomenological Lagrangians. I *Phys. Rev.* **177** 2239–47

[23] Callan C G, Coleman S, Wess J and Zumino B 1969 Structure of phenomenological Lagrangians. II *Phys. Rev.* **177** 2247–50

[24] Azatov A, Grojean C, Paul A and Salvioni E 2015 Taming the off-shell Higgs boson *J. Exp. Theor. Phys.* **120** 354–68

[25] ATLAS Collaboration 2023 Effective field theory interpretation of the measurement of off-shell Higgs boson production from $ZZ \to 4\ell$ and $ZZ \to 2\ell 2\nu$ decay channels with the ATLAS detector (available at: https://cds.cern.ch/record/2860128)

[26] CMS Collaboration 2024 Measurement of the Higgs boson mass and width using the four-lepton final state in proton–proton collisions at $\sqrt{s} = 13$ TeV (arXiv:2409.13663 [hep-ex])

[27] Brehmer J, Louppe G, Pavez J and Cranmer K 2020 Mining gold from implicit models to improve likelihood-free inference *Proc. Natl Acad. Sci.* **117** 5242–9

[28] Brehmer J, Cranmer K, Louppe G and Pavez J 2018 A guide to constraining effective field theories with machine learning *Phys. Rev. D* **98** 052004

[29] Brehmer J, Kling F, Espejo I and Cranmer K 2020 MadMiner: machine learning-based inference for particle physics *Comput. Softw. Big Sci.* **4** 3

[30] Cranmer K, Brehmer J and Louppe G 2020 The frontier of simulation-based inference *Proc. Natl Acad. Sci.* **117** 30055

[31] ATLAS Collaboration 2024 An implementation of neural simulation-based inference for parameter estimation in ATLAS *Rep. Prog. Phys.* accepted (arXiv:2412.01600[hep-ex])

[32] CMS Collaboration 2019 Measurements of the Higgs boson width and anomalous *HVV* couplings from on-shell and off-shell production in the four-lepton final state *Phys. Rev.* D **99** 112003

[33] CMS Collaboration 2025 Constraints on standard model effective field theory for a Higgs boson produced in association with W or Z bosons in the H$\to$ b$\bar{b}$ decay channel in proton-proton collisions at $\sqrt{s} = 13$ TeV *J. High Energ. Phys.* **2025** 114

[34] DØ Collaboration 2004 A precision measurement of the mass of the top quark *Nature* **429** 638–42

[35] CDF Collaboration 2006 Top quark mass measurement from dilepton events at CDF II with the matrix-element method *Phys. Rev. D* **74** 032009

[36] Barreiro Megino F *et al* 2024 Operational experience and R&D results using the Google Cloud for high-energy physics in the ATLAS experiment *Int. J. Mod. Phys. A* **39** 2450054

[37] ATLAS Collaboration 2008 The ATLAS experiment at the CERN large hadron collider *JINST* **3** S08003

[38] ATLAS Collaboration 2010 *ATLAS Insertable B-Layer: Technical Design Report* ATLAS-TDR-19; CERN-LHCC-2010-013 (available at: https://cds.cern.ch/record/1291633)

ATLAS Collaboration 2012 *ATLAS Insertable B-Layer: Technical Design Report Addendum* ATLAS-TDR-19-ADD-1; CERN-LHCC-2012-009 (available at: https://cds.cern.ch/record/1451888)

[39] Abbott B *et al* 2018 Production and integration of the ATLAS insertable B-layer *JINST* **13** T05008

[40] Avoni G *et al* 2018 The new LUCID-2 detector for luminosity measurement and monitoring in ATLAS *JINST* **13** 07017

[41] ATLAS Collaboration 2017 Performance of the ATLAS trigger system in 2015 *Eur. Phys. J. C* **77** 317

[42] Aad G 2025 Software and computing for Run 3 of the ATLAS experiment at the LHC *Eur. Phys. J. C* **85** 234

[43] Andersen J R 2013 Handbook of LHC Higgs cross sections: 3. Higgs properties (arXiv:1307.1347 [hep-ph])

[44] Ghezzi M, Gomez-Ambrosio R, Passarino G and Uccirati S 2015 NLO Higgs effective field theory and $\kappa$-framework *J. High Energy Phys.* JHEP07(2015)175

[45] ATLAS Collaboration 2023 Measurement of the Higgs boson mass in the $H \to ZZ^* \to 4\ell$ decay channel using 139 fb$^{-1}$ of $\sqrt{s} = 13$ TeV *pp* collisions recorded by the ATLAS detector at the LHC *Phys. Lett. B* **843** 137880

[46] Passarino G 2012 Higgs interference effects in $gg \to ZZ$ and their uncertainty *J. High Energy Phys.* JHEP07(2015)175

[47] Mattelaer O and Ostrolenk K 2021 Speeding up MadGraph5_aMC@NLO *Eur. Phys. J. C* **81** 435

[48] ATLAS Collaboration 2023 Luminosity determination in *pp* collisions at $\sqrt{s} = 13$ TeV using the ATLAS detector at the LHC *Eur. Phys. J. C* **83** 982

[49] ATLAS Collaboration 2020 ATLAS data quality operations and performance for 2015–2018 data-taking *JINST* **15** 04003

[50] ATLAS Collaboration 2020 Performance of electron and photon triggers in ATLAS during LHC Run 2 *Eur. Phys. J. C* **80** 47

[51] ATLAS Collaboration 2020 Performance of the ATLAS muon triggers in Run 2 *JINST* **15** 09015

[52] ATLAS Collaboration 2022 The ATLAS inner detector trigger performance in *pp* collisions at 13 TeV during LHC Run 2 *Eur. Phys. J. C* **82** 206

[53] Bothmann E *et al* 2019 Event generation with Sherpa 2.2 *SciPost Phys.* **7** 034

[54] Buccioni F, Lang J -N, Lindert J M, Maierhöfer P, Pozzorini S, Zhang H and Zoller M F 2019 OpenLoops 2 *Eur. Phys. J. C* **79** 866

[55] Cascioli F, Maierhöfer P and Pozzorini S 2012 Scattering Amplitudes with Open Loops *Phys. Rev. Lett.* **108** 111601

[56] Denner A, Dittmaier S and Hofer L 2017 Collier: a fortran-based complex one-loop library in extended regularizations *Comput. Phys. Commun.* **212** 220–38

[57] NNPDF Collaboration R D 2015 Parton distributions for the LHC run II *J. High Energy Phys.* JHEP04(2015)040

[58] Höche S, Krauss F, Schönherr M and Siegert F 2013 QCD matrix elements + parton showers. The NLO case *J. High Energy Phys.* JHEP04(2013)027

[59] Cascioli F, Höche S, Krauss F, Maierhöfer P, Pozzorini S and Siegert F 2014 Precise Higgs-background predictions: merging NLO QCD and squared quark-loop corrections to four-lepton + 0,1 jet production *J. High Energy Phys.* JHEP01(2014)046

[60] Caola F, Melnikov K, Röntsch R and Tancredi L 2015 QCD corrections to ZZ production in gluon fusion at the LHC *Phys. Rev. D* **92** 094028

[61] Anastasiou C, Melnikov K and Petriello F 2005 Fully differential Higgs boson production and the di-photon signal through next-to-next-to-leading order *Nucl. Phys. B* **724** 197–246

[62] Catani S and Grazzini M 2007 Next-to-next-to-leading-order subtraction formalism in hadron collisions and its application to higgs-boson production at the large hadron collider *Phys. Rev. Lett.* **98** 222002

[63] Grazzini M, Kallweit S and Wiesemann M 2018 Fully differential NNLO computations with MATRIX *Eur. Phys. J. C* **78** 537

[64] Anastasiou C, Duhr C, Dulat F, Herzog F and Mistlberger B 2015 Higgs Boson gluon-fusion production in QCD at three loops *Phys. Rev. Lett.* **114** 212001

[65] Passarino G 2014 Higgs CAT *Eur. Phys. J. C* **74** 2866

[66] Alwall J, Frederix R, Frixione S, Hirschi V, Maltoni F, Mattelaer O, Shao H -S, Stelzer T, Torrielli P and Zaro M 2014 The automated computation of tree-level and next-to-leading order differential cross sections and their matching to parton shower simulations *J. High Energy Phys.* JHEP07(2014)079

[67] Sjöstrand T, Ask S, Christiansen J R, Corke R, Desai N, Ilten P, Mrenna S, Prestel S, Rasmussen C O and Skands P Z 2015 An introduction to PYTHIA 8.2 *Comput. Phys. Commun.* **191** 159

[68] ATLAS Collaboration 2014 ATLAS Pythia 8 tunes to 7 TeV data, ATL-PHYS-PUB-2014-021 (available at: https://cds.cern.ch/record/1966419)

[69] Ball R D *et al* NNPDF Collaboration 2013 Parton distributions with LHC data *Nucl. Phys. B* **867** 244

[70] Biedermann B, Denner A, Dittmaier S, Hofer L and Jäger B 2016 Electroweak corrections to $pp \to \mu^+\mu^-e^+e^- + X$ at the LHC: a Higgs Boson background study *Phys. Rev. Lett.* **116** 161803

[71] Biedermann B, Denner A, Dittmaier S, Hofer L and Jäger B 2017 Next-to-leading-order electroweak corrections to the production of four charged leptons at the LHC *J. High Energy Phys.* JHEP01(2017)033

[72] Frixione S, Hirschi V, Pagani D, Shao H -S and Zaro M 2015 Electroweak and QCD corrections to top-pair hadroproduction in association with heavy bosons *J. High Energy Phys.* JHEP06(2015)184

[73] ATLAS Collaboration 2010 The ATLAS Simulation Infrastructure *Eur. Phys. J. C* **70** 823

[74] Agostinelli S 2003 Geant4—a simulation toolkit *Nucl. Instrum. Meth. A* **506** 250

[75] Sjöstrand T, Mrenna S and Skands P 2008 A brief introduction to PYTHIA 8.1 *Comput. Phys. Commun.* **178** 852–67

[76] ATLAS Collaboration 2016 The Pythia 8 A3 tune description of ATLAS minimum bias and inelastic measurements incorporating the Donnachie–Landshoff diffractive model (available at: https://cds.cern.ch/record/2206965)

[77] ATLAS Collaboration 2021 Muon reconstruction and identification efficiency in ATLAS using the full Run 2 *pp* collision data set at $\sqrt{s} = 13$ TeV *Eur. Phys. J. C* **81** 578

[78] ATLAS Collaboration 2024 Electron and photon efficiencies in LHC Run 2 with the ATLAS experiment *J. High Energy Phys.* JHEP05(2024)162

[79] ATLAS Collaboration 2017 Jet reconstruction and performance using particle flow with the ATLAS Detector *Eur. Phys. J. C* **77** 466

[80] Cacciari M, Salam G P and Soyez G 2008 The anti-$k_t$ jet clustering algorithm *J. High Energy Phys.* JHEP04(2008)063

[81] Cacciari M, Salam G P and Soyez G 2012 FastJet user manual *Eur. Phys. J. C* **72** 1896

[82] ATLAS Collaboration 2021 Jet energy scale and resolution measured in proton–proton collisions at $\sqrt{s} = 13$ TeV with the ATLAS detector *Eur. Phys. J. C* **81** 689

[83] ATLAS Collaboration 2016 Performance of pile-up mitigation techniques for jets in *pp* collisions at $\sqrt{s} = 8$ TeV using the ATLAS detector *Eur. Phys. J. C* **76** 581

[84] ATLAS Collaboration 2019 Forward jet vertex tagging using the particle flow algorithm, ATL-PHYS-PUB-2019-026 (available at: https://cds.cern.ch/record/2683100)

[85] Bolognesi S, Gao Y, Gritsan A V, Melnikov K, Schulze M, Tran N V and Whitbeck A 2012 Spin and parity of a single-produced resonance at the LHC *Phys. Rev. D* **86** 095031

[86] Cranmer K, Lewis G, Moneta L, Shibata A and Verkerke W 2012 HistFactory: a tool for creating statistical models for use with RooFit and RooStats (available at: https://cds.cern.ch/record/1456844)

[87] Ramachandran P, Zoph B and Le Q V Searching for activation functions 2017 (arXiv:1710.05941 [cs.NE])

[88] Papamakarios G, Nalisnick E, Rezende D J, Mohamed S and Lakshminarayanan B 2021 Normalizing Flows for Probabilistic Modeling and Inference *J. Mach. Lear. Res.* **22** 2617

[89] Cranmer K, Pavez J and Louppe G 2015 Approximating likelihood ratios with calibrated discriminative classifiers (arXiv:1506.02169 [stat.AP])

[90] Cranmer K 2015 Practical statistics for the LHC (arXiv:1503.07622 [physics.data-an])

[91] Hastie T, Tibshirani R and Friedman J H 2009 *The Elements of Statistical Learning: Data Mining, Inference and Prediction* (*Springer Series in Statistics*) (Springer) (available at: https://books.google.com/books?id = eBSgoAEACAAJ)

[92] Garrido L and Juste A 1998 On the determination of probability density functions by using neural networks *Comput. Phys. Commun.* **115** 25–31

[93] Rizvi S, Pettee M and Nachman B 2024 Learning likelihood ratios with neural network classifiers *J. High Energy Phys.* JHEP02(2024)136

[94] Kingma D P and Ba J 2014 Adam: a method for stochastic optimization (arXiv:1412.6980 [cs.LG])

[95] Dozat T 2016 Incorporating Nesterov momentum into Adam *4th Int. Conf. on Learning Representations* p 1 (available at: https://dblp.org/rec/conf/iclr/2016.html)

[96] Cowan G, Cranmer K, Gross E and Vitells O 2011 Asymptotic formulae for likelihood-based tests of new physics *Eur. Phys. J. C* **71** 1554
Cowan G, Cranmer K, Gross E and Vitells O 2013 *Eur. Phys. J. C* **73** 2501 (erratum)

[97] Niculescu-Mizil A and Caruana R 2005 Predicting good probabilities with supervised learning *Proc. of the 22nd Int. Conf. on Machine Learning (ICML '05)* (Association for Computing Machinery) pp 625–32

[98] Agarwal B, Jones S, Kerner M and Manteuffel A 2025 Complete NLO QCD corrections to *ZZ* production in gluon fusion *Phys. Rev. Lett.* **134** 031901

[99] Catani S, Krauss F, Webber B R and Kuhn R 2001 QCD matrix elements + parton showers *J. High Energy Phys.* JHEP11(2001)063

[100] Gieseke S, Kasprzik T and Kühn J H 2014 Vector-boson pair production and electroweak corrections in HERWIG++ *Eur. Phys. J. C* **74** 2988

[101] Efron B and Tibshirani R J 1994 *An Introduction to the Bootstrap* ed Y Bengio and Y LeCun (CRC Press) (available at: https://books.google.com/books?id = MWC1DwAAQBAJ)

[102] ATLAS Collaboration 2020 Recommendations for the modeling of smooth backgrounds, ATL-PHYS-PUB-2020-028 (available at: https://cds.cern.ch/record/2743717)

[103] Neyman J 1937 Outline of a theory of statistical estimation based on the classical theory of probability *Phil. Trans. R. Soc. A* **236** 333–80

[104] Praestgaard J and Wellner J A 1993 Exchangeably weighted bootstraps of the general empirical process *Ann. Probab.* **21** 2053

[105] Pinto A, Wu Z, Balli F, Berger N, Boonekamp M, Chapon É, Kawamoto T and Malaescu B 2024 Uncertainty components in profile likelihood fits *Eur. Phys. J. C* **84** 593

[106] ATLAS Collaboration 2020 Higgs boson production cross-section measurements and their EFT interpretation

in the $4\ell$ decay channel at $\sqrt{s} = 13$ TeV with the ATLAS detector *Eur. Phys. J. C* **80** 957
ATLAS Collaboration 2021 *Eur. Phys. J. C* **81** 398 (erratum)
ATLAS Collaboration 2021 *Eur. Phys. J. C* **81** 29 (erratum)
[107] CERN 2020 *CERN Open Data Policy for the LHC Experiments* CERN-OPEN-2020-013 (available at: https://cds.cern.ch/record/2745133)
[108] ATLAS Collaboration 2025 ATLAS computing acknowledgements, ATL-SOFT-PUB-2025-001 (available at: https://cds.cern.ch/record/2922210)
[109] ATLAS Collaboration 2024 Total cost of ownership and evaluation of Google cloud resources for the ATLAS experiment at the LHC *Comput. Softw. Big Sci.* **9** 2